Experimental Investigation of Polycyclic Aromatic Hydrocarbons (PAHs) in Hydrogen-Enriched Diffusion Flames.

Chinonso Emma Ezenwajiaku

Submitted in partial fulfilment of the requirements

for the degree of Doctor of Philosophy at

University College London

July 2021

I, Chinonso Emma Ezenwajiaku confirm that the work presented in this thesis is my own. Where information has been derived from other sources, I confirm that this has been indicated in this thesis.

Dated: 5th July 2021

ABSTRACT

Polycyclic aromatic hydrocarbons (PAHs) are the carcinogenic components of soot. Detailed understanding of the underlying processes of PAH formation and growth is required for the development of effective strategies to curtail PAH formation and reduce soot emissions from combustion systems. One such approach is the use of hydrogen (H_2) as an alternative energy vector which is in-line with the global push for transition towards low carbon energy systems. Therefore, understanding the effects of H_2 addition in hydrocarbon fuels on PAH formation process is key to its full utilisation in combustion devices to reduce pollutant emissions.

This thesis presents an experimental methodology to analyse PAH formation and growth characteristics of laminar inverse diffusion flames of various H_2-enriched hydrocarbon fuel mixtures using simultaneous planar laser induced fluorescence (PLIF) imaging of PAHs and hydroxyl radicals (OH). Methane was also separately added to the same hydrocarbon fuels to study effects of fuel (carbon-hydrogen) composition in comparison to H_2 addition. Additionally, argon, nitrogen, and carbon dioxide were used as control diluents to study the diluting effects of H_2 addition in hydrocarbon flames.

PAH fluorescence intensity values were observed to increase with increasing length along the flame front, L_f, for all conditions tested, however this rate of increase reduced with H_2 addition. The reduction in PAH with H_2 addition might be attributable to an anticipated reduction in acetylene and propargyl concentrations, and reduced H-atom abstraction rates, which reduced the

availability of active sites for PAH growth. Furthermore, the addition of both H_2 and CH_4 was found to reduce the growth rate of PAH, with H_2 demonstrating higher reductions. The PAH growth rate in this thesis refers to the rate of increase of the PAH LIF signal as the length along the flame front, L_f, increases. For both fuel additions (CH_4 and H_2), two distinct regions in the PAH growth curve were observed; a steep growth region followed by a slower growth region. This suggests that for PAH and soot formation, though first ring formation plays a significant role, it is not the only important step for PAH and soot formation. Other PAH growth processes could be playing significant roles as well.

IMPACT STATEMENT

The work carried out in this thesis aims to provide underpinning science on PAH formation and growth characteristics through an experimental analysis of laminar inverse diffusion flames of various hydrogen-enriched hydrocarbon mixtures. The scientific outcomes from this work could be of benefit to both academia and industry associated with the fields of pollutant emission (PAH and soot formation), fire research, synthesis/preparation of different carbon materials such as fullerene, graphite, carbon black, carbon nanofiber/nanotube, and graphene as well as contribute to the utilisation of hydrogen as an energy vector.

The findings of this study suggest a positive impact of hydrogen addition to all the hydrocarbon fuels tested in reducing the formation and growth of PAHs. This is expected to translate to a reduction in soot formation which is a key pollutant from the combustion of hydrocarbons from both light and heavy duty transport vehicles as well as power generation plants. A key potential impact of this finding is that it promotes the use of hydrogen as a non-carbon energy vector, which is in line with the decarbonisation strategy of the power and propulsion sectors. Utilisation of hydrogen-hydrocarbon mixtures (as done in this study) takes advantage of the positives associated with hydrogen combustion (including reduction of soot/carbon emissions) and presents a feasible intermediate solution while efforts are made to develop combustion systems suitable for 100% hydrogen combustion.

On the dissemination front, this research work has led to two collaborations: first with the computational modelling group of Professor Swaminathan at the University of Cambridge. This resulted in a publication in the International Journal of Hydrogen Energy titled "***Study of polycyclic aromatic hydrocarbons (PAHs) in hydrogen-enriched methane diffusion flames***" (https://doi.org/10.1016/j.ijhydene.2019.01.253). The findings from this publication have potential impact through provision of experimental data which can help in validating PAH formation computational models and improving reaction mechanism schemes.

Secondly, the research methodology developed in this project was utilised for another study conducted in collaboration with Dr Roberto Volpe's group at Queen Mary University of London to investigate the formation of tar and tar precursors during biomass pyrolysis. The findings from the study can provide valuable scientific input towards the development of technologies for the synthesis of green chemicals and energy vectors through thermochemical breakdown of biomass. This work resulted in a publication titled: "***In-situ observation of the evolution of polyaromatic tar precursors in packed-bed biomass pyrolysis***" in the journal - RSC Reaction Chemistry & Engineering (https://doi.org/10.1039/D1RE00032B). Additionally, two other manuscripts based on Chapters 5 and 6 of this thesis are in advanced stages of preparation at the time of preparing this thesis.

Furthermore, the results from this study were accepted for presentation at both the Combustion Aerosol Conference 2019 and the Joint SIG Meeting on Spray

and Combustion 2019 (UK Fluids network – Combustion science, technology,

and applications group). The presentation was well received at both sessions.

ACKNOWLEDGEMENT

My sincere gratitude goes to my supervisors: Professor Ramanarayanan Balachandran, Professor Alistair Greig and Dr. Midhat Talibi for their contributions towards the success of this work. A special thanks to Professor Balachandran for his vast knowledge, expertise, duty of care, assistance and unparalleled guidance which made doing science under him both tasking and pleasurable. Am deeply grateful to Dr. Talibi for showing me the ropes around the lab, his encouragement and constant assistance whenever required motivated me to always strive for the best. Many thanks to Professor Greig for chairing my MPhil to PhD upgrade panel. I am grateful to God for the opportunity to work with the best supervisory team!

A big thank you goes to the Petroleum Technology Development Fund (PTDF) for sponsoring this research work. A special mention to Hajiya Waziri-Adamu, Wahab Gbenga and Bolanle Agboola for their invaluable help with all my requests at PTDF.

Special thank you to the technicians in the workshop who manufactured my IDF burner and other parts used for the rig set-up. I duly appreciate my amiable colleagues: Dr. Adesile, Dr. Christopher, Dr. Victor, Seun (Amanda), Hywel, Ahmad and Zuhaib who made the sojourn in the thermodynamics laboratory these four years interesting. Also, I wish to thank the MechEng finance department for their help with purchase of consumables for my experiments.

TABLE OF CONTENTS

3.0 Experimental methodology   73

LIST OF FIGURES

LIST OF TABLES

NOMENCLATURE

Abbreviations

ABF   Appel-Bockhorn-Frenklach

CDF   Counterflow diffusion flame

2D-LOSA   2D line of sight attenuation

FWHM   Full width-half maximum

GCMS   Gas chromatography mass spectrometry

HACA   H-abstraction-C_2H_2-addition

HAB   Height above burner

HENG   Hydrogen-enriched natural gas

ICCD   Intensified charge coupled devices

IC   Internal combustion

IDF   Inverse diffusion flame

LIF   Laser-induced fluorescence

LII   Laser induced incandescence

MBMS   Molecular beam mass spectrometry

MPI   Multi-photon ionisation

NDF   Normal diffusion flame

PM   Particulate matter

PAC   Phenyl addition/cyclisation

PAH   Polycyclic aromatic hydrocarbon

SNR   Signal to noise ratio

SPI   Single photon ionisation

SVF   Soot volume fraction

Slpm   Standard litres per minute

TOFMS   Time of flight mass spectrometry

TEF   Toxic equivalence factor

USEPA   United States environmental protection agency

VUV   Vacuum ultraviolet

Molecular Formula

C_2H_2 Acetylene

C_6H_6 Benzene

CO_2 Carbon dioxide

CO Carbon mono oxide

C_2H_6 Ethane

C_2H_4 Ethylene

He Helium

H_2 Hydrogen

CH_4 Methane

CH_3 Methyl

$C_{10}H_8$ Naphthalene

O_2 Oxygen

C_6H_5 Phenyl

C_3H_8 Propane

C_3H_3 Propargyl

C_3H_6 Propylene

Subscript

sum Cumulative sum of the PAH line profile

$sum, 0$ Cumulative sum of the PAH line profile of the reference case

pk Peak

CHAPTER ONE

1.0 INTRODUCTION

1.1 MOTIVATION

Global population rise coupled with intensified rates of industrialisation of developing countries will ensure continuous increase in energy demands worldwide for the foreseeable future. It has been projected that from 2020 to 2040, energy consumption will increase by 30% (USEIA, 2016). Even though efforts to diversify the world energy mix by utilising alternative sources of energy such as solar, wave, wind, tidal, geothermal and nuclear energy are yielding significant results, fossil fuels are still expected arguably to play a complementary role for energy supply in the coming decades. This is more relevant for the power generation and transportation sectors due to their heavy reliance on fossil fuel; it is noteworthy that more than 60% of the barrels of crude oil consumed yearly are used in internal combustion (IC) engines for power generation and transport (Fu *et al.*, 2013; Reitz, 2013; Wang and Chung, 2019; Liu *et al.*, 2021). The continued use of these conventional hydrocarbon fuels (gasoline, diesel, natural gas, coal, wood and oil) for energy provision poses a significant environmental and health risk as they are major sources of hazardous pollutant emissions like carbon dioxide (CO_2), carbon monoxide (CO), nitric oxide (NO_x), unburned hydrocarbons (UHC) and soot. Soot (also known as black carbon) is produced from pyrolysis or the incomplete combustion of hydrocarbon fuels and composed mainly of carbon with traces of hydrogen and oxygen (Wang and Chung, 2019). Soot is of particular interest due to its ubiquitous nature and significant contribution to

the emissions of $PM_{2.5}$, which are a group of fine particles with diameters less than 2.5μm. $PM_{2.5}$ can be transported more efficiently into the human lungs through the respiratory tracts and is capable of producing devastating health effects (Richter and Howard, 2000; Eveleigh, 2015). Studies have shown that prolonged exposure to soot particles can cause cancer and other cardiopulmonary diseases (Holme *et al.*, 2019; Li *et al.*, 2019; Sari, Esen and Tasdemir, 2020). This is primarily due to the presence of polycyclic aromatic hydrocarbons (PAHs) which are the precursors of soot formation and can also get adsorbed on the surface of exhaust soot particles (Ramanakumar *et al.*, 2008; Niranjan and Thakur, 2017).

Polycyclic Aromatic Hydrocarbons (PAH) are hydrocarbons with two or more benzene rings fused together in either linear, cluster or angular molecular arrangement. PAHs can persist long-term in the environment, often being carried over long distances without significant degradation. For example, Björseth and Lunde (1977) observed that PAHs emitted in the United Kingdom were transported to as far as southern Norway while Tamamura *et al.* (2007) reported (using back trajectory analysis) similar long-range transportation of PAHs without significant degradation between Japan and the loess region in China.

Additionally, several research studies have shown that PAHs undergo metabolism inside the human body to release derivatives that combine with human DNA and proteins to induce mutagenic activities in human cells (Farmer *et al.*, 2003). Other health effects like decreased immune function, breathing problems and abnormalities in lung functions have been linked to

24

chronic exposure to PAHs (Harvey, 1991; Abdel-Shafy and Mansour, 2016). Additionally, recent epidemiological studies on occupational worker exposures to PAH mixtures have shown relation to cases of lung, skin, gastrointestinal and bladder cancers (Kiriluk *et al.*, 2012; Rehman *et al.*, 2020). More details on the study of PAH as a causative agent for cancer can be found in Refs. (Mastrangelo, Fadda and Marzia, 1996; Shen *et al.*, 2014; Rengarajan *et al.*, 2015).

Furthermore, PAHs emitted to the atmosphere can get adsorbed on to dust particles and subsequently photo-oxidised in the presence of ultra-violet (UV) radiation from the sun. Photo-oxidation from the UV radiation has been shown in literature to increase the toxicity of PAHs (Ukaogo, 2015). These photo-oxidised PAHs can migrate from the atmosphere to the soil using air as the primary transport vector (Manzetti, 2013). For example, Ni *et al.* (2011) estimated that in Shenzhen, China, about 10-15% of PAHs in the air were transported to the soil during autumn season in 2010 due to the increase in rainfall. Accumulation of PAHs in the soil can affect plants adversely as PAHs have been shown to exhibit lipid peroxidation and phytotoxicity in plants (Pašková *et al.*, 2006). Also, increase in the concentration of PAHs in the soil can result in the contamination of nearby water bodies via soil erosion and subsequently harm aquatic life. Pollution of the rivers and lakes can also result from the high molecular weight PAHs (that is, above 4 rings PAHs) which have been found to adsorb on particles and precipitate at the base of water bodies like rivers, oceans, ponds and lakes due to their insolubility in water (Maliszewska-Kordybach, 1999; Ukaogo, 2015).

Given the environmental hazards posed by the presence of PAHs and the associated health risks as elucidated above, several governmental agencies have made efforts at classifying various PAHs into groups in order to highlight the most hazardous PAHs; the United States Environmental Protection Agency (USEPA) have designated 16 PAHs as priority pollutants while the International Agency for Research on Cancer (IARC) has also identified 8 PAHs as probable or possible human carcinogens (see Table 1.1) (EEA, 1999). The classification by EPA used the toxic equivalence factor (TEF) method which was based on the following factors: the adverse effect of the PAHs on humans (toxicity), reactivity and its abundance and persistence in the environment (Erika *et al.*, 2012; Andersson and Achten, 2015; Jia *et al.*, 2020). Benzo(a)pyrene - B[*a*]P was utilised as the reference compound for the EPA classification (Nisbet and LaGoy, 1992). While the classification by IARC is based on extensive experimental evidence obtained from *in vitro* studies done on tissues and cells of animal species and mechanistic data from humans exposed to the PAHs (updated as new evidences are obtained) (Jameson, 2019; IARC, 2020). These classifications have helped focus PAH investigations to a priority group between 2 – 6 rings PAHs. Additionally, stringent regulations on PAH concentrations in the environment have been set to as low as reasonably practicable (ALARP) by many governmental agencies globally to limit the health effects and environmental damage due to PAH pollution. For example, European Union Council Directive (Directive 2004/107/EC and EC 2019/1021) stipulates that the concentration of PAH using B[*a*]P as a marker in ambient air should not exceed a target value of 1 ng/m^3 (EU, 2019). Also, under Euro 6 emission standards, either diesel or

petrol engines should not emit more than 5 mg/km of particulate matter (PM) (EU, 2007). These values are updated regularly as government policies change.

To tackle these problems posed by PAH emissions and in response to various stringent government regulations, intense research efforts have been focused on finding alternative renewable sources of energy. Various alternative sources of energy have been proposed in literature and are at different stages of deployment globally. Some of these sources include fuel cells, electric vehicles, wind, solar, tidal and hydrogen. Of all these energy sources, hydrogen is of major interest as it is a clean energy carrier and considered a viable fuel option for the decarbonisation of the transportation, power generation and manufacturing sectors of the global economy (USDOE, 2020). These sectors are considered as the largest three sectors of the global economy and highest contributors of pollutant emissions including PAHs (USDOE, 2020). This prospect for hydrogen has increased the global demand for pure hydrogen over the last 30 years as shown in Figure 1.1 (IEA, 2019). Despite these good prospects for hydrogen, its widespread utilisation is still very low presently, due to the challenges with storage and production of hydrogen (Gu, Chu and Liu, 2016). These challenges negatively affect funding from national governments and industry contribution as well for the hydrogen economy research (Solomon and Banerjee, 2006; IEA, 2019). However, in recent times, the use of hydrogen as an energy source has received significant attention due to the role it has been projected to play in the bold net zero carbon targets set by various countries (such as the UK and Japan) in

response to climate change (Great Britain, Department for Business, 2019; Elaine, 2020; Tsukimori, 2020). This has provided the motivation for renewed concerted research efforts towards the use of hydrogen to diversify the global energy mix and reduce particulate emissions.
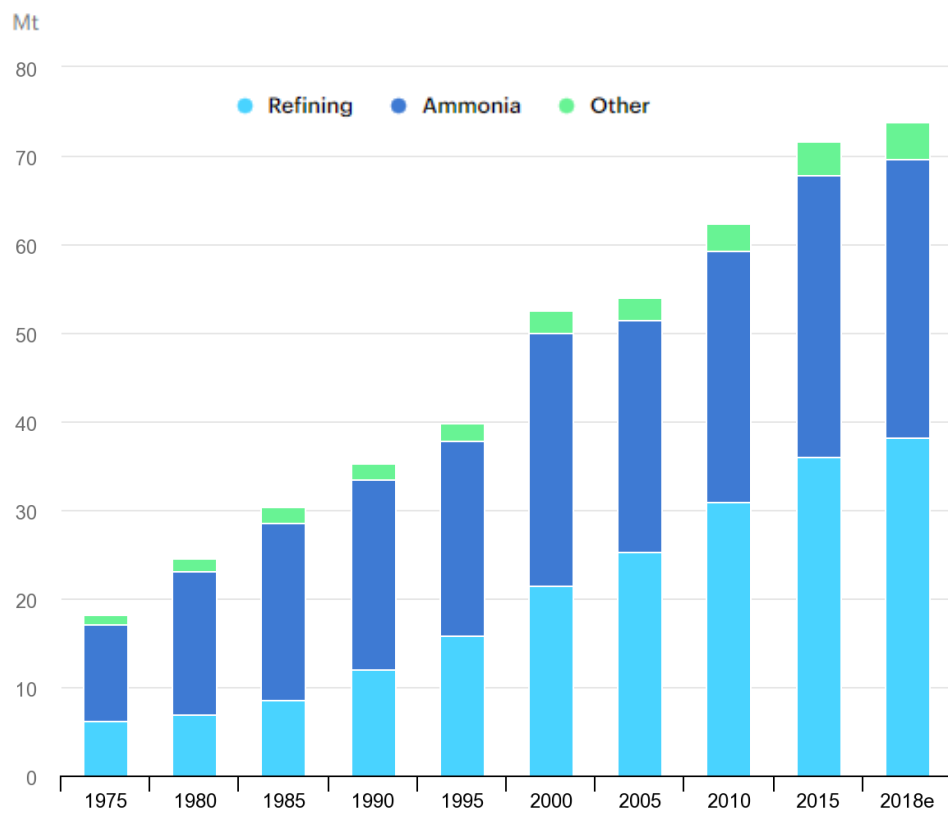
Figure 1.1: Global demand for pure hydrogen from 1975 to 2018 in megatons, Mt (IEA, 2019). The legend shows the different sources of the pure hydrogen

Table 1.1: Classification of PAHs by USEPA and IARC as pollutants and carcinogens (EEA, 1999; IARC, 2020)

PAH	USEPA Priority Pollutants (16 PAHs)	IARC Probable or possible human carcinogens
Naphthalene	✔	✔
Acenaphthylene	✔	
Acenaphthene	✔	
Fluorene	✔	
Anthracene	✔	
Phenanthrene	✔	
Fluoranthene	✔	
Pyrene	✔	
Benz[a]anthracene	✔	✔
Chrysene	✔	✔
Benzo[b]fluoranthene	✔	✔
Benzo[k]fluoranthene	✔	✔
Benzo[a]pyrene	✔	✔
Dibenz[a,h]anthracene	✔	✔
Indeno[1,2,3-cd]pyrene	✔	✔
Benzo[g,h,i]perylene	✔	

1.2 OVERARCHING AIM OF THE THESIS

Due to the environmental and health effects of soot emissions and the additional deleterious effects of soot deposits on the maintenance and efficiency of combustion devices, the study of the processes leading to soot formation is imperative. Since PAHs have been identified as a key precursor and building blocks (discussed later in chapter 2) to soot formation and also

the toxic component of soot particles, it is important to develop strategies to reduce PAH formation in order to limit formation and growth of soot particles. Hydrogen has shown great promise in this regard as it does not produce carbon emissions on combustion, and hence has potential to improve combustion properties and reduce pollutant emissions. Additionally, most of the chemical kinetic studies on PAH and soot growth available in literature (discussed in Chapter 2) showcase the importance of hydrogen atom in the intermediate steps involved in the reaction mechanisms for the formation and growth of PAHs and soot. Hence, the effect of hydrogen addition to hydrocarbon fuels is an important factor which needs to be studied as a strategy for the reduction of PAHs and soot. Therefore, the overarching aim of this study is to investigate the formation and growth of PAHs in a non-premixed (diffusion) flame configuration (applicable to practical combustion systems) – using multi-component fuel mixtures, primarily focusing on understanding the effect of hydrogen on PAH reduction.

1.3 STRUCTURE OF THESIS

This report describes the experimental study of PAH formation and growth characteristics in a laminar inverse diffusion flame (IDF) configuration using multi-component fuel mixtures composed of hydrogen, hydrocarbons (C1 – C3) and non-reactive diluents. Simultaneous imaging of OH and PAH PLIF technique was employed for this study.

Chapter 1 presents the introduction and motivation for this study. The overarching aim of the study is also set out in this chapter.

Chapter 2 focuses on literature survey of relevant past works related to PAHs including formation and growth mechanisms as well as techniques utilised for the study of PAH. It also highlights the importance of PAH investigation in reducing soot formation in IDF flame configuration using laser based optical diagnostics. It concludes with a gap analysis to establish the scientific questions this work seeks to answer and its contribution to the body of knowledge relevant to PAH emissions. Following on from the gap analysis, the specific objectives for this work are also presented.

Chapter 3 describes the experimental methodology including a detailed description of the experimental set up used for this study. It also explains the methods of analysis and the uncertainty/errors to be considered when interpreting the results from this work.

Chapter 4 presents result of PAH formation in hydrogen enriched methane inverse diffusion flame and comparison with 1-D flame simulations. **Chapter 5** presents results of PAH formation and growth in binary fuel mixtures of either hydrogen or methane with C1-C3 hydrocarbons while **Chapter 6** presents results of PAH formation when hydrocarbon fuels are diluted with non-reacting gases. Conclusions and further work are summarised in **Chapter 7**.

CHAPTER TWO

2.0 LITERATURE REVIEW

2.1 PAH OVERVIEW

2.1.1 Sources of PAH

Several sources of PAH emissions to the environment exist which can be broadly classified into three major types – pyrogenic, petrogenic, and biological (Abdel-Shafy and Mansour, 2016). The pyrogenic sources refer to those produced by combustion or pyrolytic reactions, petrogenic sources refer to PAHs produced as a result of crude oil processing and utilisation and biological sources cover PAHs produced due to synthetic bacterial or algal action on vegetation causing decay.

These sources described above can be natural or anthropogenic (pollution due to human activity). Main natural sources include bush or forest fires and volcanic eruptions while anthropogenic sources range from incomplete combustion of fossil fuels, exhaust from automobiles, aircraft and power plants, oil spillage, wood burning, tobacco smoke, waste incineration, crude oil refining processes, coal processing and other industrial processes. Natural sources do not contribute significantly to the overall global PAH emissions; most PAH emissions reported globally are as a result of incomplete combustion and pyrolysis of fossil fuels in engines and gas turbines due to increased industrial activities (Maliszewska-Kordybach, 1999).

2.1.2 Characteristics of PAH

PAHs can be characterised by their vapour pressure, aqueous solubility and boiling points (Kim *et al.*, 2013; Abdel-Shafy and Mansour, 2016). The molecular weight and structure of PAHs determine these physical properties; for example, the vapour pressure of PAHs reduces as the molecular weight increases (Akyüz and Çabuk, 2010) and the boiling points can vary from 200 °C for 2-ring PAHs to about 600 °C for 10-ring PAHs (Achten and Andersson, 2015). PAHs are very soluble in organic solvents compounds (lipophilic) but the aqueous solubility reduces as more rings are added to the PAH (Abdel-Shafy and Mansour, 2016). PAHs can exist in the liquid, gaseous and solid phase. During combustion, smaller PAHs are formed initially in the gaseous phase. These smaller PAHs grow to larger PAHs and continue to increase in size (via dimerisation and various growth routes to be discussed later) until it reaches comparable molecular masses of the incipient soot particles (solid phase). (Masclet, Bresson and Mouvier, 1987; D'Anna, 2008; Slavinskaya *et al.*, 2012). PAH molecules from the vapour phase are also able to adsorb on to the matrix of exhaust soot particles, this adsorption is primarily dependent on the PAH vapour pressure (Mastral and Callén, 2000). Additionally, PAHs are sensitive to light - they absorb in the UV and visible spectra with each ring structure identified by a unique UV/visible spectrum thus each isomer possesses a different UV/visible absorbance spectrum (Randall L.Vander Wal, 1996; Kim *et al.*, 2013). This characteristic has been exploited for the identification and speciation of PAHs using optical diagnostics. Furthermore, most PAHs fluoresce and emit characteristic wavelengths of light when they

are excited by a light source with enough energy (Masih *et al.*, 2010). This is utilised in the laser induced fluorescence technique for the study of PAH formation in flames and other pyrolytic processes.

2.2 PAH FORMATION

Soot formation is a complex process involving various stages as shown in Figure 2.1. The decomposition of the fuel molecules and subsequent formation of small PAHs (especially first ring formation) are considered to be the critical steps which determine the overall rate of soot formation in most hydrocarbon mixtures (McEnally *et al.*, 2006). The formation of the first ring and its interaction with other intermediate species for further growth to larger PAHs have been argued to depend on the starting fuel molecules while there is no consensus on the general route to further growth of PAHs and subsequent soot formation (McEnally *et al.*, 2006; Shukla and Koshi, 2011). This area of PAH study (PAH formation) remains an important stage in need of further investigation for complete understanding of the soot formation process. In this section, relevant literatures on the dominant theories of first ring formation and growth of PAHs are reviewed.

2.2.1. First ring formation

The formation of the first aromatic ring (benzene) is key in the study of PAH formation and growth primarily because it has been identified by many studies as the rate-limiting step in the series of reactions leading to the formation of larger aromatic compounds (Cole *et al.*, 1984; Frenklach, 2002; Hansen *et al.*,

2012). Several possibilities for the first aromatic ring formation exist in literature for aliphatic base fuels and have been reviewed below.

(1) fuel decomposition   *(2) aromatics formation*

Fuel → Decomposition Products → Small Aromatic Hydrocarbons (~1 to 3 rings)

(3) aromatics growth

Large Aromatic Hydrocarbons (> 3 rings)

Large Soot Particles ← Small Soot Particles ← Large Aromatic Hydrocarbons (> 3 rings)

(5) particle growth   *(4) particle inception*
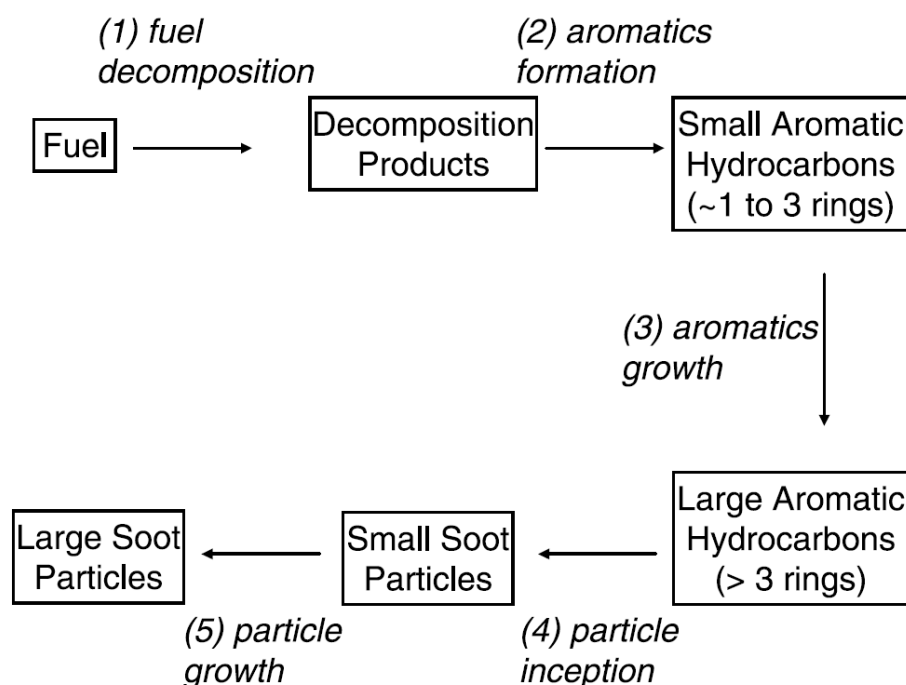
Figure 2.1: Soot formation stages from fuel molecule decomposition through PAH formation to large soot particles (McEnally *et al.*, 2006)

The quantitative assessment of aromatics formation in flames of aliphatic fuels was first attempted by Cole *et al.* (1984). To assess feasible formation mechanisms, the authors compared predicted formation rates with values estimated from experimental mole fraction profiles which were obtained by molecular beam sampling coupled to mass spectrometry (MBMS) in a near-sooting 1,3-butadiene premixed flat flame. They proposed the reaction sequence below (R1 – R4) as a viable means of first aromatic ring formation in a butadiene flame. First, H is abstracted from the fuel molecule by hydrogen

radicals to form 1,3-butadienyl radical $(1,3-C_4H_6)$. Then 1,3-butadienyl radical $(1,3-C_4H_6)$ identified as an important intermediate species for this sequence undergoes ring closure and hydrogen loss to form benzene through this free radical mechanism.

$$1,3 - C_4H_6 + H^* \rightleftharpoons 1,3 - C_4H_5^* + H_2 \tag{R1}$$

$$1,3 - C_4H_5^* + C_2H_2 \rightarrow C_6H_7^* \tag{R2}$$

$$C_6H_7^* \rightarrow c - C_6H_7^* \tag{R3}$$

$$c - C_6H_7^* \rightarrow C_6H_6 + H^* \tag{R4}$$

Frenklach and Warnatz (1987) performed a detailed modelling study of PAH formation in a burner-stabilised sooting low pressure C_2H_2- O_2- Ar flame. They proposed two pathways for the formation of first aromatic ring in the low temperature and high temperature regions of the flame respectively. In the pre-reaction zone (lower temperature), the reaction sequence (R5- R8) was found to be the most dominant route for benzene formation. It is important to note that the prefixes n and c refer to normal (straight chain) molecules and cyclic molecules respectively.

$$C_2H_2 + H \rightarrow C_2H_3 \tag{R5}$$

$$C_2H_3 + C_2H_2 \rightarrow n - C_4H_5 \tag{R6}$$

$$n - C_4H_5 + C_2H_2 \rightarrow n - C_6H_7 \tag{R7}$$

$$n - C_6H_7 \ \rightarrow \ c - C_6H_7 \ \rightarrow C_6H_6 + H \ \text{(Via cyclisation)} \hspace{3cm} \text{(R8)}$$
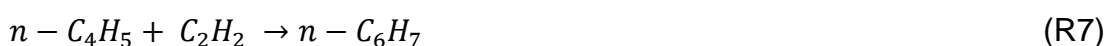
But in the main reaction zone (high temperature), due to the increase in temperature and the resultant increase in the decomposition rate of the radicals, cyclisation via reactions: R9 - R10 was reported as the dominant route for the formation of benzene. Here, the $n - C_4H_3$ is produced mainly from the H abstraction from vinylacetylene (C_4H_4).

$$n - C_4H_3 + \ C_2H_2 \ \rightarrow n - C_6H_5 \hspace{4cm} \text{(R9)}$$

$$n - C_6H_5 \ \rightarrow C_6H_5 \hspace{5cm} \text{(R10)}$$

These pathways described above as proposed by Cole et al. (1984) and Frenklach and Warnatz (1987) are referred to as the even-carbon-atom pathways and have been corroborated by other studies (Colket, 1986; Harris, Weiner and Blint, 1988).

However, Miller and Melius (1992) studied the same flame as Frenklach and Warnatz (1987) using chemical kinetic modelling and dismissed reactions R7 – R10. They argued that $n - C_4H_3$ and $n - C_4H_5$ transform rapidly into their resonantly stabilised isomers: iso$-C_4H_3$ and $iso - C_4H_5$ and so could not be available in high concentrations for the reactions to occur. Alternatively, they proposed the odd-carbon-atom pathway through a combination reaction of two resonance stabilised free propargyl radicals (R11) which rearrange to form benzene (or phenyl and H atom). This pathway was supported by other studies (Kern and Xie, 1991; Stein *et al.*, 1991; Hansen *et al.*, 2012) and has been used as the basis for the explanation of PAH formation in more recent studies

(Senkan and Castaldi, 1996; Roesler *et al.*, 2003; Yoon, Lee and Chung, 2005; Yoon, Anh and Chung, 2008; Golea *et al.*, 2012; Yan *et al.*, 2019).

$$C_3H_3 + C_3H_3 \rightarrow C_6H_6 \text{ or } C_6H_5 + H \tag{R11}$$

Other pathways (R12 and R13) based on either the odd or even-carbon-atom were also recommended by the studies in Refs. (Melius *et al.*, 1996; Moskaleva, Mebel and Lin, 1996; Ikeda *et al.*, 2000) for benzene formation.

$$C_5H_5 + CH_3 \rightarrow C_6H_6 + H + H \tag{R12}$$

$$C_3H_3 + C_2H_2 \rightarrow c - C_5H_5 \tag{R13}$$

R13 combines the benefits of two key reactants for PAH formation; the very stable propargyl radical and the readily available acetylene (PAH building block) to form cyclopentadienyl which rapidly reacts to form benzene (Ikeda *et al.*, 2000; Frenklach, 2002).

Furthermore, it is pertinent to note that a few studies have argued that it is possible that the formation of benzene might not necessarily be the rate limiting step in the growth of PAHs, rather suggesting that the growth of PAHs can be through direct formation of multi-ring PAHs (Richter and Howard, 2000; Frenklach, 2002), condensation of polyacetylenes (Haynes and Wagner, 1981), C_4H_x species combination (Bockhorn *et al.*, 1983) and self-recombination of larger radicals (e.g. R14 - the combination of two cyclopentadienyl moiety to form naphthalene and two H atoms (Melius *et al.*, 1996)) without going through benzene as an intermediate.

$$C_5H_5 + C_5H_5 \rightarrow C_{10}H_8 + H + H \qquad\qquad\qquad \text{(R14)}$$
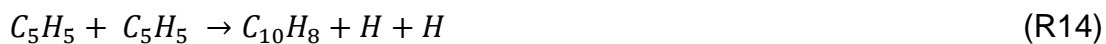
Even though there exists an extensive research effort focused on the reaction sequences for the formation of first ring aromatics, there seem to be no consensus yet on the dominant pathway for the formation of benzene. However, it is agreed that in aliphatic hydrocarbon fuels, the formation of benzene is the first step to the formation and further growth of PAHs. This proceeds mostly either through the odd or even carbon-atom pathways or a combination of both depending on the fuel and operating conditions (Richter and Howard, 2000; Frenklach, 2002; McEnally *et al.*, 2006).

2.2.2 Growth of PAHs

As stated earlier in Section 2.2.1, though there is presently no generally accepted dominant mechanism for the formation of benzene, there is a consensus in the combustion community on PAH growth to soot via a "building block" sequence involving either ions, species, gas phase molecules or larger radical recombination or a combination of some of them. For the growth of PAH beyond first ring formation, many possibilities have been postulated in literature which include H-abstraction- C_2H_2 -addition (HACA) mechanism (Frenklach, 2002), PAH dimerisation (Siegmann, Hepp and Sattler, 1995; Kislov *et al.*, 2005; Mercier *et al.*, 2019; Faccinetto *et al.*, 2020a; Frenklach and Mebel, 2020), growth by other species involving methyl, propargyl, cyclopentadienyl including multi-ring PAH formation and surface growth by PAHs (Frenklach and Wang, 1991; Benish *et al.*, 1996; Richter and Howard, 2000; Miller, Pilling and Troe, 2005) and polymerisation of polyynes (Krestinin,

1998, 2000; Cherchneff, 2011). However, of these above possibilities, the HACA mechanism is the most widely accepted and would be briefly described below.
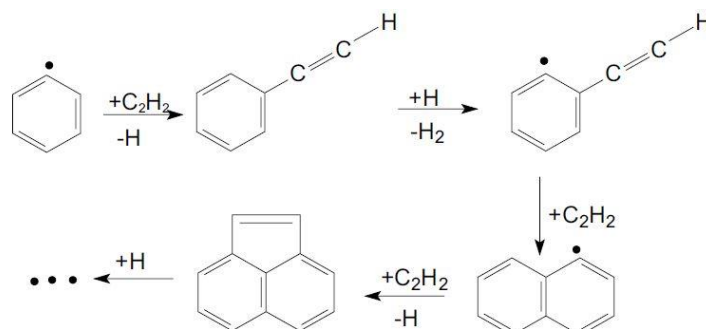
Figure 2.2: H-Abstraction-C_2H_2-Addition reaction pathway of PAH growth (Xi and Zhong, 2006)

As shown in Figure 2.2 above, HACA mechanism involves two steps that proceed in a repetitive sequence:

(i)   Hydrogen atom abstraction from the aromatic molecule by another hydrogen atom via collision to produce a radical intermediate and gaseous hydrogen.

$$A_i + H \rightleftharpoons A_{i-} + H_2 \qquad \text{(R15)}$$

Where A_i is the aromatic molecule with i peri-condensed rings and A_{i-} is the corresponding radical

40

(ii) C_2H_2-addition – addition of acetylene gas molecule to the radical site formed by the H abstraction process thus enhancing PAH growth and cyclization continuously.

$$A_{i-} \; + \; C_2H_2 \; \rightleftharpoons Products \hspace{4cm} \text{(R16)}$$

.

The degree of reversibility of reaction R16 determines the contribution of the step to the growth of PAH. The simple process described above subsists when the starting fuel molecule is aliphatic. But when the starting fuel molecule is aromatic, it proceeds in a slightly different manner, starting with PAH–PAH recombination process but quickly reverts to the HACA mechanism after the initial reaction stages (Frenklach *et al.*, 1988; Wang and Frenklach, 1997; Frenklach, 2002; Xi and Zhong, 2006).

More recently, some modelling studies observed that the utilisation of the HACA mechanism for PAH formation under-predicted PAH concentration in flames when compared with experimental results. Consequently, a few additional mechanisms were proposed either as alternatives or complementary to the HACA mechanism for accurate modelling of PAH formation and growth in flames. These have been described in the following paragraphs.

Shukla and Koshi (2010) performed a chemical kinetic analysis of the formation pathways of the gas-phase products of the pyrolysis of benzene and acetylene mixtures in a flow tube reactor and observed that the growth of PAHs were initiated and accelerated efficiently by reaction routes involving phenyl

radicals. They termed this mechanism phenyl addition/cyclisation (PAC). PAC growth mechanism involves the addition of phenyl radical to any fusing site of an aromatic species followed by dehydrocyclisation which leads to the formation of a larger PAH molecule (product) with two new additional fusing sites. As a result of the continuous generation of additional fusing sites for further ring growth, they reported that PAC routes are fast and form PAC products capable of endless production of PAH. A typical example of PAC is shown in R17 and R18 for the formation of benzo[*e*]pyrene (5-ring PAH) from phenanthrene (3-ring PAH) and dibenzo[*b,pqr*]perylene (7-ring PAH) from benzo[*e*]pyrene respectively.

$$C_{14}H_{10} \xrightarrow{+C_6H_5/-H} C_{20}H_{14} \xrightarrow{-H_2} C_{20}H_{12} \tag{R17}$$

$$C_{20}H_{12} \xrightarrow{+C_6H_5/-H} C_{26}H_{16} \xrightarrow{-H_2} C_{26}H_{14} \tag{R18}$$

Comparing PAC and HACA mechanisms, Shukla and Koshi (2011) reported that with regards to PAH growth rate, though PAC mechanism is very efficient and fast, it is not capable of forming symmetrical PAHs while the HACA mechanism (although slower) was found to be very efficient at producing symmetrical PAHs (more stable when compared to non-symmetrical PAHs). However, at temperatures relevant to flames (high temperatures above 1370K), the authors observed a collaboration between PAC and the HACA mechanism and noted that the most efficient PAH growth occurred at the condition where HACA and PAC were both present (Shukla *et al.*, 2008; Shukla and Koshi, 2010).

Similar to C_2H_2, methyl (CH_3) radical is significantly produced from the pyrolysis and oxidation of aliphatic and aromatic hydrocarbons (Georganta *et al.*, 2017). Though it is not a stable species as it reacts rapidly with other radicals and neutral species, Shukla et al. (2010) postulated that PAH formation via methyl addition/cyclisation is a feasible mechanism for PAH growth. They performed pyrolysis experiments in a flow tube reactor of toluene and toluene/acetone mixtures and obtained the PAH mass spectra using time of flight mass spectrometry (TOFMS). A typical MAC growth route involves the addition of one or more methyl radicals to the fusing site of PAH with subsequent dehydrocyclization to form cyclotetra/penta-fused or benzenoid structure. Their results showed that MAC has a unique capacity of inducing sequential growth of PAH. Other studies tested the viability of the MAC mechanism for PAH growth. Georganta *et al.* (2017) studied numerically, the conversion of phenanthrene to pyrene by methyl radicals using a detailed reaction mechanism (author-developed mechanism) in laminar premixed methane and ethane flames. They observed that the reactions based on methyl addition were not able to compete with the C_2H_2 based addition reaction for the production of pyrene. Schenk *et al.* (2015) studied the formation of PAHs in opposed flow flames of n-butane, *i*-butane, *i*-butene, and *i*-butanol using molecular beam mass spectrometry (MBMS) with electron ionisation (EI) and gas chromatography mass spectrometry (GCMS) techniques to identify important contributors to PAH formation and growth. They observed that contrary to the conclusion by Georganta *et al.* (2017), reactions based on methyl radicals were very important steps in the molecular growth of PAH. They also concluded that the formation and growth of PAH is

based on several pathways with multiple building blocks rather than a single species. This assertion was confirmed by the comparative study of Shukla and Koshi (2011) who compared the efficiency of the PAC, HACA and MAC mechanisms experimentally by detecting the gas phase reaction products of the pyrolysis of pure toluene and toluene with benzene/acetylene mixtures using the vacuum ultraviolet (VUV) single photon ionisation (SPI) TOFMS technique. Their results showed the interdependency of the three mechanisms; PAC was very efficient for successive growth, HACA filled the triple fusing sites formed by the PAC mechanism and MAC expanded the cyclotetra/pentafused structures (formed by the interaction of the HACA and PAC mechanisms) into benzenoid structures. They proposed a combination of all three mechanisms for the construction of a general and optimum mechanism for PAH/soot formation and growth in order to cover a wide range of operating conditions for combustion.

Other mechanisms that has been proposed for PAH growth include Diels-Alder, H atom migration, ionic species, cyclopentadienyl moiety, PAH dimerisation, reactive coagulation/condensation can be found in the Refs. (Hepp, Siegmann and Sattler, 1995; Weilmünster, Keller and Homann, 1999; Richter and Howard, 2000; Fialkov, Dennebaum and Homann, 2001; Frenklach, 2002; Kislov et al., 2005; McEnally et al., 2006; Slavinskaya et al., 2012; García-Rodeja and Fernández, 2019; Mercier et al., 2019; Fernández, 2020). There is no consensus yet on a generalised mechanism for PAH growth which is capable of capturing the wide range of pyrolysis and combustion conditions investigated in literature (Shukla and Koshi, 2011).

2.3 PAH MEASUREMENTS

2.3.1 Flame configuration

To understand the complex processes involved in formation of PAH, various open flame configurations have been used including premixed and non-premixed flames (Vander Wal, 1996; Blevins *et al.*, 2002; McEnally and Pfefferle, 2002; Katta, Blevins and Roquemore, 2005; Santamaría *et al.*, 2006). However, non-premixed or diffusion flames have been shown to be more suitable to track the early stages of PAH formation and understand fuel molecular structure effects on soot formation (Sidebotham and Glassman, 1992). Furthermore, Bejaoui *et al.* (2014) studied PAH LIF signatures produced in non-premixed and premixed flames using UV and visible laser excitation wavelengths and concluded that the classification of PAHs based on size as height above burner (HAB) increases is possible in the non-premixed flame configuration but not in the premixed flame mode. The authors explained that in premixed flame, all observed sizes of PAH form early, close to the burner lip and continue to exist as the HAB increases in the premixed flame configuration. Two types of the diffusion flames in the co-flow mode are commonly used for PAH investigations: the normal diffusion flame (NDF) and the inverse diffusion flame (IDF). In the NDF configuration, the fuel is supplied through a central tube surrounded by the oxidiser in an annular ring. Here, the combustion products are formed in the centre of the flame and transported through the main reaction zone of the flame where they get significantly oxidised and carbonised thus minimising the amount of soot (and PAH) formed (Blevins *et al.*, 2002; Santamaría *et al.*, 2006). This makes the study of PAHs

difficult in the NDF configuration as the setup alters the combustion products as they form. However, in the IDF configuration, the oxidiser is supplied through the central tube and the fuel is passed through the annular ring. As a result, the combustion products are formed on the fuel-rich side of the reaction zone and convected away from the main reaction zone hence obviate significant oxidation and carbonisation (Blevins *et al.*, 2002; Santamaría *et al.*, 2006; Mikofski *et al.*, 2007). Thus, PAHs and soot formed in IDF are unaltered by its setup. In this regard, the IDF provides a good separation between the pyrolysis and oxidative process in the flames and as a result, produces relatively larger amount of PAH and soot compared to the NDF. Additionally, Dobbins (2007) compared nanoparticles (including PAHs) sampled from inverse diffusion flames and diesel engine exhaust and reported similarity in the chemical composition of both samples. Also, air staging technique which is employed in the primary combustion zones of many burner designs, often mimics the IDF structure more than the NDF structure (Ballester *et al.*, 1997; Shaddix *et al.*, 2005). Hence, the IDF configuration is more appropriate for the study of PAH formation and growth, and relevant to practical combustion devices.

2.3.2 PAH measurement techniques

Generally, detection of PAHs in flames are broadly classified into intrusive and non-intrusive diagnostics. The intrusive techniques involve the use of a probe to sample species from the flame for either online or offline quantitative/qualitative analysis while the non-intrusive technique utilises optical diagnostics (mostly laser-based) to obtain spatial, temporal and time-

resolved qualitative PAH information from the flame. A major difference between both detection methods is that the intrusive techniques perturb the flow field, temperature profile and the concentration profiles of the flame region under investigation while the non-intrusive ones do not. An experimental evidence of probe effects on quantities measured was provided in the study by Stepowski *et al.* (1981) that studied low pressure propane-oxygen flame. The authors compared the local OH concentration profiles obtained via LIF and sampling to understand perturbation effects (due to probe usage) in the flame. Their results showed that the concentration of OH in the preheat zone of the flame decreased when the quartz nozzle was introduced into the flame due to the probe taking away heat energy.

A brief discussion on the most common techniques for both measurement techniques (or diagnostics) are presented below.

2.3.2.1 Intrusive detection techniques

- **Molecular beam mass spectrometry (MBMS)**

Flame sampling MBMS is an important tool used for the detection of stable intermediate species, resonant stabilised radicals and other hydrocarbons involved in the formation of PAHs in the flame (Hansen *et al.*, 2009). Sampling analysis by MBMS is popular for investigations in laminar low-pressure flames for studying the formation of benzene and PAH (McEnally *et al.*, 2006; Hansen *et al.*, 2009). By direct calibration, quantitative characterisation of molecules up to naphthalene has been achieved in literature (Bohm *et al.*, 2000; Defoeux

et al., 2005) while for higher carbon molecules in the range $C_{20}H_x - C_{48}H_x$, characterisation has only been qualitative (Ahrens *et al.*, 1998).

The MBMS technique involves the extraction of the PAH species from the flame which can be achieved using a microprobe coupled with an online molecular beam extraction system. Generally, the extracted species are cooled down when passed through the small vacuum probes at high pressure which expands them supersonically into a region of lower pressure forming a molecular beam. Subsequently, the molecular beam is ionised through either electron-impact ionisation (EI), single-photon vacuum ultraviolet (VUV) or multi-photon ionisation (MPI) before they are analysed by mass spectrometry (MS) using either quadrupole mass filters or time of flight (TOF) devices (Hansen *et al.*, 2009). Though EI has been widely applied in flames, it has low sensitivity and selectivity (Qi and McIlroy, 2005). To avoid this limitation, the resonance enhanced multiphoton ionisation (REMPI) was preferred as a better choice for measuring PAHs with the additional capability of separating the isomers due to its resonant feature especially for non-sooting flames. This was confirmed by Kamphus *et al.* (2008) who studied formation of small PAHs in laminar premixed low-pressure propene and cyclopentene flames using MBMS coupled with EI and REMPI consecutively. They reported improved measurement sensitivity and selectivity with the REMPI method. Additionally, Li *et al.* (2009) in their experimental study of low pressure fuel-rich toluene showed that the sensitivity and uncertainties of measurements using VUV from synchrotron sources or laser frequency generated radiations are similar to REMPI. Further details of this method can be found in Ref. (Qi, 2013).

The main challenge with MBMS analysis is quantifying the PAH concentration profiles especially the intermediates of larger aromatic species due to their characteristic low vapour pressure. Increased uncertainties have been reported in literature as a result of the difficulty in the internal calibration of species due to the temperature variation between the calibration concentration and extracted PAH concentration (Ahrens *et al.*, 1998; Kohse-Höinghaus *et al.*, 2002; Kamphus, Braun-Unkhoff and Kohse-Höinghaus, 2008).

- **Gas Chromatography – Mass Spectrometry (GCMS)**

This method is similar to the MBMS as both involve sampling with quartz microprobe and coupling to a mass spectrometer. The difference between both techniques is in the sampling methodology. Here, the PAHs from particulates are trapped in XAD-2 or XAD-4 adsorbent/resin and subsequently extracted using either the accelerated solvent extractor (ASE) as in Ref. (Dandajeh *et al.*, 2017a) or the classical widely employed Soxhlet extraction method (Prado *et al.*, 1984). The extraction is done with various solvents including methylene chloride, methanol and dichloromethane for the recovery of PAH compounds. The extracted PAHs are then analysed with the GCMS for quantitative and qualitative PAH information with standard calibration. This method is used for analysis in open flames (Prado *et al.*, 1985), reactors (Dandajeh *et al.*, 2017b) and IC engines (Barbella *et al.*, 1990; Fleurat-Lessard, Pointet and Renou-Gonnord, 1999; Gong, Hochmuth and Weatherburn, 2003). The possibility of PAH loss due to the different steps involved in the transfer of extracted PAHs before analysis presents a major disadvantage for this method particularly for the offline mode as commonly used for engine analysis. However, in open

flames direct analysis can be achieved in an online mode to reduce the PAH loss as demonstrated in Ref. (Senkan and Castaldi, 1996).

- **Jet cooled laser induced fluorescence (JC-LIF)**

This method was developed by Mercier *et al* (2008) utilising flame extraction using axially oriented thin quartz microprobe (see Figure 2.3). The extract is sent into a jet-cooled analysis chamber through a nozzle designed to promote isentropic expansion of the free jet. The laser induced fluorescence technique (LIF) is used immediately thereafter to image the species under cooled/supersonic condition and record the spectra. Under this condition (that is, low temperature and pressure conditions), the authors concluded that the vibronic spectra of the molecules became structured and simplified which reduced the possibility of electronic transitions, thus allowing selective detection of the PAH species using LIF (Wartel *et al.*, 2010). Additionally, the very low quenching efficiency of the LIF signals inside the jet, makes it possible to relate the population of the probed PAH species to the LIF signals and hence determining absolute concentrations is possible by internal calibration using known concentration of PAH samples (small known concentration is added to the sampled PAH). Sensitivity of the JC-LIF under sooting conditions for pyrene flames has been reported to be in the parts per billion (ppb) range with $\pm 10\%$ uncertainty (Wartel *et al.*, 2011). Applications in sooting and non-sooting methane flames for different equivalence ratio for profiles of the mole fraction of pyrene, naphthalene and benzene are captured in the following Refs. (Mercier *et al.*, 2008; Wartel *et al.*, 2010, 2011). In comparison with MBMS, JC-LIF possess the advantage of simplistic experimental set up with

quantitative measurement of important PAHs in real time with good sensitivity including sooting flames (Desgroux, Mercier and Thomson, 2013). However, this method can only measure a single stable species at a time due to the calibration routine.
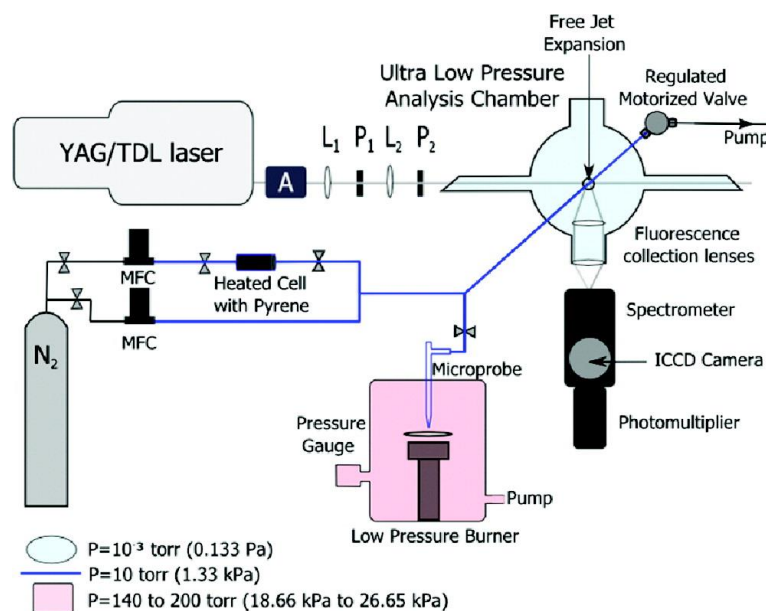
Figure 2.3: Experimental setup for the Jet cooled LIF measurements (Wartel *et al.*, 2011)

2.3.2.2 Non-intrusive detection techniques

- **Laser-Induced Fluorescence (LIF)**

Due to the high absorption coefficient and quantum yields (fluorescence efficiency) of PAHs, detection with lasers is possible even at low concentration (ppb or ppm order) (Crosley, 1981; Mercier *et al.*, 2008). However, PAHs exhibit broadband excitation and emission characteristics at flame conditions, hence individual characterisation of the distinct PAH species is not possible yet with LIF technique only. Therefore, a PAH LIF signal represents

51

fluorescence from a mixture of PAH species in different ring sets. Even though the information obtained from PAH-LIF measurements are qualitative, it remains the only method for non-intrusive PAH investigation to obtain spatially and temporally resolved information in turbulent and laminar conditions in flames.

Most PAH molecules absorb strongly over a wide range of excitation wavelengths from UV to visible with the corresponding emission wavelength dependent on the number of aromatic rings possessed by the PAH molecule (Singh and Sung, 2016). Furthermore, emitted PAH LIF spectra are influenced strongly by variations in temperature and concentration of the species in the measurement volume hence determination of the concentration of individual PAH species from the LIF signal is not trivial. Therefore, when PAHs are excited especially in the UV range, the LIF signal obtained collectively represents a mixture of PAHs which are grouped by size range using optical filtering according to their emission spectra signatures (and detection wavelength range). The emission wavelength of PAH increases with increasing number of aromatic rings. Vander Wal *et al.* (1997) reported that with excitation wavelength below 300 nm, PAH with 2 or 3 aromatic rings can fluoresce between 300-350 nm while PAHs of 4 rings or more can exhibit fluorescence in the range 300-700 nm. More specifically, investigations in Refs. (Wu *et al.*, 2006; Verhoeven *et al.*, 2013) attributed PAH fluorescence in the visible range of 400 – 480 nm to larger PAHs of 3 to 5 rings and most small PAHs (1-2 rings) attributed to fluorescence emissions in the UV range of 300 – 380 nm. The temperature dependence of PAH LIF signal occurs as a result

of collisional quenching and the Boltzmann population fraction (Eckbreth, 1996). Since, there is yet no data in literature detailing the variation of PAH quenching characteristics with temperature in the range of interest (Smyth, Shaddix and Everest, 1997; Xiao, Austin and Roberts, 2005), a few reasonable assumptions can be made to simplify the analysis of PAH LIF signals. For example, the quenching characteristics and the Boltzmann constant can be assumed constant if the temperature variation of all the flame conditions studied is not significant (Mulla *et al.*, 2016). Furthermore, if the PAH rings set in focus is not wide apart (say for 3 to 5 rings), it can be reasonably assumed that the absorption and emission spectral characteristics is largely similar (Eckbreth, 1996). Further details on the absorption and fluorescence bands of a number of PAH molecules of different sizes can be found in Refs. (Petarca and Marconi, 1989; Bejaoui *et al.*, 2014)

In sooting conditions, soot incandescence interferes with the LIF signal as seen in Refs. (Vander Wal, 1997; Shaddix *et al.*, 2005) and hence care has to be taken to ensure accurate separation of both signals. Various schemes have been proposed to solve this problem. First, is the two-wavelength laser induced incandescence (LII) method using excitation wavelengths at 532 nm and 1064 nm. The 1064 nm excitation captures only soot incandescence, while PAH and soot signal coexist in the signal when the 532nm excitation is used. Then the PAH-LIF signal is obtained from a simple subtraction between both signals (Moreau *et al.*, 2004). Another solution is to employ the delayed LII measurement technique using the 532 nm excitation taking advantage of the longer decay time for LII signal with respect to PAH-LIF signals (typically 50

53

ns decay time) to differentiate PAH contributions from soot (Geitlinger *et al.*, 1998; Shaddix *et al.*, 2005) if the interest is in the LII signal. But if the desired signal is the PAH LIF, prompt detection is employed. This involves capturing the PAH PLIF signal just as the laser excites the PAH molecules in the flame using low fluence levels (Singh and Sung, 2016). Even though excitation schemes in the visible range at 460, 488, 514 and 563 nm utilising argon lasers/dye laser were reported in literature (Miller, Mallard and Smyth, 1982; Beretta *et al.*, 1985; Petarca and Marconi, 1989) for the detection of large PAHs, the UV excitation scheme (around 248 and 283 nm) is preferred as it favours simultaneous imaging of OH (useful for temperature related information in the flame) and PAH species (Smyth, Shaddix and Everest, 1997; Hayashida *et al.*, 2006).

Several studies have employed the LIF technique in the study of PAH in open flames. Liu *et al.* (2018) studied the effect of doping laminar gasoline NDF with various alcohols (methanol, ethanol and n-butanol) on PAH growth characteristics using planar laser-induced fluorescence (PLIF). They observed that increasing the alcohol ratio decreased PAHs monotonously with methanol identified as the most significant in inhibiting the PAH growth process. Also, Yamamoto and Takemoto (2013) studied PAH formation in a propane IDF using PAH LIF and GC-MS techniques. They concluded that PAH LIF signals compares well with the benzene and naphthalene concentrations obtained from GC-MS measurements in their study. Additionally, Vander Wal (1998) utilised combined LIF-LII to observe distributions of both PAH and sooting regions within a droplet flame and a steady state C_2H_4 IDF/NDF flame

respectively. Other studies on PAH PLIF in IDF configuration can be found in Ju, Oh and Shin (2005), Mikofski *et al.* (2006), Shaddix and Williams (2009), Yamamoto and Takemoto (2014). Hence, literature shows that the LIF technique is well suited for the study of PAH formation in diffusion flames.

2.4 PREVIOUS WORKS ON THE EFFECTS OF BINARY FUEL MIXTURES ON PAH FORMATION

Since PAH has been established as a key precursor to soot formation, understanding its formation and the underlying growth mechanisms are key to the success of the research efforts towards reducing particulate emission and meet the increasing stringent regulations by governmental agencies. As a result, several studies have investigated PAH formation in different binary fuel mixtures to investigate fuel composition effects on PAH formation and build reliable data of key reactions (and their kinetics) for accurate numerical modelling of PAH formation, growth and oxidation in hydrocarbon combustion (Wang and Frenklach, 1997). This has improved the understanding of the role of fundamental factors (such temperature, residence time) towards the influence on PAH growth and hence revealed strategies which can be exploited for the reduction of PAH formation in practical combustion devices. In this section, the relevant literatures on this subject (effects of binary fuel mixtures) are reviewed under two headings: binary mixtures with chemically reacting fuels and those with non-reacting fuels. Subsequently, synergistic effects observed due to the interaction between different fuel molecules in binary mixtures have been discussed.

2.4.1 Effects of binary mixtures with chemically reacting fuels on PAH formation

Researchers have studied the effects of adding H_2 to hydrocarbon fuels on PAH formation and growth. This interest stems from H_2 being a clean and sustainable energy carrier, and has shown promise for the improvement of combustion properties and reduction of pollutant emissions when blended with hydrocarbon fuels for combustion (Wang *et al.*, 2019). In their numerical study of H_2-C_2H_4-Air diffusion flames, Guo et al. (2006) reported a reduction in PAH growth rate with addition of up to 24% H2. This reduction was attributed to the higher concentration of H_2 molecule closer to the burner lip and lower H atom concentration in the surface growth regions which lowers the abstraction rate of PAHs. They also observed that for a given condition of H_2 addition, the combined effect of high temperature, higher concentration of benzene (first aromatic ring) and acetylene enhanced PAH growth rate as the height above the burner (HAB) increased resulting in higher concentration of pyrene at higher heights. Liu *et al.* (2014) studied numerically the effect of adding H_2 to the fuel stream of CH_4 diffusion flames on PAH formation. They observed a reduction in the mole fraction of PAHs (both benzene and pyrene) with the addition of 30% by volume of H_2 for all the HAB considered. Du et al. (1995) investigated the effects of adding various additives including H_2 to counterflow diffusion flames of C_2H_4, C_3H_8 and $n-C_4H_{10}$ on soot formation. They used the local velocity gradient to determine the characteristic soot inception rate (relevant to PAH growth) and laser line extinction measurement for soot volume fractions (SVF). Their results showed that although H_2 addition

increased the flame temperature consistently, the sooting inception limits and SVF reduced for all conditions. They attributed this effect to the following reasons: (a) the preferential diffusion of H_2 in strained counterflow diffusion flame (CDF) possibly reduced the concentration of soot precursors (PAH) thereby reducing the soot formation rate, (b) H_2 addition reduces the carbon supply of the main fuel and (c) increased concentration of H_2 in the mixture reverses the H abstraction reaction of the HACA mechanism ($A_i + H \leftrightarrow A_i^- + H_2$) thus limiting the involvement of the aromatic radical in further mass addition reactions and consequently, reducing the concentration of PAHs available for further growth to soot. Do *et al.* (2021) studied the influence of H_2 as a fuel additive on the soot nucleation process in a laminar atmospheric premixed CH_4 flame using JCLIF and GC-MS. The authors replaced 10% of N_2 in the oxidiser with same amount of H_2 and observed that the peak mole fraction of PAHs (C_6H_6, naphthalene ($C_{10}H_8$) and pyrene ($C_{16}H_{10}$) were reduced significantly (about 26%, 58% and 76 % for C_6H_6 , $C_{10}H_8$ and $C_{16}H_{10}$ respectively). The authors explained that adding H_2 in the oxidiser contributed only to increase the concentration of O and OH while reducing the amount of H atoms available for further PAH growth. They suggested that this accelerated the oxidation processes of PAHs which resulted in the overall reduction of peak PAH mole fractions. Also, their results showed that soot particle nucleation process only initiated when the concentrations of C_6H_6, $C_{10}H_8$ and $C_{16}H_{10}$ were 16 ppm, 1 ppm and 22 ppb for all studied flames. The authors suggested that these values might be the controlling concentration for the inception of soot particle formation. Xu *et al.* (2020) studied the effect of H_2 addition on soot formation in counterflow diffusion flame (CDF) of C_2H_4 and

CH_4 using LII. They reported that with up to 20% H_2 addition (v/v), the soot volume fraction (SVF) reduced in both C_2H_4 and CH_4. With C_2H_4, the authors attributed the reduction in SVF to the chemical inhibition of PAH growth and soot inception process with H_2 addition. But with CH_4, the authors explained that the reduction in SVF could be as a result of increased concentration of H radicals which impeded the formation of C_3H_3 and consequent reduction in the formation of C_6H_6 formation and soot inception rate. Additionally, their results showed that the effect of H_2 addition in only CH_4 was dependent on the mole fraction of O_2 in the oxidiser. Furthermore, Wang et al. (2020) studied numerically and experimentally the effect of adding H_2 to C_2H_4 on soot formation in a laminar co-flow diffusion flame. The oxidiser was in the ratio of 30% O_2 − 70% CO_2 to typify conditions relevant to oxygen-enriched combustion technology like exhaust gas recirculation and flue gas recirculation. The authors used CoFlame code coupled with an extended ABF mechanism and 2D-line of sight attenuation (2D-LOSA) for the study respectively. Their results showed that with addition of up to 50% H_2 (v/v), the total soot loading was suppressed for all flames investigated for both numerical and experimental campaign. The authors attributed this to the increase in the mole fractions of H and H_2 which resulted to a corresponding reduction in the mole fraction of C_3H_3 (identified as the dominant PAH and soot formation pathway for their study) and consequently reduction in PAHs and soot nucleation. The authors also suggested that reductions in the total soot loading could also be linked to the chemical coupling effect between H_2 and CO_2 additions which further reduced the soot nucleation rate and surface growth reactions.

The effect of addition of other hydrocarbon fuels (including liquid fuels) on PAH and soot formation have also been studied. Golea *et al.* (2012) conducted a 1-D modelling study whereby ethanol was added to benzene premixed flame to study the effect of oxygenated fuels on PAHs. The authors reported a decrease in PAH concentration with increase in the volume of ethanol in the mixture. This effect was attributed to the reduction in the concentration of acetylene and propargyl which are key species for the formation of PAH. Both species decreased with increase in the volume of ethanol in the mixture. They concluded that since all the PAHs in their study were formed from the phenyl radical, which in-turn was formed due to H abstraction from benzene, the mechanism of PAH reduction could be that the ethanol merely diluted the sooting benzene in the mixture without influencing its combustion chemistry. More explanations on the PAH reduction mechanism with the addition of ethanol was provided by Wu *et al.* (2006) in their study of fuel rich C_2H_4 premixed flat flame doped with ethanol for equivalence ratios ($\emptyset$) of 2.34 and 2.65 using PAH LIF and PREMIX flame code calculations. Ethanol was shown in their results to influence the formation of larger PAH species more than the smaller PAHs especially at $\emptyset = 2.34$. In agreement with the trends reported by Golea et al. (2012), the experimental results from the study by Wu et al. (2006) also indicated that increase in ethanol percentage reduced PAH concentration. The authors suggested from their numerical results, that ethanol affects PAH formation via two routes: first, it can decompose via two steps (involving the breakage of the $C - O$ bond) to form C_2H_4, CH_3 and carbon monoxide (CO). Both C_2H_4 and CH_3 subsequently undergo additional reactions leading to the formation of various precursor species. Secondly, ethanol is capable of

59

undergoing H abstraction at three different sites to form radical species that reacts further to form aromatic species and carbon monoxide (CO). For both cases, the authors removed all ethanol-bound carbon capable of contributing to the formation of CO from the reaction pathway leading to PAH formation in the model. This is because the strength of the triple bond in CO hinders its contribution to the formation of PAHs as also noted by Curran *et al.* (2001). They showed via a carbon flow analysis that only 5% of the carbon participated in the propargyl formation (which was reported as the primary route to the formation of the first aromatic ring in ethanol flames), and hence concluded that ethanol addition reduced PAH formation by starving the process of carbon participating in the formation of the precursor particles. Similar mechanism of carbon starvation was reported by Wu *et al.* (2006) as the reason for the reduction in PAH concentration in the premixed C_2H_4 flame with the addition of dimethyl ether (DME) employing the PAH-LIF technique.

Yan *et al.* (2019) studied formation of PAH and soot in C_2H_4 counter flow diffusion flames (CDF) doped with ethanol and methanol respectively using LIF and LII techniques. They observed that though both ethanol and methanol are clean fuels, they produced opposite effects on PAH and soot formation when added to C_2H_4 diffusion flame; while methanol reduced the concentration of PAH/soot monotonically, the addition of ethanol produced a non-monotonic effect on PAH/soot formation. The authors offered the following explanation for the contrasting effects: methanol decomposed primarily to carbon mono-oxide (CO) while enhancing the formation of H_2 via H abstraction in the intermediate steps. The combined effects of dilution by CO and chemically

suppressing incipient benzene ring formation by H_2 reduced the formation of PAH and soot in methanol doped C_2H_4 flame. But ethanol decomposes to produce increased concentration of methyl radicals which enhanced the C_3H_3 recombination reaction known for promoting growth of large size PAHs and consequently increase soot formation. For both cases, the results from the chemical kinetic analysis showed that the effect of addition of either ethanol or methanol on the formation of benzene ring propagated the growth rate of larger size PAH concentration (e.g pyrene) using the HACA-based mechanism of PAH growth. Lemaire *et al.* (2013) utilised two-colour LII/LIF to study PAH and soot formation characteristics when rapeseed methyl ester (RME) is added to commercial diesel using a spray burner and reported about 36% reduction in PAH LIF signal intensity and 44% reduction in total soot yield with 30% addition of RME to the diesel. Hwang *et al.* (1998) studied the effects of adding oxygen (O_2) on PAH and soot formation in counterflow C_2H_4 flames using PAH LIF and laser extinction techniques respectively. The authors reported that the addition of small amount of O_2 in C_2H_4 increased PAH and soot formation. This was attributed to the increase in C_3 species via C_3H_3 recombination reactions. The authors explained that in the soot inception zone, oxygen atom (from the added oxygen gas) reacts with C_2H_2 which is the most abundant species in the flame reaction zone to form methylene radicals (CH_2) which undergoes further reactions to form C_3H_3 as shown through these two key steps: $C_2H_2 + O \rightarrow CH_2 + CO$ and $C_2H_2 + CH_2 \rightarrow C_3H_3 + H$. Thereafter, C_3H_3 formed undergoes self-recombination reactions to form benzene, thus enhancing incipient ring formation.

Most conventional fuels and natural gases utilised in practical combustion systems are complex fuel mixtures (Sarathy *et al.*, 2015). The component fuel molecules in these mixtures play an important role in determining the sooting tendency (soot volume fraction, soot particle size and PAHs) of these practical fuels (Wang and Chung, 2019). As a result, some studies have represented these fuels by mixing hydrocarbon fuels to understand the effects of fuel composition on the formation of PAHs and soot (Roesler *et al.*, 2003; Trottier *et al.*, 2007; Park *et al.*, 2017; Wang *et al.*, 2018; Yan *et al.*, 2019). Additionally, these studies have shown that chemical interactions between various molecules in binary/ternary mixtures reveal kinetic pathways which provide insight to some complex processes of PAH and soot formation mechanisms which are elusive with single component fuel investigations (Wang and Chung, 2019).

A major observation from these studies is the synergistic effects on PAH/soot formation as a result of mixing various hydrocarbon fuels together. Synergistic effect refers to the case where the PAH concentration formed from the combustion of the binary fuel mixture is higher than that of the pure fuel. This synergistic effect due to binary mixtures has been observed in various works (Hwang, Chung and Lee, 1998; Roesler *et al.*, 2003; Yoon, Lee and Chung, 2005; Trottier *et al.*, 2007; Yoon, Anh and Chung, 2008; Liu *et al.*, 2011; Park *et al.*, 2017). These are briefly reviewed next:

Park *et al.* (2017) studied the effects of fuel composition on PAH and soot formation in counterflow diffusion flames of gasoline surrogates using LIF, laser induced incandescence (LII) and chemical kinetic modelling. Their work

focused on binary mixtures of *n*-heptane/*iso*-octane, *n*-heptane/toluene, *iso*-octane/toluene and ternary mixtures of *n*-heptane/*iso*-octane/toluene. For the binary mixtures with toluene, the authors observed a synergistic effect on PAH formation with increasing toluene ratio. They explained that benzyl radicals from the dehydrogenation of toluene was key to the synergistic effect on PAH concentration observed. Roesler *et al.* (2003) investigated binary mixtures of CH_4 and *n*-heptane in premixed flames, and CH_4/C_2H_4 mixtures in co-flow diffusion flames and flow reactor. They obtained detailed PAH speciation with gas chromatography (GC) coupled with flame ionisation detector (FID) and mass spectrometry (MS) while soot volume fraction was achieved with LII. The authors observed that the addition of CH_4 in C_2H_4 increased the formation of PAH and soot in the reactor and co-flow diffusion flame while no increase was seen for the premixed flame of CH_4/*n*-heptane. Methyl radicals from CH_4 were implicated as being responsible for the synergistic effect on PAH in binary mixtures of CH_4/C_2H_4 in the diffusion flame and reactor, which the authors claimed enhances PAH formation and growth from the propargyl recombination reaction (odd-carbon numbered species). Liu *et al.* (2011) investigated the effect of DME addition to C_2H_4 diffusion flame on PAH and soot formation using PLIF and LII respectively. Also, they observed a synergistic effect on PAH and soot as the volume of DME in the binary mixture increased and attributed it to increase in methyl radical concentrations produced from the dissociation of DME which enhanced the formation of PAH. Hwang *et al.* (1998) studied PAH and soot formation characteristics in a binary mixture of C_2H_4 and C_3H_8 in both counterflow and co-flow diffusion flame configurations to isolate the flow and flame structure effects. PAH LIF and laser

63

extinction techniques were utilised for the measurements of PAH concentration and soot volume fractions. Their results showed that the addition of small amount of C_3H_8 to C_2H_4, the PAH LIF signals and SVF increased significantly for both flame configurations even though the concentration of C_2H_2 and adiabatic temperature were lower for all mixtures. This was attributed to the role of C_3H_3 recombination reactions in the formation of incipient PAH ring and its subsequent growth. However, at certain propane ratios in the mixture, the authors observed a complementary role between the C_3H_3 radical and C_2H_2 for further growth of PAH to soot particles. They concluded that the while C_3H_3 is important for incipient ring formation in these mixtures, C_2H_2 addition via the HACA mechanism remains relevant for further PAH growth to soot particles. Yoon *et al.* (2005) investigated the synergistic effects on PAH and soot formation when each of CH_4, C_2H_6, C_3H_8, and C_3H_6 were mixed with counter-flow C_2H_4-base diffusion flame using PAH-LIF, LII (for SVF) and numerical simulations. They observed that small additions of C_2H_6 or C_3H_8 to C_2H_4 significantly increased the PAH LIF and LII signals when compared with the signals from either the ethylene base fuel or the C_2H_4/C_3H_6 mixture. This was attributed to the increased formation of propargyl radical (C_3H_3) that enhanced incipient ring formation. Using their numerical results, the authors proposed a possibility that the dominant role of methyl radical (CH_3) generated from the thermal decomposition of C_2H_6 and C_3H_8 in the low temperature region is a valid explanation for the formation of C_3H_3 which caused the observed synergistic effects. Yoon *et al.* (2008) studied the synergistic effects on PAH formation in mixtures of dimethyl ether (DME) with CH_4, C_2H_6, C_3H_8 and C_2H_4 in counter-flow diffusion flame configuration using LIF technique and

numerical calculations. The addition of DME to C_2H_4 was reported to increase PAH formation but reduced PAHs when added to CH_4, C_2H_6, and C_3H_8. This increase referred to as the synergistic effect was attributed to the combinatory role of C_3H_3 self-recombination reactions and high concentration of C_2H_2. The authors explained that numerical calculations showed that DME flames produce less amount of O radicals and significant amounts of CH_3 and subsequently C_3H_3 in the low temperature region where PAH formation prevails. Additionally, the effectiveness of DME addition in enhancing PAH formation was shown to depend on the concentration of C_2H_2. Hence, they concluded that the observed synergistic effect on PAH formation was governed mainly by the role of CH_3 but also depends on the amount of C_2H_2 in the low temperature region where PAH forms.

2.4.2 Effect of binary mixtures with non-reacting fuels on PAH formation

Zhang *et al.* (2018) studied the effects of adding CO_2 and water vapour on PAH formation in laminar premixed ethylene-oxygen-argon flames using laser induced fluorescence (LIF) and kinetic simulation. They observed a monotonic decrease in PAH LIF intensity as the addition of both CO_2 and water vapour increased with water vapour showing better effectiveness in PAH reduction than CO_2 . The authors reported that the addition of CO_2 increased the backward reaction rate of $CO + OH \rightleftharpoons CO_2 + H$, hence decreasing the concentration of H radical and increasing the OH radical concentration. Similarly, the addition of water vapour increased the backward reaction rate of

$OH + OH \rightleftharpoons O + H_2O$ and $CH_3 + OH \rightleftharpoons CH_2{}^* + H_2O$ resulting in increased formation of OH radical. The authors attributed the reduction in PAHs to this increase in OH radical (enhanced oxidation rate) and depletion of H radical (reduced H abstraction rate). Oh and Shin (2006) studied the effect of adding CO_2 to the oxidiser (O_2) in a co-flowing C_3H_8 non-premixed flame on soot formation. Time-resolved laser induced incandescence (TIRE-LII) and TEM photography were used to measure soot volume fraction, primary particle size, primary particle number concentration (relevant to the soot inception region). They also estimated the specific soot growth rates from the plot of soot particle diameter and time. In the inception region (relevant to PAH growth and condensation), their results showed that with the addition of CO_2, the primary particle size and the soot volume fraction decreased while the primary particle number concentration increases. This was attributed to the reduction in flame temperature, dilution of reactive species and direct chemical effect due to the presence of CO_2. They also observed that the addition of CO_2 had no significant effect on the estimated specific soot growth rates; the estimated soot growth rates only showed a dependence of about 20% on the concentration of O_2 in the oxidiser. McEnally and Pfefferle (2000) studied the effect of adding N_2 to laminar non-premixed CH_4 and C_2H_4 flames on the formation of propyne (C_3H_4) and benzene (C_6H_6). The authors extracted the gas samples with a quartz microprobe and used photoionisation/time of flight mass spectrometry to detect and analyse centreline profile concentrations of C_3H_4 and C_6H_6. Their results showed a reduction in maximum centreline concentrations of both species with increase in N_2 volume flow rate. The authors explained that increase in the level of N_2 in the fuel stretch the profile

towards the flame tip leading to an increase in the residence time available for the diluents to interact with the species and consequently, decreasing the maximum concentrations of C_3H_4 and C_6H_6. Sirignano and D'Anna (2020) studied the effect of CO_2 addition to the oxidiser on PAH and soot formation in a C_2H_4 counterflow diffusion flame (CDF) using LIF, LII techniques and chemical kinetic modelling. The authors reported that with the addition of up to 78% CO_2 (v/v), reduction in soot particles are more significant compared to those of PAHs. This was attributed to the thermal effect (temperature reduction) induced as a result of CO_2 addition since the soot particles are formed mainly in the high temperature region of the flame. Using the modelling results, the authors explained that though a chemical effect of CO_2 addition cannot be excluded as the reason for the reductions observed, it seemed less significant when compared to the effect produced in their result due to reduction in temperature (thermal effect) as a result of CO_2 addition.

2.5 SUMMARY

The following conclusions can be reached from the literature survey:

- PAHs are formed initially in the gaseous phase at high temperatures but begin to transform into the solid phase as the temperature reduces via condensation. PAH molecules from the vapour phase are also capable of adsorbing onto the matrix of another solid particle (such as exhaust soot particles) depending on the difference in vapour pressure between both structures. This attribute makes it possible for PAHs to

function as precursors to soot formation as well as get adsorbed onto the matrix of the soot particle.

- Formation of the first aromatic ring (benzene) has been identified as the important step in the series of reactions leading to the formation of larger PAHs and consequently soot formation. Thus, highlighting the importance of the study of PAH formation and growth in the efforts to reduce pollutant emission (soot formation).

- The formation and growth of PAHs have been proposed to follow various mechanisms including the HACA, MAC, PAC, and PAH dimerisation. The hydrogen atom (H atom) has been shown to be a key species in the reactions involved in most of these named mechanisms.

- Various open flame configurations have been used to study PAH formation including premixed flames, normal diffusion, and inverse diffusion flames. However, the inverse diffusion flame configuration was shown as well suited for fundamental study of PAH formation as its set-up enables a separation of the pyrolytic reactions from the oxidation reactions within the flame. Hence, the PAHs formed are not altered by the flame set-up.

- A variety of techniques, both intrusive and non-intrusive, have been employed for the study of PAH formation and growth in open flames. The intrusive methods involve physically probing the flame with a quartz microprobe to extract gas species (or samples) and subsequently analysing these samples using techniques such as MBMS or GCMS. The non-intrusive methods are mainly optical diagnostics which involve the use of laser devices to study the flame for the desired species at the

right wavelength. The fluorescence from the excited species (due to the energy from the laser probe) are optically filtered and subsequently detected using ICCD cameras. These non-intrusive techniques have an added advantage of providing good spatial resolution.

- The reduction in the formation of PAHs (and soot) has been investigated using various strategies including the addition of reactive gases (e.g., H_2, O_2, etc.), non-reactive gases (e.g., CO_2, N_2, etc) to primary hydrocarbon fuels. Additionally, binary/ternary hydrocarbon mixtures have been employed to study fuel compositional effects on PAH formation. The interaction between the fuel molecules in some of these binary/ternary hydrocarbon fuel mixtures revealed the existence of synergistic effects on PAH/soot formation. Synergistic effect refers to the case where the PAH concentration formed from the combustion of the binary fuel mixture is higher than that of the pure fuel.

2.6 GAP ANALYSIS

The review of literature covering the proposed growth mechanisms for the formation of the first aromatic ring (benzene), subsequent growth to larger PAHs and then to soot particles shows that the hydrogen atom (H atom) through various dehydrogenation processes is a key species in these mechanisms. Despite this, most studies in literature have focused on investigating the effect of adding H_2 on soot formation. However, PAH has been established as a key precursor to soot formation and some numerical studies have suggested that setting up the PAH section of soot formation models is key in achieving good agreement between numerical and

experimental results (Chernov *et al.*, 2014). Additionally, to the best of the author's knowledge there had been no previous extensive study of the effects of H_2 addition on PAHs (or PAH LIF) in inverse diffusion flames. Therefore, it is more beneficial to understand the effect of H atom via H_2 addition on PAH formation in simple hydrocarbon fuels such as CH_4, C_2H_6 and, C_2H_4 using the inverse diffusion flame configuration (due to the advantages over other flame configurations outlined previously in section 2.3.1). Of these simple hydrocarbon fuels, it is important to put more emphasis on CH_4 for the following reasons: firstly, CH_4 is a major component of natural gas. Natural gas is an important fossil fuel because it contributed a significant one-third of the total energy demand in the last decade (IEA, 2020). Secondly, CH_4 is a key component of biogas which is a renewable fuel and lastly, CH_4 is the second largest contributor to greenhouse gas emissions after CO_2 (USEPA, 2020). Therefore, additional emphasis on CH_4 is justified as its usage concerns the present efforts to reduce dependence on the use of fossil fuels (through H_2-enriched natural gas), and contribution to the renewable fuel sources (through biogas).

The review of literature on binary hydrocarbon fuel mixtures clearly shows that fuel composition plays an important role in PAH, and subsequently soot formation and growth. Most studies present these effects as a general trend of PAH response as height above burner increases. This approach could shroud key information that would aid better comparison between hydrocarbon fuels with different molecular structures. For example, C_3H_6 will form more PAHs than CH_4 in terms of the concentration as HAB increases because of its

molecular structure and carbon content (lower H:C ratio). However, is it possible to reach a point where PAH formation in both hydrocarbon fuels match (i.e., can the growth rate of PAH be controlled)? Or is the rate of growth comparable in both hydrocarbon fuels despite significant variation in magnitude of PAHs formed? To the best of the author's knowledge, no studies have made such comparisons based on the rate of PAH growth. Therefore, a more thorough understanding of the underlying mechanisms of PAH growth is needed for these fuels particularly when mixed with H_2. The addition of H_2 can be used to modify the H:C ratio of the fuel mixture hence allowing investigation of molecular structure effects on PAH formation. The comparison based on H:C ratios for hydrocarbon fuels is important as it could potentially help develop quantitative correlations between PAH growth and fuel molecular structure, which can then be applied to any hydrocarbon fuel. This is not only important for the effort to reduce PAH formation; it is also relevant to other industries, such as those that synthesise carbon nanotubes. Hence, there is need to understand the dependence of PAH growth on both PAH LIF signal (concentration) and the H:C ratios of different fuel mixtures. It is important to reiterate here that PAH growth rate as referred in this study concerns the rate of change in the PAH LIF signal along the flame front.

Soot formation has been shown in literature to be a complex process involving several reactions. Yet, the formation of first ring PAH has been consistently regarded in literature as the important step for soot formation and used for setting up soot models. However, with better methodologies and techniques available, it is important to revisit the question: Is first ring PAH (benzene)

71

formation the only important step for soot formation? There is evidence in literature that this might not be the case. The answer to this question would help broaden the approach to PAH formation and growth in both experimental and numerical studies. The comparison of PAH formation in hydrocarbon mixtures based on the rate of growth (as described in the previous paragraph) could be very helpful towards answering this question.

The specific objectives of this study are therefore:

- To set-up and optimise PAH PLIF system to detect 3-5 ring PAHs and use this system simultaneously with OH PLIF to get flame location.
- Understand the effect of binary fuel mixtures composed of varying levels of H_2 in C1-C3 hydrocarbon fuels on PAH formation and growth.
- Understand the effect of H_2 - enriched natural gas (simulated with CH_4) on PAH formation.
- Perform data reduction and image analysis to determine PAH growth rate in C1-C3 hydrocarbon fuels mixtures in relation to the flame front location.
- Estimate PAH growth rate function from the binary hydrocarbon fuel mixtures (involving H_2 and CH_4).
- Understand diluent effect of H_2 addition to hydrocarbon fuels on PAHs using control diluents.

CHAPTER THREE

3.0 EXPERIMENTAL METHODOLOGY

This chapter presents a description of the experimental apparatus and a general introduction of the flow configurations utilised in this work. The experimental techniques and the methodology employed for the image reduction and analysis in this work are also detailed in this chapter.

3.1 IDF BURNER FACILITY

Under this section, the inverse diffusion flame burner designed for this study is described. Also, the details of the flow meters and a general description of the flow conditions employed for this study are presented.

3.1.1 IDF burner design

The burner used for this study is based on Inverse Diffusion Flame (IDF) configurations described in Refs. (Blevins *et al.*, 2002; Mikofski *et al.*, 2006). The IDF configuration has been shown to be best suited for the study of PAH formation and growth due to the possibility of stratification of PAHs according to ring size as HAB increases (detailed in section 2.3.1) (Blevins *et al.*, 2002; Bejaoui *et al.*, 2014). The burner consisted of three coaxial stainless-steel tubes. The central tube for the oxidiser flow was surrounded by the inner and outer annular co-flows for the passages of fuel mixtures and nitrogen gas respectively. The inner diameters of the central tube, inner and outer co-flow tubes were 10, 30 and 64 mm respectively. To reduce the effect of rim thickness, the burner exit was tapered to a knife edge for all the three tubes.

Nitrogen gas was passed in the outer co-flow to shield the flame from ambient air conditions and hence minimise air entrainment effects. A combination of steel balls (of diameters 3 mm and 5 mm), wire mesh and honeycomb were utilised for flow smoothening and straightening of the co-flow gases. A sectional view of the burner is shown in Figure 3.1.
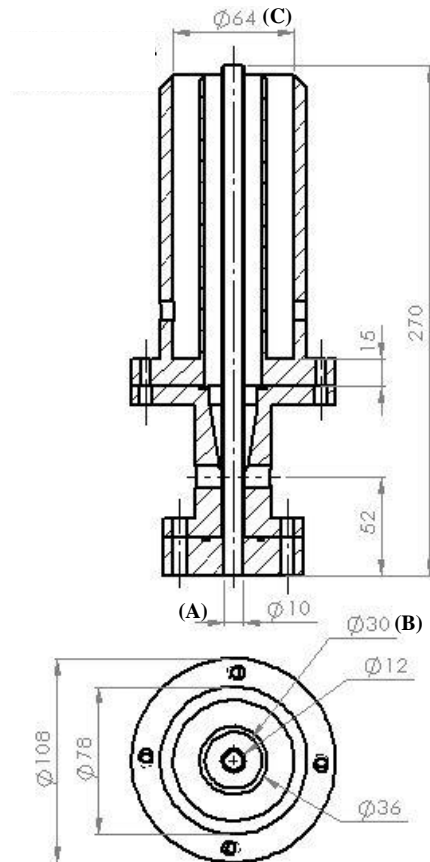
Figure 3.1: (a) Side and (b) top view cross sections of the inverse diffusion flame burner showing the inner and outer diameters of the central and inner and outer co-flow annular passages for the air (**A**), fuel (**B**), and nitrogen (**C**) respectively.

3.1.2 Flow measurement and flame conditions

The compressed air used for this study was supplied from a central system in the laboratory. It was filtered prior to entering the flow meter while the other

gases - methane (CH_4), ethane (C_2H_6), ethylene (C_2H_4), propane (C_3H_8), propylene (C_3H_6), hydrogen (H_2), nitrogen (N_2) carbon dioxide (CO_2), and argon (Ar) were CP grade gases with 99.99% purity procured from BOC, UK. Thermal mass flow meters from Vögtlin instruments and Bronkhorst flow meters fitted with high precision needle valves were employed for the control and measurement of all gas flows to the burner. The flow meters have an accuracy of $\pm$ 1.5% of the full-scale deflection (FSD).

Tables showing the details of the flow conditions for the flames investigated in this work will be presented in their respective result chapters for ease of reference. Hence, a general description is presented here. This study was conducted in three major parts.

First, the effect of H_2 addition to fuel on PAH formation characteristics was investigated in a CH_4 IDF flame. The level of H_2 was varied from 0% to 20% (v/v).

In the second part, two sets of experiment were done. In the first set, H_2 was added in varying percentages to each of the designated primary fuels (CH_4, C_2H_6, C_2H_4, C_3H_8, and C_3H_6) to study the effect of H_2 addition on PAH formation characteristics and also create a well resolved range of H:C ratio for PAH growth rate analysis which will be described later. For the second set of experiments, CH_4 was added to each of the primary fuels listed above. These two sets of experiments were used to investigate differences in PAH formation characteristics when H_2 is added as a molecule compared to when it is bound

to carbon in a hydrocarbon fuel (as in CH_4). The addition of CH_4 allowed a wider range of H:C ratios to be obtained for PAH growth rate comparison.

In the third part, the effect of diluents addition on PAH formation characteristics was investigated by separately adding N_2, CO_2, and Ar in varying percentages to CH_4, C_2H_6, and C_2H_4 consecutively.

In all the cases, the desired volumes of the secondary gases were premixed with the primary fuels reasonably far upstream (about 1400 mm) of the burner exit to ensure homogenous mixture and a fully developed flow is achieved.

3.2 LASER IMAGING SET-UP AND OPTICAL LAYOUT

Under this section, the laser system, imaging set-up and the optical arrangement utilised for this study is explained. The schematic for the laser and camera setup (including the optics) is shown in Figure 3.2.

3.2.1 Laser system

The PLIF technique was utilised for the simultaneous imaging of the OH and PAH species in this investigation. It is pertinent to note that the OH imaging in this study was to obtain the flame front for all the conditions tested, which was used later for the flame normal analysis (as described in section 3.4.1). To achieve this, two laser systems were employed – Nd:YAG laser and a tunable dye laser.

For OH radical excitation, a frequency-doubled output from an Nd: YAG laser $(Litron^{©}, Nano - PIV)$ was used to pump a tunable dye laser $(Fine\ Adjustments^{©}, Pulsare - S\ model)$ equipped with Rhodamine 6G dye. The fundamental wavelength output from the dye laser was frequency-doubled and tuned to near 283 nm to pump the Q1(5) transition of the $A^2\sum^+ \leftarrow X^2\prod$ (1,0) band with approximately $160\ mJ/cm^2$ laser fluence. This excitation wavelength/band was chosen because of its sensitivity to temperature (Kostka *et al.*, 2009). This is important for this study since the peak temperature region is denoted by the peak OH concentration and used to track the flame front for the analysis presented in this study (detailed explanation are presented in section 3.4). The laser beam was shaped (described in detail in section 3.2.1.2) into a laser sheet for planar measurement.

ICCD - Intensified Charge coupled device
FA – Filter A: UG11 + WG 305
FB – Filter B: BG 12 + GG 420
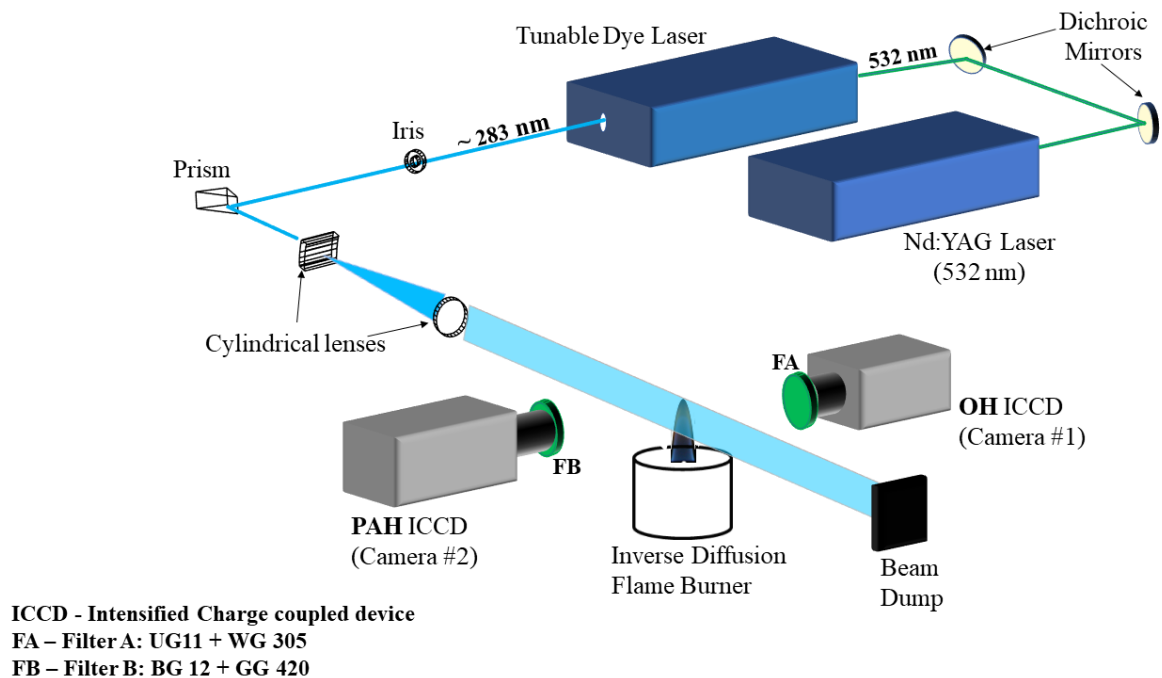
Figure 3.2: Schematic of the experimental arrangement used for simultaneous planar laser induced fluorescence imaging of PAH and OH.

PAH species were also excited with the same laser sheet described for the OH radical excitation to enable simultaneous OH-PAH measurements. Literature is replete with studies showing interferences from soot particles as a result of resonant radiation from laser induced incandescence on PAH LIF measurements in non-premixed flames (Vander Wal, 1997; Lee, Yoon and Chung, 2004; Xiao, Austin and Roberts, 2005; Singh and Sung, 2016). A soot isolation technique as described by Chakraborty and Chakravarthy (2018) was used to confirm the absence of soot interference in the region of interest for all the flames studied. The soot isolation technique involves imaging the flame using a colour DSLR camera fitted with a 650 nm bandpass filter and extracting the red pixel intensities from the RGB matrix. Thereafter, BG-3 filter is used to separately image the flame to obtain CO_2 emission and subtracted from the red pixel intensities obtained above. The resulting image is then approximated to the soot distribution in the flame (that is, representative of infrared radiation from the soot). As an additional step, the laser fluence level was maintained at a constant value of $160 \ mJ/cm^2$ for all other studies. This is similar to the strategy used in Refs. (Yoon, Anh and Chung, 2008; Singh and Sung, 2016) to obviate noise from soot incandescence.

3.2.1.1 Laser beam calibration

To obtain the OH transition indicated above, the OH spectra from the dye laser was calibrated with OH spectra from LIFBASE calculations (Luque and Crosley, 1999). A lean premixed methane flame ($\emptyset = 0.75$) was stabilised on the flat flame burner designed by Talibi (2011) and a triggered burst scan of the dye laser was employed between the wavelength range of 282.5 nm and

284.3 nm with a resolution of 0.0125 nm per scan to excite OH radicals in the flame. 20 PLIF images were captured per scan (which corresponds to a specific wavelength within the specified range). In the LIFBASE calculation, the same range of wavelength and resolution in the experiment were maintained. The system was set to thermalised and linear LIF regime was selected while keeping the fluorescence detection range to between 300 nm and 350 nm. The sum of the intensities in each averaged image per scan from the experiment was calculated with MATLAB and saved in a text file which was imported into LIFBASE software for comparison. Subsequently, the peaks of both spectra (experiment and simulation) were compared against the OH transition branch activated in the software to obtain the wavelength and transition band of the desired OH line (see Figure 3.3) for this work.
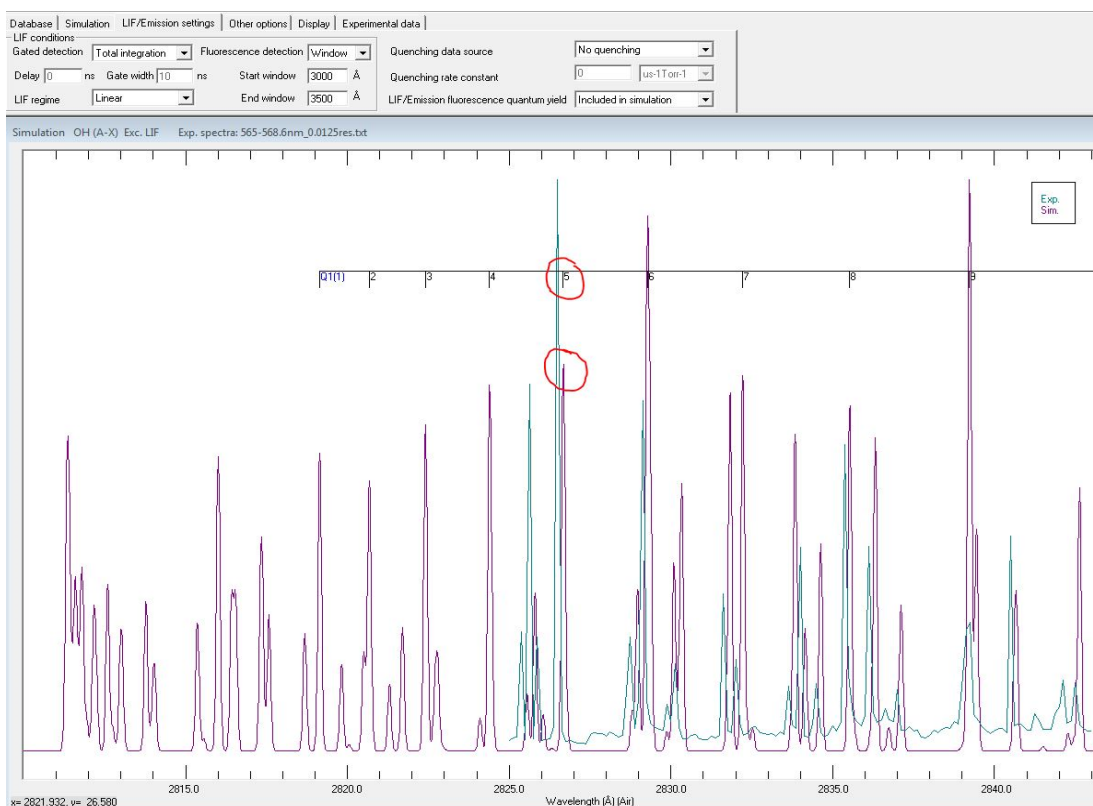
Figure 3.3: The comparison between OH spectra obtained in experiments and using LIFBASE simulations to obtain the desired OH transition - Q1(5)

3.2.1.2 Laser beam shaping

For simultaneous planar imaging of the OH and PAH species, the laser beam at the exit of the dye laser with diameter of approximately 6 mm was shaped into a laser sheet. This was accomplished with a combination of a right angle prism, plano-concave cylindrical lens (f = -40 mm) and bi-convex lens (f = 500 mm) converting the beam to a light sheet of height 50 mm and thickness of 150 μm determined by the scanning knife edge technique (Balachandran, 2005). The location of the sheet was adjusted to coincide with the central axis of the burner for all measurements.

The scanning edge technique involves placing a knife edge with its direction perpendicular to the laser sheet and gradually blocking sections of the laser sheet until the entire sheet thickness is covered. The energy of the laser sheet is measured for every movement of the knife edge (in microns) keeping the energy sensor at a fixed location. The laser energy obtained is plotted against the distance covered. Subsequently, the fit to the curve of the energy against distance is differentiated to obtain the average intensity profile of the laser sheet. Thereafter, the distance from the centre of the beam (peak value in the graph) to where the laser intensity dropped to $1/e^2$ of the peak value is estimated and multiplied by two to obtain the laser sheet thickness. This obtained thickness was used in determining the laser fluence values indicated throughout this thesis. Both graphs are shown in Figure 3.4 below:
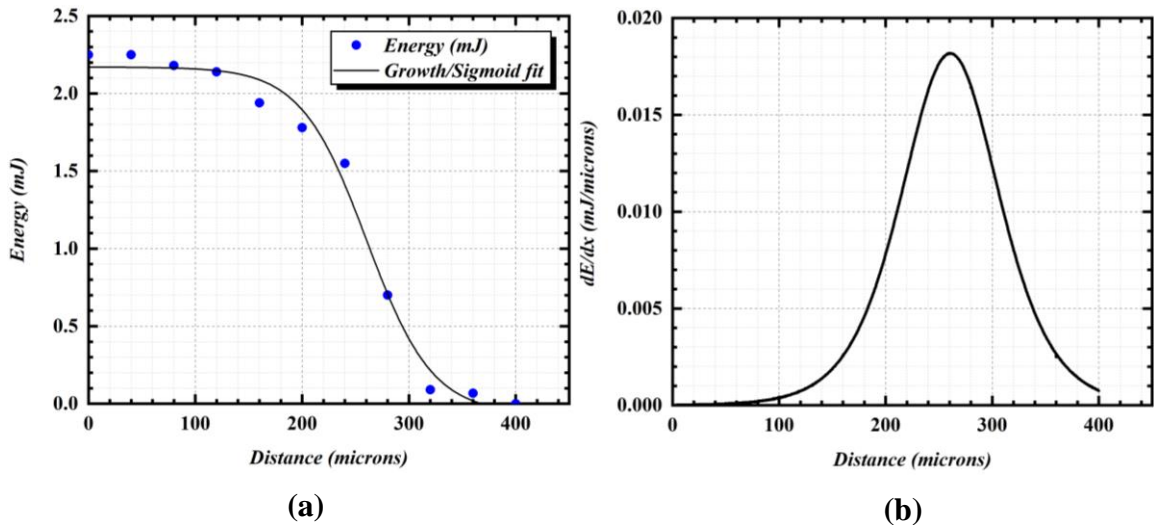
Figure 3.4: Laser energy in mJ plotted as a function of distance in microns and (b) its derivative - dE/dx presented as a function of distance in microns (representing the average laser intensity profile), where E and x represents the energy and distance respectively.

Furthermore, to understand the relationship between the laser intensity and PAH LIF signal, preliminary tests were conducted using the pure CH_4 flame condition whereby the laser fluence was varied incrementally from 40 mJ/cm^2 to 180 mJ/cm^2. At each laser fluence level, 200 PAH PLIF images were accumulated and analysed to obtain the PAH LIF signal profile as the height above burner lip increased. Thereafter, the peak PAH LIF signal for each fluence level was extracted for further analysis. Subsequently, the extracted peak PAH LIF signals for all the fluence levels investigated were normalised with the maximum PAH LIF signal (that is the maximum value within the extracted PAH LIF signal values) and presented as a function of laser fluence in mJ/cm^2 in Figure 3.5. It can be seen from Figure 3.5 that at laser fluence of 107 mJ/cm^2 and above, the PAH-LIF signal was independent of the laser intensity (saturated). A similar observation regarding the saturation of PAH fluorescence with respect to variation in laser energy was reported by Vander

Wal (1997). Hence, the laser fluence chosen for this study was maintained at a value above 107 mJ/cm^2 to ensure that observed changes were not due to increasing laser fluence levels. The other factor considered in choosing the laser fluence for this study such as the shot-to-shot fluctuations of the laser are detailed later in section 3.6.
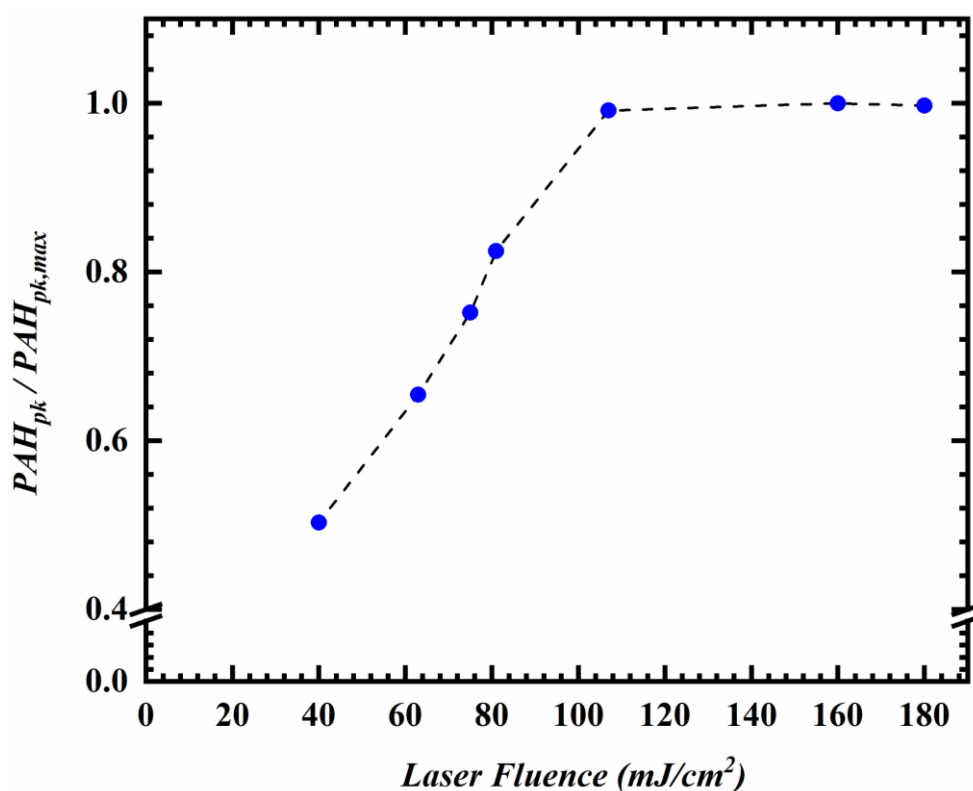
Figure 3.5: Normalised peak PAH LIF signal as a function of the laser fluence.

3.3 IMAGING AND DETECTION SYSTEM

The fluorescence from the OH radicals and PAH species were imaged simultaneously by two intensified charge coupled devices (ICCDs) placed perpendicular to the direction of the laser sheet on either side of the burner. The ICCD cameras used in this study were TSI PowerView 1.4MP CCD fitted

with Videoscope VS4-1845 intensifiers. A TSI LaserPulse synchroniser with model number 610035 was used to accomplish synchronisation of the timing between the camera exposure, gating of the intensifier and the laser pulse. The data is acquired through a frame grabber on the Insight 3G® software (TSI Inc.®, Minnesota, USA).

The OH fluorescence near 310 nm was captured on OH ICCD (see Figure 3.2) which was fitted with a UV 100 mm f/2.8 Cerco lens and a combination of UG11 and WG305 Schott glass filters.

For the PAH species, the fluorescence was captured on PAH ICCD (see Figure 3.2) using visible lens of two different focal lengths. This was done to ensure imaging of the full flame height, as well as capture a higher resolution image of the lower part of the flame closer to the burner lip. In the first case, an f/1.2 Nikon visible lens of focal length 50 mm was used to image up to 26 mm of the flame height hence providing higher resolution image of the PAH species closer to the burner lip (herein referred to as zoomed in imaging). For the second case, an f/2.8 Nikon visible lens of focal length 105 mm was used to image fluorescence from PAHs over the full flame height (herein referred to as zoomed out imaging).

For both cases, following the work of Wu *et al*. (2006), a combination of GG420 (high pass Schott filter) and BG12 (low pass Schott filter) were fitted to the lens to image fluorescence from PAH species of three or more rings between the wavelength range of 420 nm and 480 nm.

3.4 IMAGE PROCESSING

A number of steps were involved in processing the images. Firstly, 200 instantaneous images of OH and PAH were accumulated respectively for each test condition. The instantaneous images were median filtered with a 3×3-pixel window to reduce salt and pepper noise. The filtered images were subsequently background corrected and averaged to obtain the mean images of the OH and PAH PLIF with good signal to noise ratio (SNR) for each test condition. A sample of the averaged OH and PAH images are shown in Figure 3.6 (a) & (b) respectively. Thereafter, the averaged PLIF image of OH was transposed onto the corresponding PAH PLIF image retaining the PAH PLIF image resolution of 25 µm/pixel using an in-house developed image warping MATLAB® routine. The transposition was based on a target image captured simultaneously on OH ICCD and PAH ICCD cameras. Identical points in the target images obtained simultaneously on both ICCD cameras were tracked to form a transformation matrix. Based on the transformation matrix, images of OH LIF and PAH LIF are matched to sub-pixel accuracy to obtain the transformed image as described above (Mulla *et al.*, 2016). An example of the combined image obtained from transposing the averaged images of OH and PAH is shown in Figure 3.6 (c). This is done for each respective test conditions and saved for further processing to extract information regarding the PAH formation characteristics.
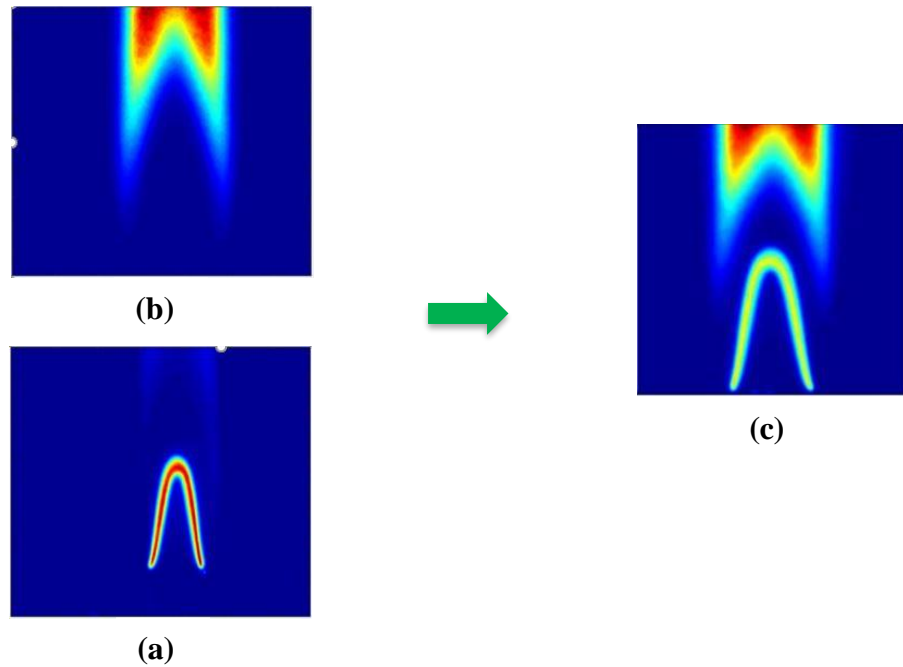
Figure 3.6: The process of transposing averaged images of (a) OH PLIF onto (b) PAH PLIF to obtain (c) the combined OH-PAH transposed images

In diffusion flames, the peak temperature region has been shown to coincide with peak OH concentration (Mikofski *et al.*, 2007). In respect of this, the peak OH location is used to denote peak temperature locations in the flame due to the non-availability of well resolved temperature data. Therefore, in this study the flame front was represented by the loci of peak OH signal at different heights in the OH PLIF image as shown in Figure 3.7. The peak position of the OH LIF in Figure 3.7 (a) is tracked to obtain the loci which is denoted as the flame front and shown in Figure 3.7 (b). Note that the intensity of the OH LIF signal was adjusted to highlight the lines in Figures 3.7 (b) and 3.7 (c) for clarity. The flame front is divided into two equal halves (left and right). One half (left half was used for the analysis in this work) is retained for further analysis

(note that either half is suitable for analysis as demonstrated in section 4.2). The position of the burner lip is represented by the top side of the blue square shown in Figures 3.7 (a), 3.7 (b) and 3.7 (c). Relative to the burner lip, a starting point, y_o which was kept constant for all cases investigated is determined on the chosen half and terminated at a height just before the curvature region in the flame front (see Figure 3.7 (b)) to obtain the line shown in Figure 3.7 (c). This line is referred to as the length along the flame front, L_f and was utilised as the base axis for the PAH analysis based on the flame normal statistics which will be discussed later in this section. The flame height measured from the burner lip to the peak location of the OH LIF along the central axis is shown in Figure 3.7 (b).

(a) (b) (c)
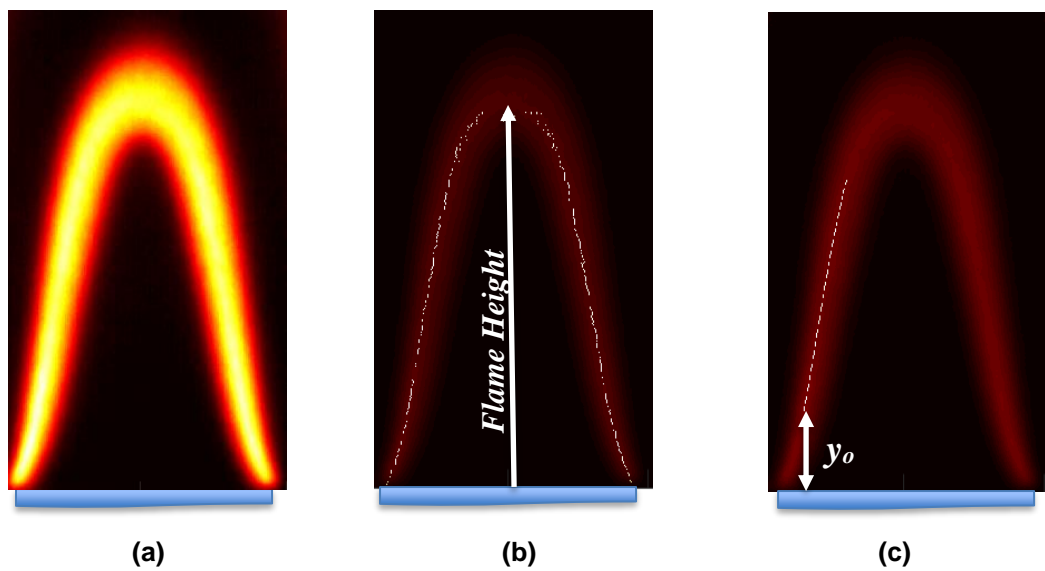
Figure 3.7: Images showing the (a) OH LIF (b) loci of the peak OH LIF signal denoted as the flame front (c) length along the flame front, L_f and the determined starting point for L_f denoted as y_o. The burner is presented by the top side of the blue square. Flame height is also shown in (b)

As described in section 3.3, the processing and analysis of the obtained images for PAH formation characteristics was achieved using two approaches: the zoomed in and the zoomed out approach. For both approaches, the laser sheet is the same while the field of view and the pixel resolution are different because of the difference in the focal lengths of the visible lens used for each (see description in section 3.3). For the zoomed in approach, the analysis of the PAH formation characteristics was referenced to the flame front (or flame position). This method of analysis incorporates the conical shape of the flame which allows meaningful comparison of the results from this work with modelling results. However, the OH profile which represents the flame front is present only up to about 15 mm above the burner lip. Therefore, analysis of PAH formation characteristics at higher heights (typically up to and above 15mm) is not possible using the zoomed in approach. Hence, the zoomed out imaging approach is employed. In this approach, the PAH formation characteristics at higher heights above the burner lip was analysed independent of the flame front. Both approaches are described in detail in the following sections.

3.4.1. Change in PAH with respect to the flame position (Flame Normal Statistics)

Figure 3.8 shows the combined OH-PAH PLIF image annotated with the parameters utilised for the image analysis in this study. In this approach, a section of the obtained flame front is dedicated as the length along the flame front, L_f with respect to a chosen initial height, y_o above the burner lip (see Figure 3.8 (a)). L_f is representative of the height above burner as used by

several studies but with reference to the conical shape of the flame. This is to allow meaningful comparison with modelling results.

To determine the PAH profile, a perpendicular axis, n, is established with respect to L_f starting from y_o $(= 1.85\ mm)$. The PAH profile normal to the flame front is then determined along the distance, x_n on the normal line starting from the reference point on L_f into the PAH region. This is repeated consecutively for every pixel location on L_f to obtain data on PAH formation as the distance along L_f increases. For every PAH profile determined, the peak value of the PAH signal is extracted and denoted as PAH_{pk}, while the area under the PAH profile is calculated to obtain PAH_{sum}. The profile widths of the PAH (w_{PAH}) and OH (w_{OH}) are established using the full-width half maximum (FWHM) of their respective profiles. Also, the distance between the peak locations of the OH and PAH signals is determined and denoted as x_{pk}. Both x_{pk} and w_{PAH} were normalised with w_{OH} and shown in Figure 3.8 (b). The change in PAH_{pk} or PAH_{sum} of the PAH profile as the L_f increases yielded the PAH formation characteristics for the flame conditions studied. Additionally, it is pertinent to note that the PAH_{sum} accommodates any variation in the peak-to-peak distance (x_{pk}) and w_{PAH} at different L_f.
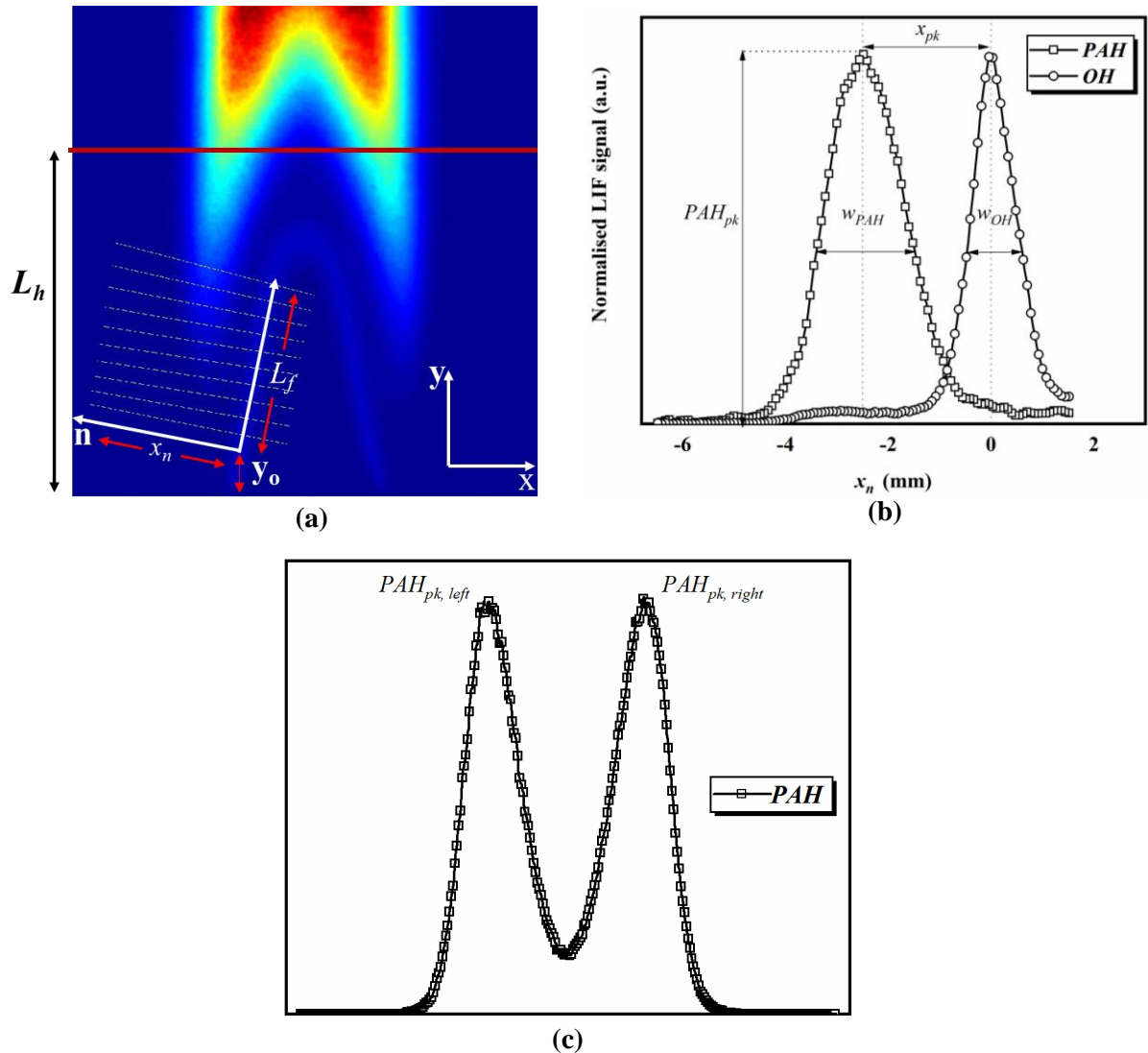
Figure 3.8: (a) An example of a combined PAH and OH LIF image showing the various coordinate systems employed for this work, (b) PAH and OH line profile along the normal 'n', at a distance of 8 mm along the flame front (L_f) (c) PAH line profile at HAB of 20 mm (at $y = L_h$ in Fig.3.6a)

3.4.2 Change in PAH with respect to the vertical height above the burner lip

In this approach, the change in PAH LIF signal is presented with respect the height above the burner lip, independent of the location of the flame. As shown in Figure 3.8 (a), the x and y axis representing the horizontal and vertical

cartesian co-ordinates with respect to the central axis of the burner lip is utilised for this analysis. Here, a reference location the y-axis is established (say L_h as in Figure 3.8 (a)) and then the PAH profile is determined along the x axis at this location. A typical PAH profile obtained using this approach at a height above the burner lip of 20 mm (that is, y = L_h) is shown in Figure 3.8 (c). The peak PAH signal for each side of the flame is denoted as $PAH_{pk,left}$ and $PAH_{pk,right}$ for the left and right sides respectively. Similar to the approach in section 3.4.1, the total amount of PAHs along the x-axis at any given distance, y, from the burner lip is determined for both sides of the flame as PAH_{sum}. The axisymmetric nature of the flame can be seen from the symmetry observed between the PAH LIF signal profile for the left and right side of the flame as shown in Figure 3.8 (c).

3.5 DETERMINATION OF PAH GROWTH RATE

An important aspect of PAH study is the role it plays in the formation of soot particles. PAHs grow from smaller to larger rings, as well as increase in number/concentration, with increasing height downstream of the burner exit nozzle. These larger ring PAHs subsequently aggregate to form soot. Hence, determining the rate of this growth and the role an increase in PAH concentration plays downstream of the flame is key to understand the transition to soot formation. This growth process can be assumed to occur via any of the HACA mechanism as proposed by Frenklach (Frenklach, 2002) and dimerisation of PAHs (Mercier *et al.*, 2019; Faccinetto *et al.*, 2020b). The growth rate characteristics of PAH for most practical combustion experiments are presented as a function of the height above burner (HAB) (Park *et al.*,

91

2017; Liu *et al.*, 2018). This captures the growth characteristics in terms of distance (residence time and velocity) from the burner lip. Alternatively, modelling approaches (either 0D or 1D) consider the growth of PAH in terms of concentration as a function of time, however, this approach does not capture the height effects (spatial resolution) but relates to it using residence time.

In the work shown in this thesis, an attempt was made to transform the HAB-derived PAH data into concentration growth characteristics for PAH. This transformation is possible since PAH growth in flames is a pyrolytic process which depends on the local PAH availability and the obtained PAH LIF signal is primarily dependent on the number density of the PAH species as observed in Chapter 4 of this work. Here, the growth characteristics refer to the rate of change of PAH LIF signal with respect to distance along the flame front, L_f (which is representative of HAB). The PAH LIF images analysed using the flame normal statistics as described in section 3.4.1 was used for the PAH growth rate analysis for the following reasons: To have a meaningful comparison between PAH profiles from experiment and 1D flame simulations, the PAH analysis should be done normal to the flame front and focused on the region where the effects of heat loss and flame curvature are insignificant. Additionally, walking along the flame normal ensured that the PAH profiles were obtained along a consistent distance to the flame front (reaction zone) from point to point on L_f. Hence, it is possible to compare the PAH growth rate profiles obtained in this study with PAH growth rate profiles from 1D flame simulations under similar flame conditions. This PAH growth is assumed to be a consequence of increase in both PAH concentration and the number (or size)

of rings formed as L_f increases. For this study, growth rate of PAH concentration is determined from the established PAH LIF signal vs L_f curves. The PAH LIF curves are smoothened with a polynomial fit of second order (chosen because it showed the best fit to the data in this study) and then differentiated in segments of 0.5 mm along the length of the curve using the central difference method to achieve the first derivative ($d(PAH)/dL_f$) of each segment. The obtained derivative gives the growth rate of PAH LIF signal in this study; where $d(PAH)$ refer to the change in the PAH LIF signal and dL_f is the change in distance along the flame front.

3.6 UNCERTAINTY AND ERRORS

To verify the repeatability of the experimental set up, the same experiments were performed several times on different days, and it was found that PAH LIF signals (PAH_{sum}) was determined to be less than 1%. As discussed previously in section 3.2, where it was observed that at laser fluence of 107 mJ/cm^2 and above, the PAH-LIF signal was independent of the laser intensity (that is, PAH LIF signal saturated). Hence, maintaining laser fluence values above 107 mJ/cm^2 is key to ensure that the observed changes in PAH LIF signal with various flow conditions investigated in this thesis were independent of variations in the laser fluence levels. Additionally, the shot-to-shot energy variations of the laser used for this work was observed to be within $\pm\,10\%$. This implies that only laser fluence levels beyond 133 mJ/cm^2 will guarantee conditions above the threshold value of 107 mJ/cm^2 for PAH fluorescence saturation. Hence, for all the conditions tested, laser fluence was maintained at values above 133 mJ/cm^2. Therefore, the observed differences in PAH LIF

signal can be assumed to be independent of the fluctuations in the laser fluence.

To understand the effect of the number of images on the PAH LIF signal, accumulations of up to 800 images were captured in incremental steps of 200 images for various instances of the CH_4-only test condition. It was observed that variations in the PAH LIF signal between averaged images from 200 accumulations and higher were negligible. Consequently, average of 200 images was concluded as sufficiently reliable for data analysis in this study. Also estimated fluctuations in the distribution of the peak value and the corresponding location was within 3% for the OH and 5% for the PAH with 95% confidence interval. Additionally, signal to noise ratio (SNR) evaluated for various conditions range from 15 to 18 for OH and 12 to 20 for PAH, with higher SNR for the zoomed-in configuration compared to that of zoomed out configuration.

The accuracy of all the flow meters was ±1.5% full scale division (FSD). In addition to this value, the set volume flow rate varied by 0.2% for all the conditions tested (resulted in no effect on the global equivalence ratio using CH_4/air flow conditions). The uncertainty due to data smoothening for the determination of the growth rate of PAH LIF signal was estimated to be within ±3.5% based on the highest standard deviation obtained for all cases.

CHAPTER FOUR

4.0 EFFECT OF HYDROGEN ADDITION ON PAH FORMATION IN METHANE DIFFUSION FLAMES

Hydrogen-enriched natural gas (HENG) which consists primarily of CH_4 and H_2 (between 10 and 20% by volume) is a low carbon alternative fuel considered for use in gas turbines, automobile engines, industrial and domestic burners (Schiro, Stoppato and Benato, 2020; Do et $al.$, 2021). Trials have been conducted in Europe to ascertain the possibility of using HENG for the main gas supply (Jones, Al-Masry and Dunnill, 2018). To facilitate widespread implementation of such alternative options, it is important to understand the effect of co-combusting H_2 and CH_4 on PAH formation, and hence on pollutant soot emissions. Additionally, the significance of the H atom in PAH formation reactions was highlighted by the various literatures reviewed in Chapter 2. But there is currently limited focus in literature investigating PAH formation in single-component hydrocarbon fuels with the addition of H_2 and its impact on reducing soot formation.

Therefore, to fill the gaps elaborated above, this chapter presents results from an experimental investigation on the effects on PAH formation when H_2 is added to CH_4 inverse diffusion flame. For the purpose of comparison, the flow conditions from this study were modelled by an academic collaborator using 1-D flame calculations - CANTERA (Goodwin, Moffat and Speth, 2017) coupled with the Appel-Bockhorn-Frenklach gas-phase mechanism for the chemical reactions (Appel, Bockhorn and Frenklach, 2000). The detailed

descriptions of the model can be found in Ref. (Ezenwajiaku *et al.*, 2019). It is important to note here that the simulation results presented in this chapter were results of work performed by the academic collaborator referred above. For this chapter, both methods for image analysis namely, zoomed in and zoomed out (as previously described in section 3.4) were employed. To reiterate the purpose for both methods, the zoomed in configuration was used to obtain the PAH formation characteristics based on flame normal statistics while the zoomed out method was used to obtain information on the PAH formed independent of the flame location. This methodology based on flame normal statistics allowed meaningful comparisons to be made between the experiments and 1-D flame simulations and, for the first time, offer experimental validation of computational data related to H_2 addition effect on PAH formation characteristics in methane flames.

4.1 EXPERIMENTAL PROCEDURE AND FLOW CONDITIONS

The flow conditions for the results presented in this chapter are summarised in Table 4.1. For all the tests conducted in this section, the flow rates of CH_4, Q_{CH_4}, and air, Q_{air}, were fixed at 10 lpm and 1.5 lpm, respectively. Hydrogen (H_2) was added to the CH_4 flow line, well in advance of the flame location to ensure proper mixing. The flow rate of hydrogen (Q_{H_2}) was varied with the resolution of 0.2 lpm. Up to 2 lpm of H_2 was added to the CH_4, which is 20% by volume of CH_4. The same mole fraction of fuel mixture (CH_4 and H_2) combinations served as input to 1D flame calculations. In addition, Table 4.1 also shows the temperature at maximum PAH and the maximum temperature,

both obtained from the flame simulation work. For each case, the OH and PAH

PLIF images are accumulated simultaneously and analysed. The details of the

results and analysis is presented below:

Table 4.1: Hydrogen flow rates (Q_{H_2}) at corresponding percentage H_2 addition (Q_{H_2}/Q_{CH_4}) for fixed Q_{CH_4} (10 lpm) and Q_{air} (1.5 lpm) flow rates. The temperature at maximum PAH concentration (T at $[PAH]_{max}$) and the maximum flame temperature (T_{max}) is also shown for each H_2 addition.

H_2 addition (lpm)	% H_2 addition	T at $[PAH]_{max}$ (K)	T_{max} (K)	w_{OH} experiments (mm)	$w_{[OH]}$ simulations (mm)
0	0	1520	2152	2.61	3.41
0.2	2	1530	2159	2.51	3.41
0.4	4	1540	2165	2.50	3.27
0.6	6	1550	2171	2.51	3.41
0.8	8	1520	2178	2.44	3.41
1	10	1540	2184	2.56	3.55
1.2	12	1550	2190	2.91	3.62
1.4	14	1560	2196	2.83	3.41
1.6	16	1530	2202	2.69	3.48
1.8	18	1540	2208	2.98	3.62
2	20	1550	2213	2.81	3.69

4.2 METHANE-AIR FLAME FORMATION CHARACTERISTICS

Figure 4.1(a) shows the change in the peak PAH LIF signal (PAH_{pk}) and the

cumulative sum of the PAH line profile (PAH_{sum}) along the flame normal as a

function of 'L_f', the distance along the flame front, for the zoomed in imaging configuration. The results shown in Figure 4.1(a) are for the methane-air test conditions only, without any addition of H_2. It can be seen that PAH increases non-linearly with increasing length along the flame front. The LIF signal from PAH depends on both the number density of each type of PAHs (that is, the PAH concentration), and the structure of the PAH molecule. It is generally known from literature, that larger PAH rings fluoresce with a higher intensity (Beretta *et al.*, 1985; Zizak *et al.*, 1996; Bejaoui *et al.*, 2014). Hence, in addition to the increase in the concentration of the PAHs, the increase in LIF signal could also be due to the smaller PAHs combining and growing into larger rings further downstream in the flame. It is pertinent to note that since it was not possible to discriminate between individual PAHs, the signal shown here is only a qualitative indication of PAH formation characteristics in the flame, as described earlier.

Figure 4.1(b) presents the variation in the normalised inter-peak distance (x_{pk}) and the normalised PAH profile width (w_{PAH}) with increasing distance along the flame front, L_f; x_{pk} and w_{PAH} were normalised using w_{OH} of the respective profile. The inter-peak distance indicates how far from the flame front does maximum PAH concentration occur with the flame front represented by the loci tracing the peak OH concentration. As explained earlier, the peak OH can be approximated to the peak temperature regions with considerable accuracy for non-premixed flames. It can be seen from the figure that inter-peak distance increases almost monotonically with 'L_f'. However, the profile width (w_{PAH}) increases significantly till about 4 mm along the flame front. Up to 4 mm, the

signal intensity is weak and the signal-to-noise ratio (SNR) is relatively low, due to low levels of PAH present. Furthermore, the effects of heat loss are more significant close to the lip of the burner. Above 4 mm, the width increases, but not as sharply, indicating the role of continued production of PAHs. As evidenced from 1D flame simulations, PAH production is restricted to a fixed temperature range irrespective of H_2 addition levels (see Table 4.1), the change in x_{pk} and the w_{PAH} with increasing L_f indicates the effect of residence time. It should also be noted that the similarity in trends of PAH_{sum} and PAH_{pk}, as observed in Figure 4.1(a), exists because the profile width remains largely the same above 4 mm. Hence, only the height of the PAH profile was changing, with increasing length along the flame front, denoting higher LIF signal.
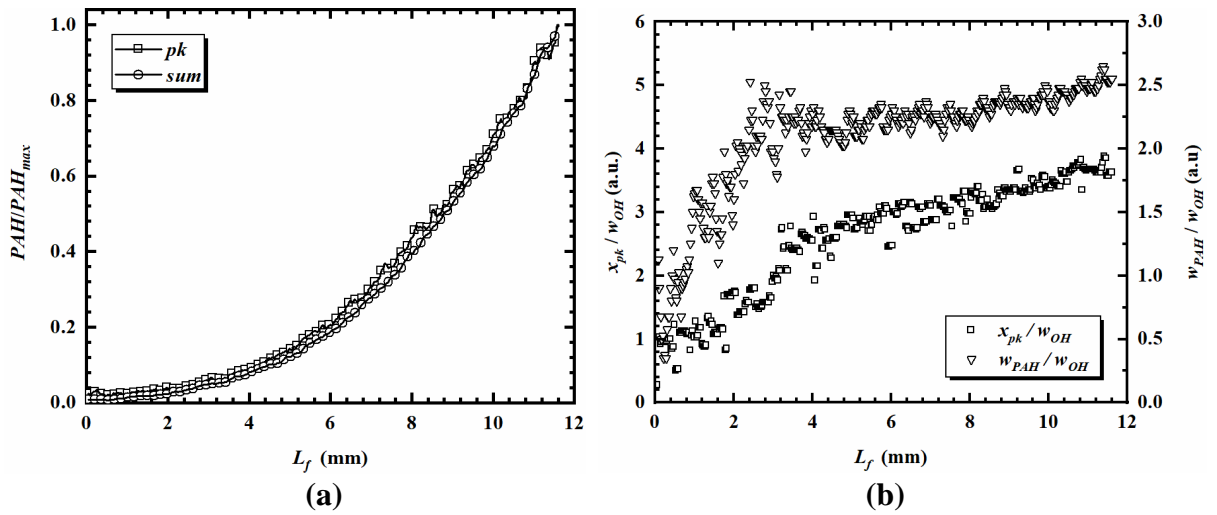
Figure 4.1: (a) Variation in normalised inter-peak PAH LIF signal (PAH_{pk}) and the cumulative sum of the PAH line profile (PAH_{sum}) as a function of length along the flame front (L_f), and (b) variation in inter-distance between OH peak and PAH peak (x_{pk}), and the PAH profile width (w_{PAH}), normalised with w_{OH}, at various L_f.

Figure 4.2 shows the change in the peak PAH LIF signal (PAH_{pk}) and the cumulative line profile (PAH_{sum}), as a function of vertical height, L_h, above the burner tip, for the zoomed out camera configuration. Similar to Figure 4.1(a), this figure also shows a monotonic increase in both PAH_{pk} and PAH_{sum} with increasing distance from the burner lip.

Similar trends of PAH concentration with respect to height above the burner have been observed in previous studies (Hepp, Siegmann and Sattler, 1995; Richter and Howard, 2000; Mikofski *et al.*, 2007). For the zoomed out configuration, since the camera lens was placed further away from the burner (in order to look at PAHs higher up the flame), the amount of light entering the camera lens from the flame was reduced (following the inverse square law relation between intensity and distance from the light source). Hence, no appreciable PAH signal was observed below L_h = 11 mm for this configuration. It can also be observed from Figure 4.2 that both the magnitude and variation in PAH_{pk} evaluated for both sides of the flame (left and right) are similar, which
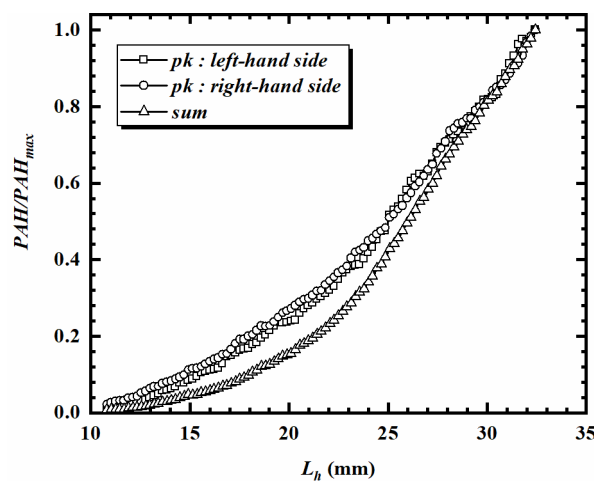
Figure 4.2: Peak PAH LIF signal (PAH_{pk}) for the left and right sides of the axisymmetric flame, and the cumulative sum of PAH line profile (PAH_{sum}) as a function of the vertical height (L_h) above the burner lip.

confirms the axisymmetric nature of the burner. Hence, from here onwards, results from only one side of the flame will be presented.

Unlike in Figure 4.1(a), a deviation can be observed between the PAH_{sum} and PAH_{pk} graphs in Figure 4.2. This is due to the fact that above the conical region (represented by OH), the two sides of the PAH profiles merge to form a bimodal distribution that incorporates w_{OH} information, resulting in variation in trends of PAH_{sum} and PAH_{pk}.

4.3 EFFECT OF METHANE AND AIR FLOW RATE

Figure 4.3 shows the effect of variation in methane flow rate, Q_{CH_4}, on the peak PAH intensity signal. It can be seen from Figure 4.3 that when the flow rate of methane is increased from 6 lpm to 12 lpm (a change of 100%), no significant change in PAH is obeserved. This shows that the effect of change in convection velocity had negligble influence on the PAH formation characteristics. This could potentially be explained by the fact that the mixing of reactants in IDF configuration is primarily diffusion-controlled. Hence, other factors, such as change in bulk velocity or change in the fluid shear stress (between the central and outer flows) might not have a significant impact for the flow conditions tested in this work. Therefore, when hydrogen is added to the fuel flow (up to 20% of the volume flow rate of methane, Q_{CH_4}), it can be safely assumed that the change in PAH characteritics is primarily due to H_2 addition and not a consequence of the variations in bulk velocity values.

The rate of change in PAH (both peak and sum) with respect to the distance, presented here, is an indicative characteristic of the sooting tendency of the
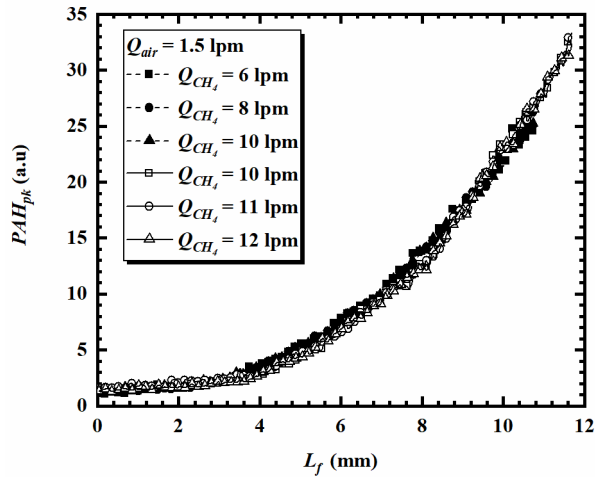
Figure 4.3: Effect of varying the methane (CH_4) flow rate on the PAH LIF signal, for a fixed air flow rate.

fuel mixture. It is clear from these results, if the air flow rate was kept constant, this PAH growth rate (change in PAH LIF signal with respect to L_f or L_h) will allow direct comparison of sooting tendencies (that is, PAH formation potential) of various fuel mixtures.

4.4 HYDROGEN ADDITION TO THE FUEL (CH_4) STREAM
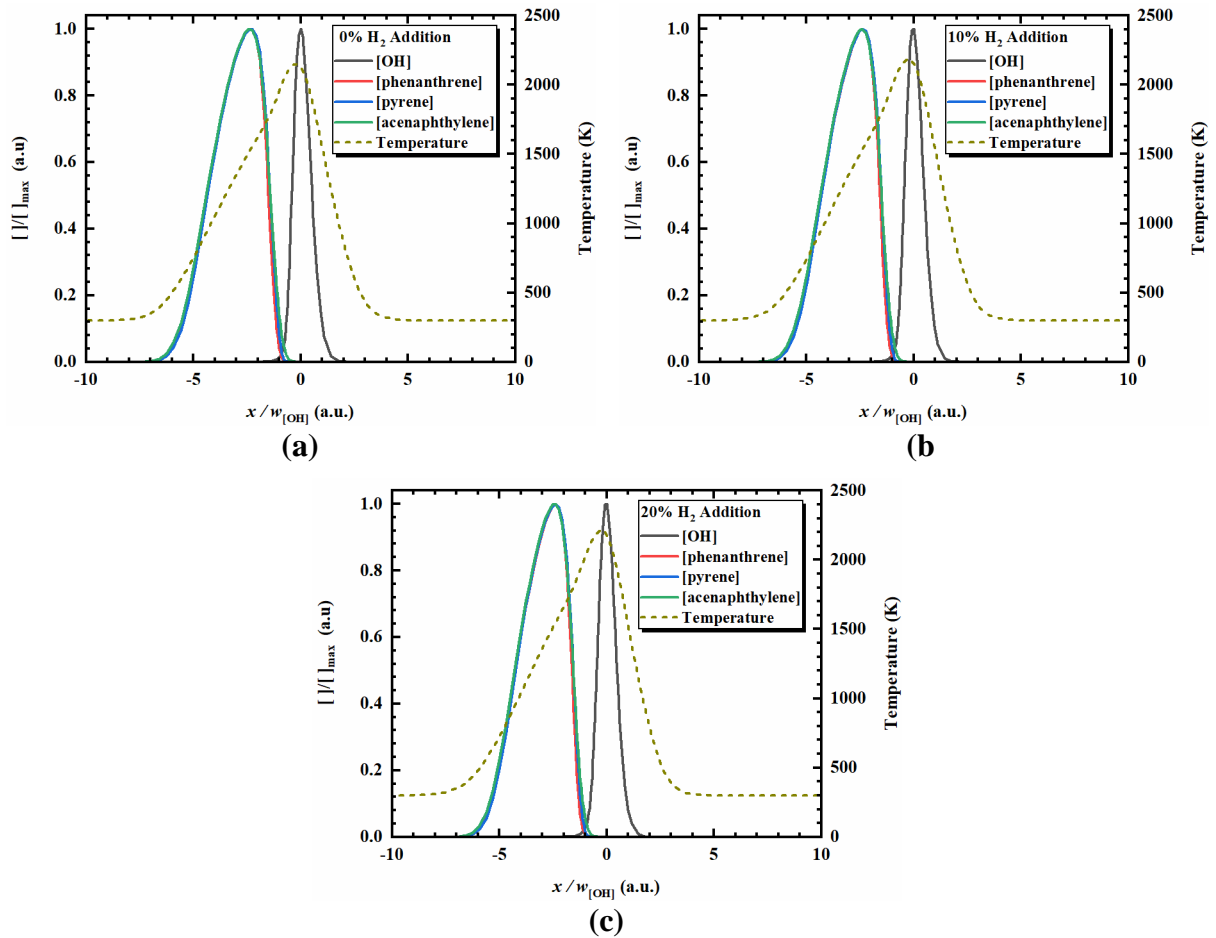
Figure 4.4: Axial profiles of [OH], three PAH species (3-ring: [phenanthrene], [acenaphthylene] and 4-ring: [pyrene]), and temperature for (a) 0%, (b) 10% and (c) 20% H_2 addition, simulated using 1-D modelling of CH_4-H_2 flame. (Note: 'x' distance is normalised with FWHM of OH concentration, $w_{[OH]}$)

Figure 4.4 shows the axial profile concentrations of OH, temperature and three PAH species – phenanthrene (3 rings), acenaphthylene (3 rings) and pyrene (4 rings) – for three different H_2 additions (0, 10 and 20%), obtained from 1-D simulations of the methane-hydrogen flame. Simulation results for other mixture conditions are available, but for brevity only three conditions are

presented. To allow accurate comparison, the x-axis has been normalised with respect to the full width-half maximum (FWHM) value of the OH profile, w_{OH}. No significant change in the PAH line profile shape is observed with increasing levels of H_2 addition. As expected, the peak temperature does show an increase, but only of about 50-70 K with increasing levels of H_2 (maximum temperature data also shown in Table 4.1).

Figure 4.5 shows the line profiles of OH and PAH species for three different H_2 additions (0, 10 and 20%) from experiments, obtained perpendicular to the flame front, at a length of 8 mm along the flame front. Similar to Figure 4.4, the x-axis for Figure 4.5 has also been normalised with respect to the FWHM value of the OH line profile, w_{OH}. A number of similarities can be observed between the computational and experimental line profiles presented in Figure 4.4 and 4.5 respectively. The normalised experimental PAH profiles similar to PAH concentration profiles from simulation start to increase at about 1 (a.u.) on the fuel side, away from the peak OH location for both sets of data. The experiments are limited in terms of resolving between individual PAH species, however the computational data shows that the different 3 and 4 ring PAH species have almost identical line profiles and are similarly affected by H_2. Hence, the experimental data can be used to represent PAHs of a certain size group with reasonable accuracy.

Figure 4.6 shows the variation in the normalised distance between the OH and the PAH peaks against different levels of H_2 addition in the fuel (CH_4) stream, for experimental ($x_{pk,exp}$) and 1-D flame simulation ($x_{pk,comp}$) studies, at a

distance of 8 mm along the flame front, L_f. The inter-peak distance x_{pk} was normalised with the x_{pk} values of the base case, $x_{pk,0}$ (that is, 100% CH_4 and 0% H_2). It can be seen from the figure that both $x_{pk,exp}$ and $x_{pk,comp}$ show an overall increase with H_2 addition. This observed trend is due to variations in adiabatic flame temperatures. Additionally, in an IDF configuration (present experimental work) combustion products and the unburnt fuel interact, which could potentially result in increased local mixture temperatures
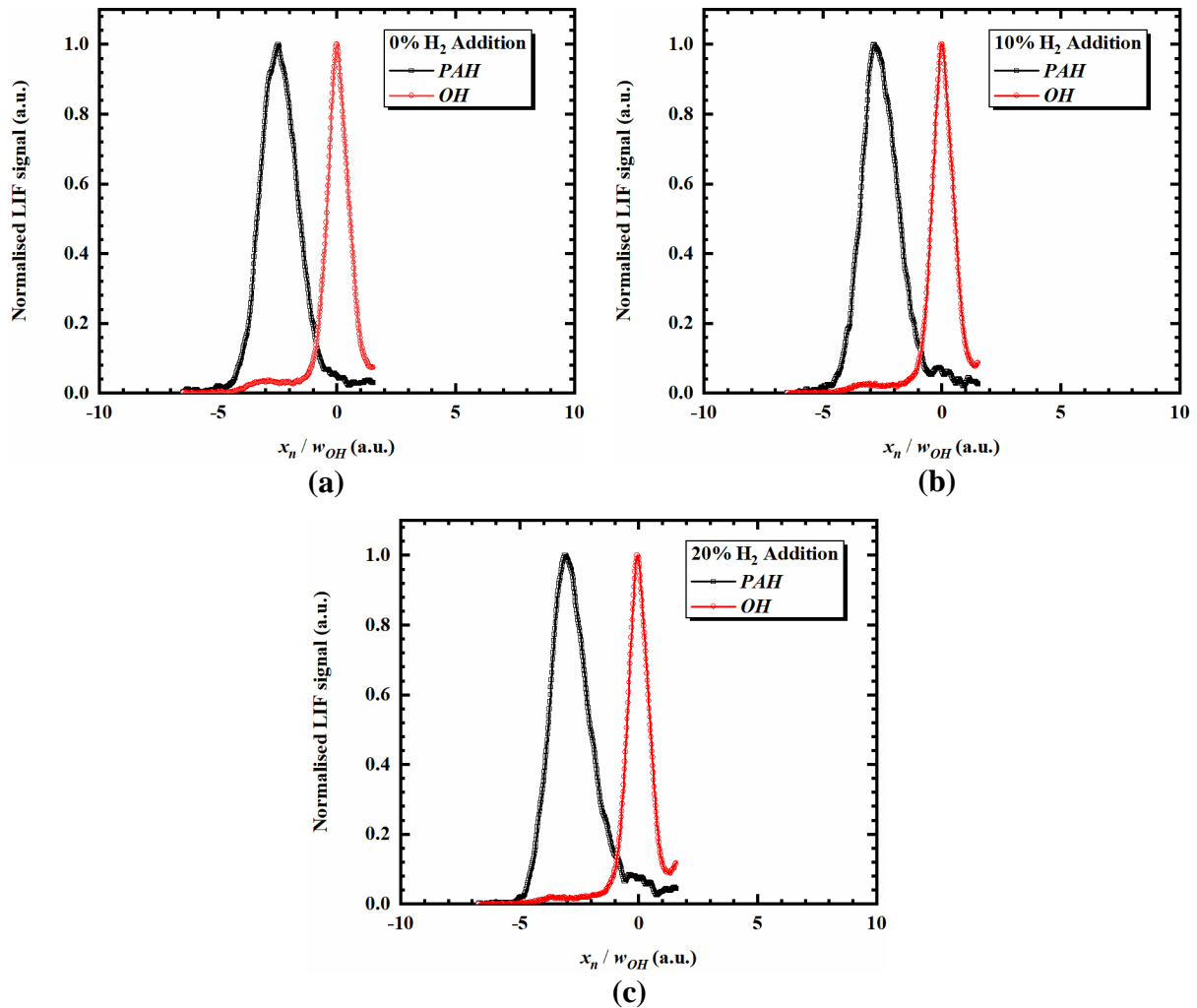
Figure 4.5: Line profiles of LIF signals OH and PAH along the normal, at a distance of 8 mm along the flame front (L_f) for (a) 0%, (b) 10% and (c) 20% H_2 addition.
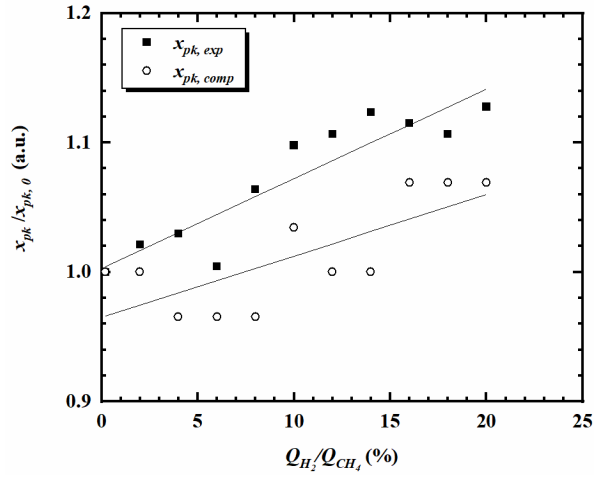
Figure 4.6: Comparison of the distance between OH peak and PAH peak (x_{pk}) normalised with base case value ($x_{pk,0}$), for various H_2 addition levels in the methane flame, for both experimental and 1-D flame simulation studies. For experiments, data was obtained at a distance of 8 mm along the flame front (L_f = 8mm).

Figure 4.7 shows the PAH_{pk} and PAH_{sum} for both the zoomed in (4.7(a) and 4.7(b)) and zoomed out (4.7(c) and 4.7(d)) camera configurations, for different levels of H_2 addition in the fuel (CH_4) stream. The zoomed in data is presented as a function of distance along the flame front (L_f), while the zoomed out data has been presented as a function of vertical height above the burner (L_h), and shows PAHs at higher heights as compared to the zoomed in graphs. It can be observed from Figure 4.7(a) that the change in the PAH signal w.r.t. the length of the flame front is highest for the methane only flame, that is, without any H_2 addition. As H_2 is incrementally added, the rate of increase of PAH_{pk} with respect to L_f, reduces. Similar trend in the reduction of PAH with H_2 is also observed at higher heights above the burner tip (Figure 4.7(c) -zoomed

out configuration), as well as in the PAH_{sum} graphs for both the configurations (Figures 4.7(b) and 4.7(d)). This characteristic reduction in PAH with H_2 addition will be further discussed in the next few paragraphs.
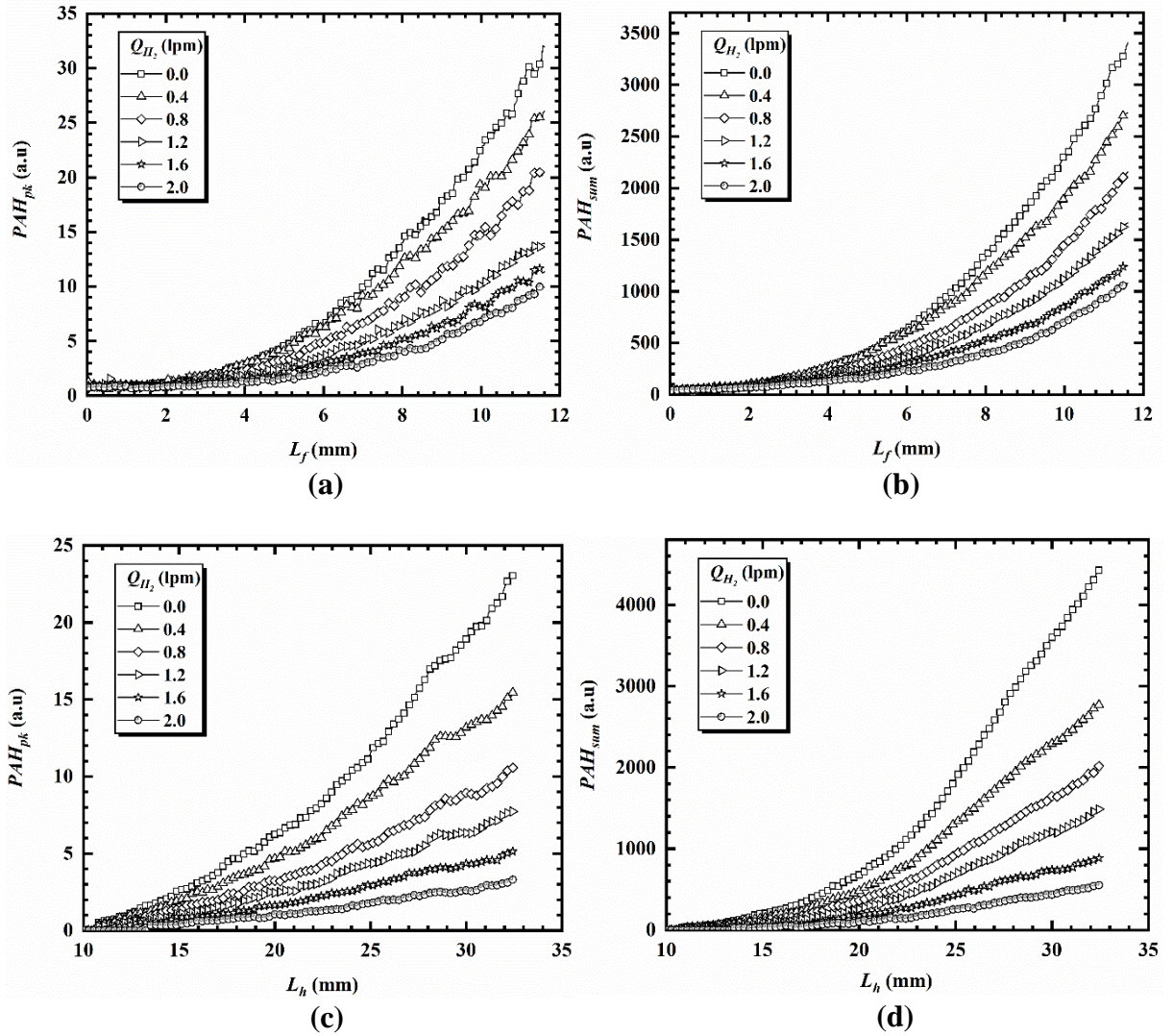
Figure 4.7: (a) Peak PAH LIF signal (PAH_{pk}) and (b) cumulative sum of PAH line profile (PAH_{sum}) as a function of L_f (length along the flame front), and (c) PAH_{pk} and (d) PAH_{sum} as a function of L_h (vertical height above the burner lip), for various H_2 addition levels.

Figure 4.8 shows the variation in the PAH_{sum} at five fixed heights above the burner lip (L_f in the case of the 'zoomed in' configuration and L_h in the case of the 'zoomed out' configuration), as a function of H_2 addition. The PAH_{sum} values have been normalised against the base case, $PAH_{sum,0}$ (that is, 100% CH_4 and 0% H_2). It can be seen from the Figure 4.8 that PAH_{sum} reduces monotonically with H_2 addition at all the heights presented. Considering the reduction in the PAH signal due to H_2 addition, it can be observed that at the lowest height presented of 5 mm (L_f) the change in the PAH_{sum} is relatively lower (70%) as compared to at the highest height where a reduction of almost 90% was observed with at the highest H_2 addition level. As noted in previous studies, larger PAHs form at higher heights above the burner (Hepp, Siegmann and Sattler, 1995; Richter and Howard, 2000; Mikofski *et al.*, 2007). Since the addition of H_2 impedes the formation of smaller PAHs, and hence preventing the formation of the larger PAHs, the effect of H_2 addition is more significant at higher heights.
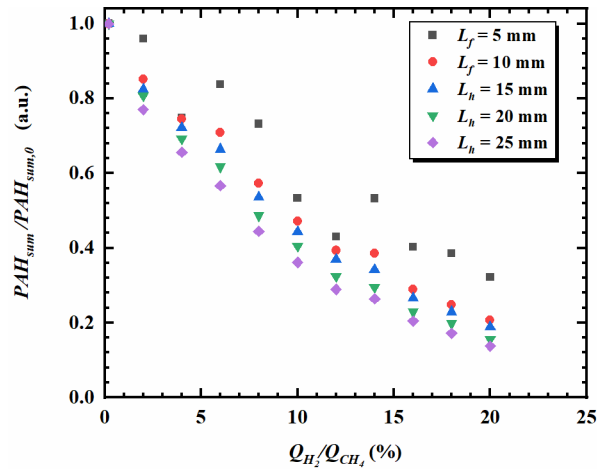
Figure 4.8: Variation in the PAH_{sum} LIF signal normalised using base case value ($PAH_{sum,0}$), as a function of percentage H_2 addition, at five different heights above the burner lip.

Figure 4.9 shows the variation in the concentrations of six species - methyl, acetylene, propargyl, acenaphthylene, phenanthrene, pyrene – as a function of H_2 addition in fuel (CH_4) stream, simulated using 1-D computational modelling. It can be seen from the figure that the addition of H_2 results in an almost 5% reduction in methyl and acetylene, about 10% reduction in propargyl and a corresponding 60% reduction in the three PAH species. Acetylene and propargyl are important species for the formation of first ring, benzene (C_6H_6), which itself is an important intermediate for subsequent formation of larger rings (Bockhorn and Schäfer, 1994; Wang and Frenklach, 1997).
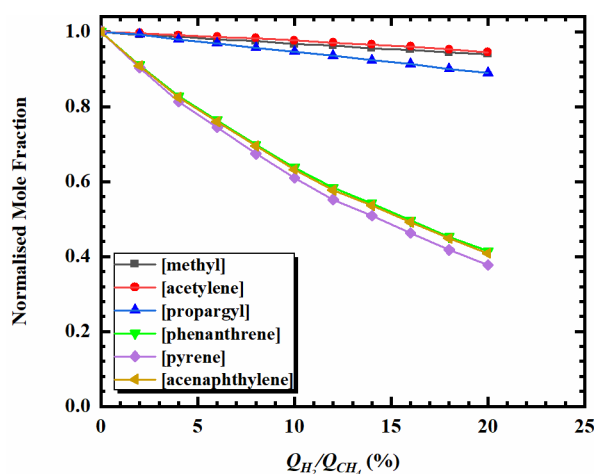
Figure 4.9: Variation in the concentrations of six species - methyl, acetylene, propargyl, acenaphthylene, phenanthrene, pyrene – as a function of H_2 addition in fuel (CH_4) stream, simulated using 1-D modelling.

Both acetylene and propargyl are building blocks of PAHs, involved in the primary reaction pathways of PAH formation. Acetylene is a crucial species of the HACA (hydrogen abstraction-acetylene addition) mechanism of PAH growth, while the recombination of propargyl is considered to be the most important cyclisation reaction in hydrocarbon flames (Frenklach and Wang, 1991; Miller and Melius, 1992; Richter and Howard, 2000; Kislov, Sadovnikov and Mebel, 2013). Hence, a reduction in the concentration of acetylene and propargyl can have a significant impact on the concentration of the larger species like acenaphthylene, phenanthrene and pyrene, as can be observed in Figure 4.9.

The reduction in PAHs with H_2 addition, as observed in both Figures 4.8 and 4.9, could be attributed to the added H_2 chemically inhibiting PAH formation. The mole fraction of OH has been observed to increase with H_2 addition to the

fuel stream, both in this work and in previous studies (Guo *et al.*, 2006; Pandey, Pundir and Panigrahi, 2007). Hence, it can be assumed that the increase in OH radicals could result in an increase in the rate of reactions which lead to higher oxidation rates of both acetylene and propargyl, hence reducing their availability to take part in the PAH formation reactions, and suppressing subsequent growth of PAHs. Another chemical effect associated with increasing the amount of H_2 in the reacting zone is the increase in the reverse rate of the H abstraction reaction ($R_1 + H \leftrightarrow R_2 + H_2$), which is a key reaction whereby H abstraction takes place to allow acetylene addition (Frenklach, 2002; Park, Choi and Yozgatligil, 2009). The abstraction of H atoms activates the surface sites of PAHs, and various hydrocarbon species such as acetylene and other PAHs then react with these active sites, hence propagating the surface growth process. The reduced H abstraction reaction rate reduces the number of sites available for acetylene addition, inhibiting surface growth of PAHs. Comparing Figures 4.8 and 4.9, it can be observed that the reduction in PAH_{sum} at 5 mm along L_f with maximum H_2 addition is about 70%, which is quite similar to the reduction in PAH concentration (approximately 60%) observed from the flame simulation studies for the same H_2 addition.

4.5 CONCLUSIONS

Some specific conclusions from this chapter are:

- PAH fluorescence signal increased with increasing height above the burner attributable to both higher concentration of PAHs as well as formation of larger rings.

- The distance between the OH and PAH peaks was observed to increase with increasing height above the burner. However, the PAH profile width remained largely similar beyond 4 mm above the burner tip. The change in the width below 4 mm was attributed to the radiative effects due to close proximity to the burner lip.

- When considering H_2 addition, both experimental and computational results showed similar PAH profile widths, with no significant change observed with H_2 addition. However, the peak PAH location from the experimental campaign was observed to shift slightly away from the OH peak (representing maximum temperature locations) with increasing H_2 addition.

- The rate of change in *PAH* with respect to the length of flame front (or height above burner) was highest for the methane only condition, with this rate reducing as H_2 was incrementally added.

- The reduction in PAH was observed to be monotonic with H_2 addition at all the heights above the burner tip, with higher reductions observed at higher heights above the burner. This was attributed to H_2 preventing the

formation of smaller PAHs at lower heights which would in turn impede the formation of larger PAHs at higher heights.

- The percentage reduction in PAH with H_2 addition at 5 mm above the burner tip was of similar magnitude to that observed from 1-D flame simulations. This is because the 1-D flame simulations cannot capture residence time, and hence are most comparable to heights closer to the burner tip but away from high strain and heat loss region.

- Based on simulation results, the reduction in PAH with H_2 addition was attributed to the increased oxidation of crucial species, such as acetylene and propargyl, hence reducing their availability for key PAH formation pathways. In addition, H_2 reduced the rate of H abstraction, hence impeding growth reactions on PAHs due to reduction of active sites for PAH growth.

CHAPTER FIVE

5.0 PAH FORMATION CHARACTERISTICS IN VARIOUS BINARY MIXTURES OF H_2 OR CH_4 WITH C1 – C3 HYDROCARBON FUELS

As described in Chapter 2, binary mixtures have been used in literature to represent the complex nature of conventional fuels and study fuel composition effects on PAH and soot formation. More importantly, as elucidated in Section 2.4, these studies showed that chemical interactions between various molecules in these binary mixtures reveal kinetic pathways which provide valuable insight to some complex processes of PAH formation. Hence, it is important to utilise these mixtures to study the effect of H_2 addition as a secondary gas (and a zero carbon fuel) on PAH formation as compared to the effect produced by using another hydrocarbon (such as CH_4, a major component of natural gas) as a secondary gas in the binary mixture. Furthermore, both mixtures could be utilised to build a database of fuel mixtures with a wide range of H:C ratios in order to study their dependence on PAH growth. Development of correlations will enable easy comparison with other mixtures of similar H:C ratios. Therefore, this chapter presents results from an experimental investigation on the PAH formation characteristics in binary mixtures of either H_2 or CH_4 and various C1 – C3 hydrocarbon fuels respectively. C1 – C3 represents the number of carbon atoms in the primary hydrocarbon fuels. The primary hydrocarbon fuels studied include: CH_4, C_2H_6, C_3H_8, C_2H_4 and C_3H_6 in the inverse diffusion flame configuration. This chapter builds on the knowledge obtained from the conclusions in the previous chapter where H_2 addition to only CH_4 was shown to reduce PAH formation. Firstly, H_2

was systematically added to more hydrocarbon fuels including saturated and unsaturated hydrocarbon fuels to study its effects on the formation and growth of PAHs. Subsequently, tests to understand the PAH formation characteristics due to the addition of CH_4 to the listed hydrocarbon fuels were carried out. The analysis approach based on the zoomed in configuration (flame normal statistics) was only used in this chapter for brevity since it was established in the previous chapter that either approach is suitable. Furthermore, the growth rate of PAH concentration in these binary mixtures were estimated with the aim of understanding how modifying the H:C ratios with the addition of H_2 and CH_4 affects the growth rate function. Lastly, the results from the analysis of these mixtures were used to comment on the differences (if any) between adding fuel bound H (through the addition of CH_4) and non-fuel bound H (through the addition of H_2) on PAH formation and growth in the hydrocarbon mixtures studied.

5.1 EXPERIMENTAL PROCEDURE AND FLOW CONDITIONS

The flow conditions for the results presented in this chapter are summarised in Table 5.1. For all the tests conducted in this section, the number of carbon atoms was maintained at a constant value of 12 for the reference case (that is, no H_2 or CH_4 addition) of each of the primary hydrocarbon fuels investigated to enable comparison between them. Hence, the flowrate of the respective primary gases (before the addition of H_2 or CH_4) was 12 slpm, 6 slpm and 4 slpm for C1 (CH_4), C2 (C_2H_6 & C_2H_4) and C3 (C_3H_8 & C_3H_6) fuels respectively. Then for each addition of the secondary fuel (H_2 or CH_4), the flow

rate of the primary fuel was adjusted to maintain a constant total volumetric flowrate of 12 slpm to eliminate bulk velocity effects. In addition, Table 5.1 shows the adiabatic flame temperature for all the mixtures calculated using GASEQ (Morley, 2005).

Table 5.1: Summary of the flow conditions for the fuel mixtures investigated. fp– Primary fuel; fs – secondary fuel; Q_{fp} – volume flow rate of primary fuel, Q_{fs} – volume flow rate of secondary fuel; Q_{air} – volume flow rate of air (fixed at 1.2 slpm), T_{ad} – adiabatic temperature; Re – Reynolds number (fuel)

fp– CH_4, fs – H_2, Q_{air} – 1.2 slpm

Q_{fp} (slpm)	Q_{fs} (slpm)	Q_{fs} (%)	H:C	T_{ad}	Re
12.0	0.0	0	4.00	2226.0	445.5
11.6	0.4	3	4.07	2231.1	440.0
11.2	0.8	7	4.14	2237.8	434.6
10.8	1.2	10	4.22	2242.8	429.4
10.4	1.6	13	4.31	2247.7	426.8
10.0	2.0	17	4.40	2254.3	419.3

fp – C_2H_6, fs – H_2, Q_{air} – 1.2 slpm

Q_{fp} (slpm)	Q_{fs} (slpm)	Q_{fs} (%)	H:C	T_{ad}	Re
6.0	0.0	0	3.00	2260.4	234.5
5.6	0.4	7	3.07	2269.3	228.5
5.2	0.8	13	3.15	2276.8	222.8

Qfp (slpm)	Qfs (slpm)	Qfs (%)	H:C	T_{ad}	Re
4.8	1.2	20	3.25	2285.6	217.3
4.4	1.6	27	3.36	2294.3	210.9
4.0	2.0	33	3.50	2301.7	207.2

fp – C_3H_8, fs – H_2, Q_{air} – 1.2 slpm

Qfp (slpm)	Qfs (slpm)	Qfs (%)	H:C	T_{ad}	Re
4.0	0.0	0	2.67	2267.3	160.5
3.6	0.4	10	2.74	2279.2	153.3
3.2	0.8	20	2.83	2290.9	147.6
2.8	1.2	30	2.95	2302.5	141.4
2.4	1.6	40	3.11	2314.1	135.8
2.0	2.0	50	3.33	2325.6	131.3

fp – C_2H_4, fs – H_2, Q_{air} – 1.2 slpm

Qfp (slpm)	Qfs (slpm)	Qfs (%)	H:C	T_{ad}	Re
6.0	0.0	0	2.00	2370.1	234.5
5.6	0.4	7	2.07	2370.3	227.0
5.2	0.8	13	2.15	2370.6	222.8
4.8	1.2	20	2.25	2371.1	216.0
4.4	1.6	27	2.36	2371.7	210.9

Q_fp (slpm)	Q_fs (slpm)	Q_fs (%)	H:C	T_ad	Re
4.0	2.0	33	2.50	2372.2	206.0

fp – C_3H_6, fs – H_2, Q_air – 1.2 slpm

Q_{fp} (slpm)	Q_{fs} (slpm)	Q_{fs} (%)	H:C	T_{ad}	Re
4.0	0.0	0	2.00	2335.0	160.5
3.6	0.4	10	2.07	2339.1	154.3
3.2	0.8	20	2.17	2343.4	147.6
2.8	1.2	30	2.29	2347.9	142.3
2.4	1.6	40	2.44	2352.4	136.6
2.0	2.0	50	2.67	2357.1	131.3

fp – C_2H_6, fs – CH_4, Q_air – 1.2 slpm

Q_{fp} (slpm)	Q_{fs} (slpm)	Q_{fs} (%)	H:C	T_{ad}	Re
6.0	0.0	0	3.00	2260.4	234.5
4.8	1.2	20	3.11	2253.6	232.9
3.6	2.4	40	3.25	2246.7	229.9
3.3	2.7	45	3.29	2245.0	228.5
3.0	3.0	50	3.33	2243.3	228.5
2.7	3.3	55	3.38	2241.6	228.5
2.4	3.6	60	3.43	2239.9	227.0

Q_fp (slpm)	Q_fs (slpm)	Q_fs (%)	H:C	T_ad	Re
1.8	4.2	70	3.54	2236.4	225.6
1.2	4.8	80	3.67	2232.9	224.2

fp – C_3H_8, fs – CH_4, Q_{air} – 1.2 slpm

Q_{fp} (slpm)	Q_{fs} (slpm)	Q_{fs} (%)	H:C	T_{ad}	Re
4.0	0.0	0	2.67	2267.3	160.5
2.8	1.2	30	2.83	2255.0	156.3
2.4	1.6	40	2.91	2250.9	155.3
2.2	1.8	45	2.95	2248.9	154.3
2.0	2.0	50	3.00	2246.8	154.3
1.6	2.4	60	3.11	2242.7	152.3

fp – C_2H_4, fs – CH_4, Q_{air} – 1.2 slpm

Q_{fp} (slpm)	Q_{fs} (slpm)	Q_{fs} (%)	H:C	T_{ad}	Re
`6.0	0.0	0	2.00	2370.1	234.5
4.8	1.2	20	2.22	2342.9	231.4
3.6	2.4	40	2.50	2314.9	228.5
2.4	3.6	60	2.86	2286.2	227.0
2.2	5.1	70	3.08	2271.4	274.4
2.2	8.8	80	3.33	2256.5	410.9

		fp – C₃H₆, fs – CH₄, Qair – 1.2 slpm			
Q$_{fp}$ (slpm)	**Q$_{fs}$ (slpm)**	**Q$_{fs}$ (%)**	**H:C**	**T$_{ad}$**	**Re**
4.0	0.0	0	2.00	2335.0	160.5
2.8	1.2	30	2.25	2303.4	157.4
2.4	1.6	40	2.36	2292.7	155.3
2.2	1.8	45	2.43	2287.3	155.3
2.0	2.0	50	2.50	2281.9	154.3

5.2 EFFECT OF H_2 ADDITION ON PAH FORMATION

Figure 5.1 shows the normalised PAH LIF signal for the five primary hydrocarbon fuels – C_2H_6, C_2H_4, C_3H_8, C_3H_6 and CH_4 - expressed as a function of percent H_2 addition (v/v) for three different heights along the flame front, L_f. For each L_f, the PAH LIF signal for various percent H_2 addition were normalised with the maximum PAH LIF signal. It can be observed in the cases of C_2H_4, C_3H_8 and C_3H_6 (Figure 5.1 (b), (c) and (d) respectively) that there is no significant variation in magnitude of the reduction levels in PAHs with the addition of H_2 as the L_f increases. This could be attributed to the following; Since formation of first ring is an important step in the growth of PAHs and subsequent soot formation (Sidebotham and Glassman, 1992; Wang and Frenklach, 1997; Michelsen, 2017), it can be deduced that for C_2H_4, C_3H_8 and C_3H_6, the formation of the first ring and subsequent growth to larger multiple

ringed PAHs occur at a very fast rate at lower heights, and reach the saturation point such that further growth at higher heights is not observed. These two effects shroud the impact of H_2 addition on PAH growth in these fuels as the height increases. However, in the CH_4 case, as can be seen from Figure 5.1 (e), addition of H_2 to CH_4 showed higher reductions at higher heights, for example a 17% H_2 addition in CH_4 resulted in a 76% and 44% reduction in PAH LIF signal for 6 mm and 4 mm heights respectively. This is consistent with observations in chapter 4 and it was attributed to the effectiveness of H_2 in impeding the growth of smaller ring PAHs closer to the burner lip. This limits the concentration of smaller ring PAHs available for growth to larger ring PAHs at higher heights above the burner lip. It is possible in the CH_4 case that though the efficiency of PAH growth is high, it does not have enough PAH concentration available to achieve the saturation point. This implies that most of the growth process would take place in the early phase where the growth process is fast hence the addition of H_2 is expected to be very effective. It is evident from Figure 5.1 that with the increase in the hydrocarbon fuel's propensity to form PAH (that is, going from CH_4 to C_3H_6), the magnitude of reduction in PAH levels with increasing height becomes less significant.

Addition of H_2 to CH_4 in this study was limited to 17%, as above that level PAH LIF signal dropped very low leading to very high uncertainty in PAH measurements. Hence comparison between the effect of H_2 addition on the primary fuels will focus on H_2 addition levels of below 17%. Comparing PAH LIF signal at 14% H2 addition (Figure 5.1) shows that the order of PAH reduction from high to low is $CH_4 > C_2H_6 > C_2H_4 > C_3H_8 > C_3H_6$. This order is

as expected due to the increasing carbon content and presence of double bonds except for propane showing lower reduction (~30%) than ethylene (~48%) with H_2 addition. This is in spite the absolute peak PAH LIF signal in ethylene (*3520 a.u.)* being more than twice that of propane (*1380 a.u.*). According to Frenklach (Frenklach, 1988), the [H]/[H2] ratio (ratio of hydrogen atom concentration to molecular hydrogen concentration) is the controlling parameter for the growth of PAH up to the formation of the first soot nuclei. The exception highlighted above could be due to the reason proposed by Gülder *et al*. (1996) for the differences they observed with the addition of hydrogen in diffusion flames of alkanes and alkenes. They explained that in C_2H_4 pyrolysis, the production of [H2] and [H] is minimal compared to the concentration produced in C_3H_8 pyrolysis, hence the addition of H_2 in C_2H_4 can be assumed to influence the [H]/[H2] ratio significantly reducing the rate of PAH production while there might be enough [H] and [H2] formed from C_3H_8 pyrolysis thereby reducing (shrouding) the effects of added molecular hydrogen on PAH reduction in C_3H_8.
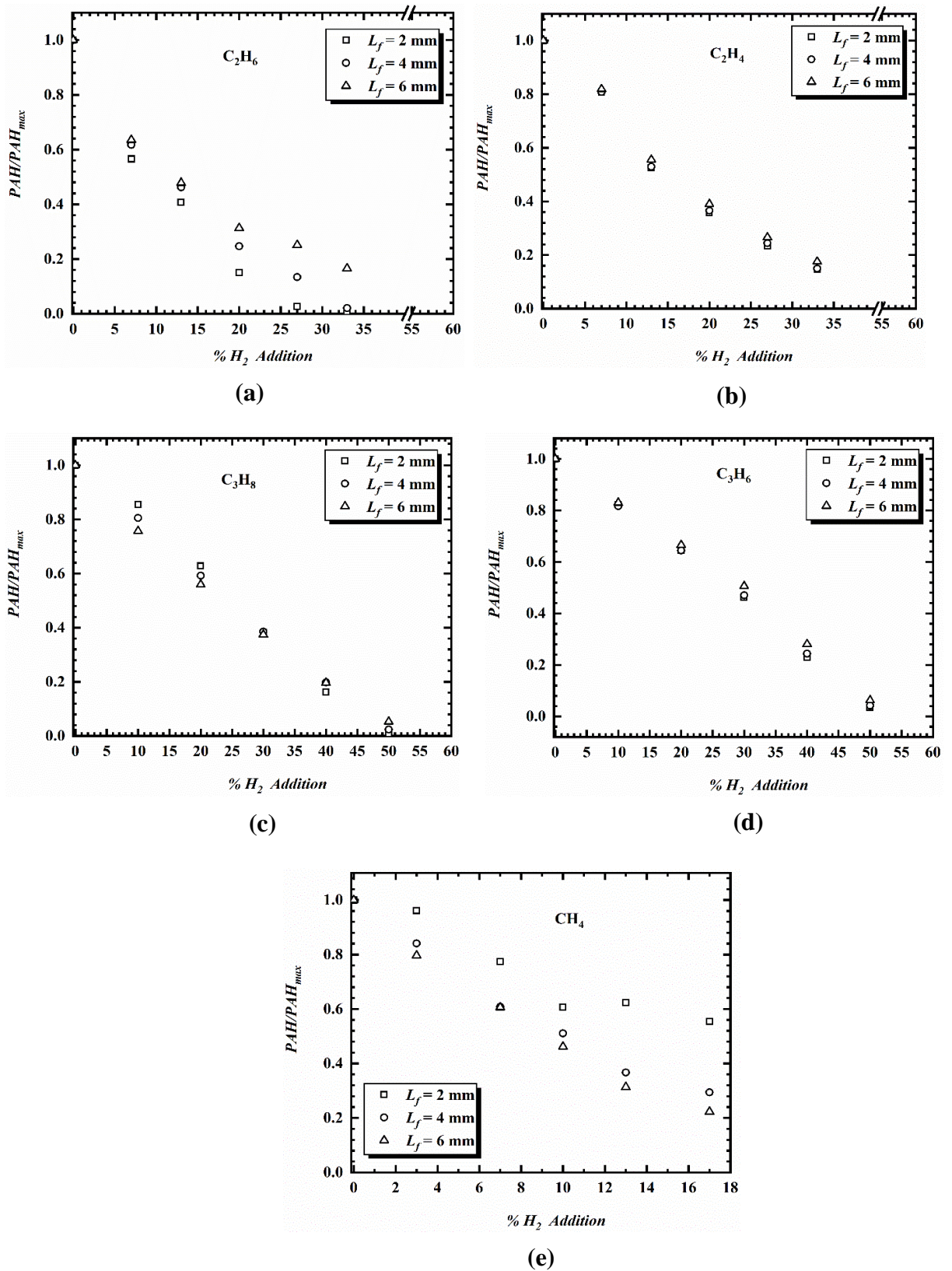
Figure 5.1: Variation in the PAH LIF signal normalised using the reference case value as a function of percent H_2 addition (v/v) at three different HAB for (a) C_2H_6 (b) C_2H_4 (c) C_3H_8 (d) C_3H_6 and (e) CH_4.

5.3 EFFECT OF CH_4 ADDITION ON PAH FORMATION

Figure 5.2 presents the normalised values of PAH LIF signal as a function of percentage CH_4 addition (v/v) for three different heights along the flame front, L_f. Each test condition was normalised with its respective reference case value (that is, primary fuel with no CH_4 addition). A monotonic decrease in PAH LIF signal with CH_4 addition is seen for all the fuels tested (Figure 5.2 (b)-(d)) except for C_2H_6 (Figure 5.2 (a)). With C_2H_6, an initial increase in PAH LIF signal is observed with CH_4 addition up to ca. 55% which then sharply reduces. It is pertinent to note also that the PAH LIF signal at all heights in the C_2H_6-CH_4 binary mixture prior to 70% CH_4 addition was higher than the reference case value. This is due to the synergistic effect between CH_4 and C_2H_6 which results in the corresponding PAH LIF signal of the binary mixture to be higher than those of each individual components in the mixture (Hwang *et al.*, 1998; Yoon, Lee and Chung, 2005). This synergistic effect will be further discussed later in this section.

It can also be observed from Figure 5.2 that the highest reduction in PAH LIF signal occurs at the lowest L_f of 2 mm for all the fuels. For example, with 40% CH_4 addition, a 30% reduction in PAH LIF signal was seen at L_f = 2 mm, while a 16% reduction was seen at 6 mm. The reason for this observation could be explained in light of the following two studies in literature. Senkan and Castaldi (Senkan and Castaldi, 1996) observed two important effects in their study of PAH formation in CH_4 combustion; firstly, the first ring formation in the CH_4 flame increased rapidly as the height increased along the reaction zone, and

secondly the rate of growth from larger ring PAHs to soot was reduced which resulted in a rich pool of gas phase PAHs upstream of the flame. In another study, Hepp *et al.* (Hepp, Siegmann and Sattler, 1995) observed some larger PAHs appearing before smaller ones which they attributed to smaller PAHs reacting efficiently via the coagulation mechanism to form larger PAHs at a rapid rate. Hence, it could be said that with the addition of CH_4 in these fuels, the rapid growth of PAHs counteracts the ability of CH_4 to reduce the growth of PAHs (both by mass growth and coagulative mechanism) such that the effect is observed maximally at the point of introduction (closer to the burner lip). Thus, the efficiency of the reaction/growth process in this region closer to the burner lip could potentially make the effect of CH_4 addition more efficient in these positions closer to the burner lip. Also, it can be seen that similar to the observation in the H_2 case, the magnitude of reduction in PAH levels as the L_f increases is relatively the same.

Furthermore, comparing PAH reduction between the different hydrocarbon fuels, it can be seen from Figures 5.2 (a) – 5.2 (d) that the trend of reduction in PAH LIF signal with CH_4 addition follows the sequence $C_3H_6 > C_2H_4 > C_3H_8 > C_2H_6$. For example, at a height of 4 mm, with 40% CH_4 addition, there were 55%, 44%, and 18% reduction in PAH LIF signal for C_3H_6, C_2H_4 and C_3H_8 respectively. Similar trends are observed for other heights and percentage CH_4 addition as shown in Figure 5.2.

Now comparing the effect of H_2 and CH_4 addition on the primary fuels, Figure 5.1 and Figure 5.2 shows that the addition of CH_4 to C_2H_4 and C_3H_6 showed

slightly more variation in PAH LIF signal between heights when compared with H_2 addition to the same fuels. Overall reduction in PAH LIF signal was more effective for all fuels with H_2 addition than CH_4 addition. It can be seen in Figure 5 that at a height of 2 mm with 30% H_2 addition, reduction levels in PAH LIF signal were 52%, 60% and 78% for C_3H_6, C_3H_8 and C_2H_4 respectively as compared to 44%, 28% and 40% for C_3H_6, C_3H_8 and C_2H_4 with 30% CH_4 addition respectively for same conditions in Figure 5.2.


(a)

(b)

(c)

(d)
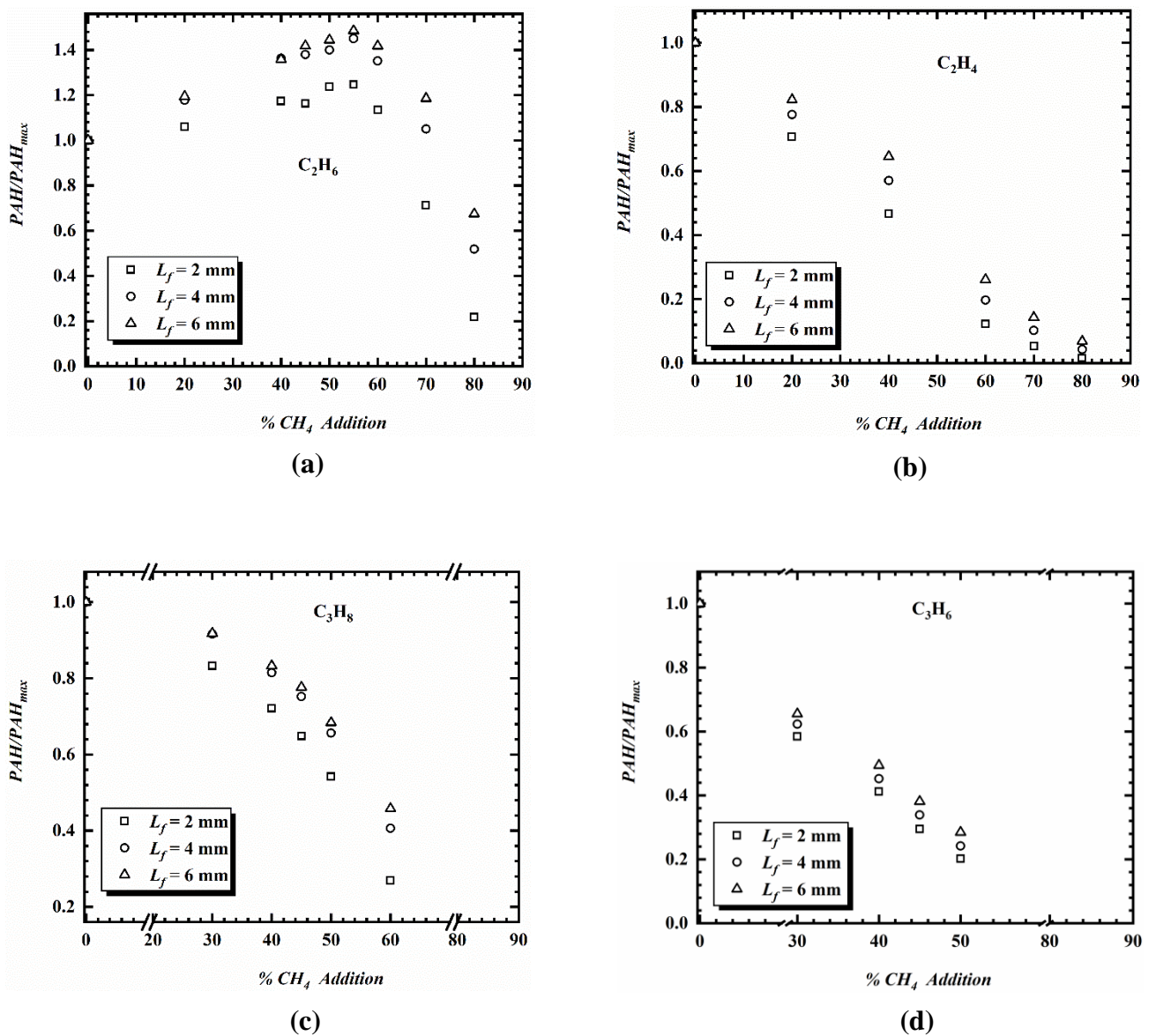
Figure 5.2: Variation in the *PAH* LIF signal normalised using the reference case value as a function of percent CH_4 addition (v/v), at three different HAB for (a) C_2H_6 (b) C_2H_4 (c) C_3H_8 and (d) C_3H_6.

126

To further explain the synergistic effect of the CH_4-C_2H_6 binary mixture, the radially integrated PAH LIF signal, $PAH(h)$, for the binary mixture was derived similar to the procedure described in Ref. (Mikofski *et al.*, 2007), and is shown in Equation 1 below. The radially integrated PAH LIF signal provides a measure of the total PAH LIF signal in the flame by factoring the change in area of the conically shaped IDF flame.

$$PAH\,(h) = 2\pi \int_0^R rp\,(r,h)\,dr \;=\; 2\pi \sum_{i=1}^R r_i p\,(r_i,h)\,\Delta r \qquad (1)$$

Where r and h represent the radial and axial positions with reference to the burner centreline and the burner exit plane, R is the radius of the integrated path length (~300 mm), the signal at (r, h) is represented by $p(r,h)$ and Δr is the pixel resolution (~0.25 mm/pixel).

Radially integrated PAH LIF signal values for C_2H_6 represented as $PAH_{C_2H_6}$ for all CH_4 addition tests were normalised with the maximum value of the radially integrated CH_4 reference case and plotted against the corresponding fuel component H:C ratio, as shown in Figure 5.3. Additionally, Figure 5.3 also shows the normalised values of the corresponding adiabatic temperature (calculated using GASEQ (Morley, 2005)) for the binary mixtures. Most reactions leading to PAH and soot formation in combustion systems have been shown to be temperature dependent (Sidebotham and Glassman, 1992; Appel, Bockhorn and Frenklach, 2000). Hence, determining the temperature of CH_4-C_2H_6 binary fuel mixture could be key to explain the observed trend in PAH formation. Figure 5.3 shows that despite the fuel bound H content

increasing (carbon content reducing) from left to right, the PAH LIF steadily increases with CH_4 addition up to a H:C of 3.38 (corresponding to 55% CH_4). Though the PAH LIF decreased beyond this H:C value, the magnitude of PAH LIF was still higher than the value of C_2H_6 reference case (represented by H:C of 3.0) up to H:C of 3.54 (corresponding to 70% CH_4). Hence, this increase in PAH levels implies some kind of a synergistic effect between CH_4 and C_2H_6 which has also been observed by previous studies (Roesler *et al.*, 2003; Yoon, Lee and Chung, 2005; Trottier *et al.*, 2007). This increase in PAH levels cannot be attributed to increased rates of H abstraction and acetylene addition (HACA). These reactions are favoured by higher temperatures (Hwang *et al.*, 1998) and adiabatic temperatures can be seen to decrease monotonically in Figure 5.3. Hence, the following paragraph presents another possible explanation of the enhancement of PAH levels due to the binary mixture of CH_4 and C_2H_6.

The role of methyl radicals ($CH_3{}^*$) in the formation of PAH has been reported previously (Bittner and Howard, 1981; Roesler *et al.*, 2003; Yoon, Lee and Chung, 2005). The thermal decomposition of C_2H_6 and CH_4 lead to the production of $CH_3{}^*$ which was shown by Roesler et al. (Roesler *et al.*, 2003) to promote the formation of PAH via the propargyl recombination reaction through the odd-carbon numbered species channel. Even though the addition of CH_4 does increase the H:C ratio of the overall mixture (that is, it lowers the carbon content), it is difficult to release the H atom from CH_4, as compared to producing $CH_3{}^*$ from C_2H_6. This is because the bond energies of the $C-C$ bond in C_2H_6 (376.1 kJ/mol) are considerably lower than that of the $C-H$

bond in CH_4 (438.6 kJ/mol) (Solomons and Fryhle, 2011; Ruscic, 2015). Hence, the concentration of $CH_3{}^*$ produced by the binary fuel mixture system possibly outweighs the effect of the H atom released thereby resulting in the enhancement of the formation of PAHs as observed in Figure 5.3.
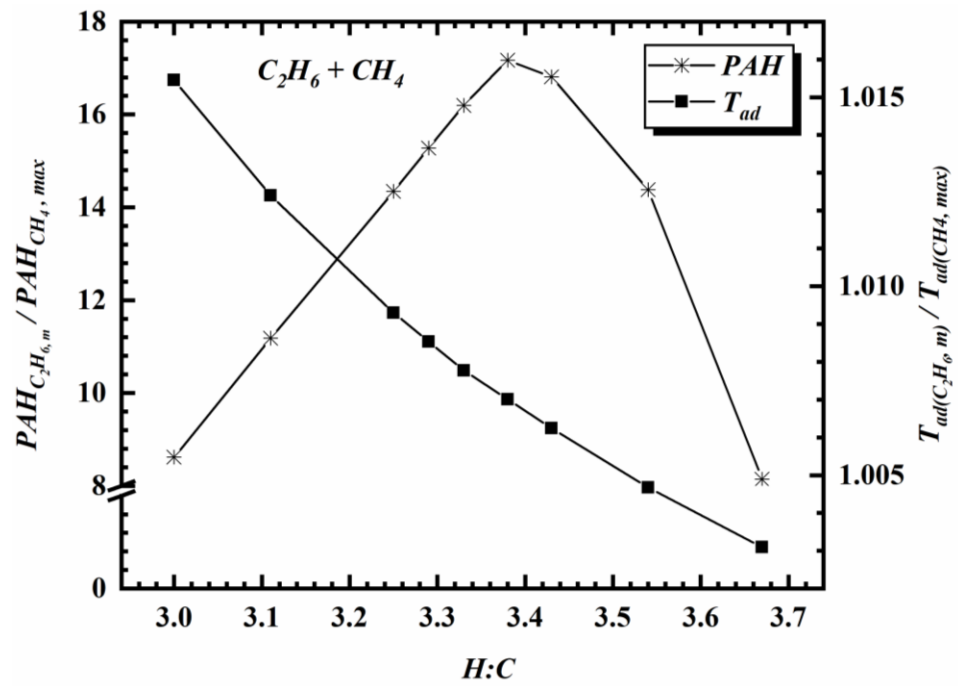
Figure 5.3: Integrated *PAH* LIF signal of a mixture of ethane and CH_4 normalised with the maximum PAH LIF signal of CH_4 expressed as a function of H:C ratios (same normalisation routine for the Mixture adiabatic temperature also presented)

5.4 OH-PAH PEAK DISTANCE AND PAH PROFILE WIDTH WITH H_2 ADDITION

Figure 5.4 presents the distance (x_{pk}) between the location of the OH and PAH peak levels, normalised with the value of the reference case ($x_{pk,0}$), plotted as a function of different percent H_2 addition for four different heights along the

flame front, L_f. The OH peak is indicative of the flame location (hence peak temperature) and is used as the reference point for the calculation of x_{pk}. Additionally, ΔT_{ad}, which is the difference between the adiabatic temperature of the reference case (0% H_2 addition) and the maximum case of H_2 addition in the binary mixture, is included on each of the graphs in Figure 5.4. A positive value of ΔT_{ad} indicates an increase in temperature while a negative value shows a decrease in temperature. It can be seen from Figure 5.4 that there is a slight increase in peak-to-peak distance with the addition of H_2 to all the hydrocarbon primary fuels, indicating that peak PAH formation occurred increasingly away from the peak temperature region in the flame as H_2 was added. Up to 20% increase in the peak distance was observed with about 30% H_2 addition for all the fuels investigated. This observed trend could be attributed to the local variation in the temperature gradient in the flame as a function of H_2 addition. This is similar to observations in Mikofski *et al.*(2007) and Shaddix *et al.* (2005) where the temperature gradient in the flow field was reported as the reason for the variations observed in the spatial locations of the peak OH, PAH and soot PLIF signals. Also, as L_f increases, there is no significant change in the peak distance trend with the addition of H_2 which shows that it is independent of the height above the burner.

Figure 5.5 shows the normalised PAH profile width (w_{PAH}) at four different heights along the flame front (L_f) presented as a function of percent H_2 addition for the five primary hydrocarbon fuels. The PAH profile width was obtained at full-width half-maximum (FWHM) and normalised with the PAH profile width of the reference case. A slight reduction in PAH profile width can

be observed with the addition of H_2 for the C2 and C3 fuels investigated. With the CH_4 and H_2 binary mixture, though the signal to noise ratio (SNR) is low due to the low concentration of PAHs, a similar trend (to the C2 and C3 fuels) can generally be observed. Additionally, the w_{PAH} along the four different L_f investigated showed similar trend for up to 25% H_2 addition in C_2H_6, up to 12 % H_2 addition in CH_4 and all H_2 additions levels in C_3H_8, C_2H_4 and C_3H_6. The divergence observed in C_2H_6 and CH_4 for conditions higher than the percent H_2 additions stated above could be attributed to possible increase in the thermal diffusivity of the binary mixture due to H_2 addition. However, the general trend remains similar across all the fuels studied.

5.5 OH-PAH PEAK DISTANCE AND PAH PROFILE WIDTH WITH CH4 ADDITION

The peak-to-peak distance (x_{pk}) between the peaks of the OH and PAH profiles normalised with the peak distance of the reference case (0% CH_4 addition) is plotted against the different percent CH_4 addition and presented for four different heights along the flame front, L_f in Figure 5.6. Contrary to observations in the H_2 addition case (Figure 5.4), different trends can be observed across the four fuels investigated. While the x_{pk} increased with CH_4 addition in the alkane primary fuels (C_2H_6 and C_3H_8), it reduced in C_2H_4 and remained constant for C_3H_6. When comparing between different L_f, it can be observed that there is no significant change in x_{pk} with the additions of CH_4 to C_2H_6 , C_3H_8 , C_2H_4 and C_3H_6 (Figure 5.6 (a) - (d)). This is similar to the observations in the H_2 addition case.
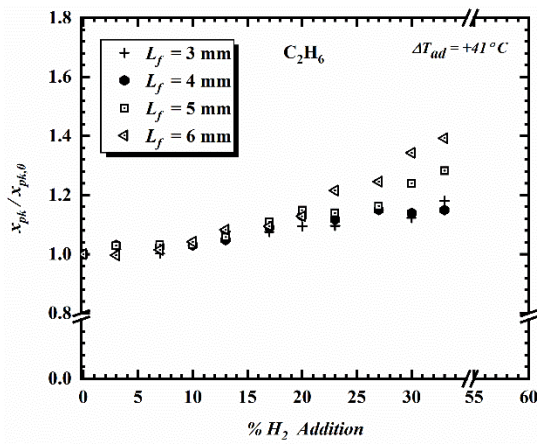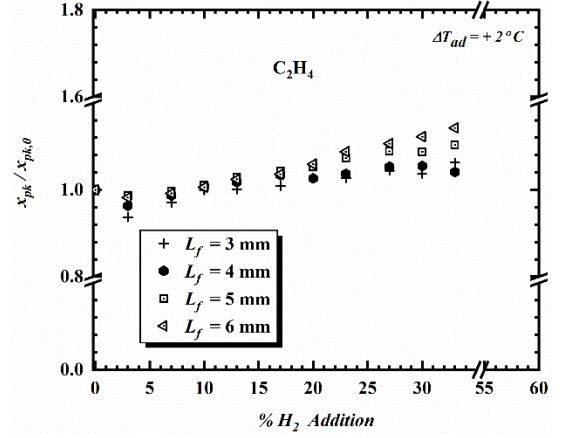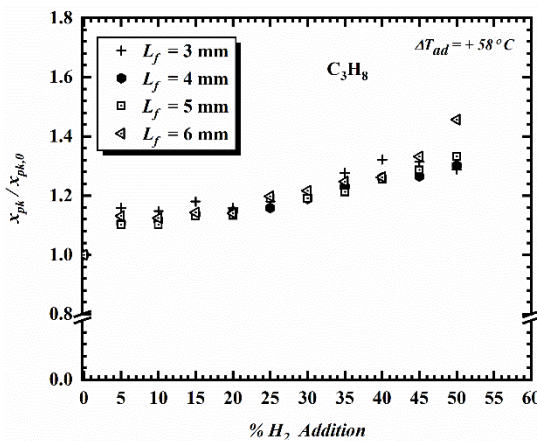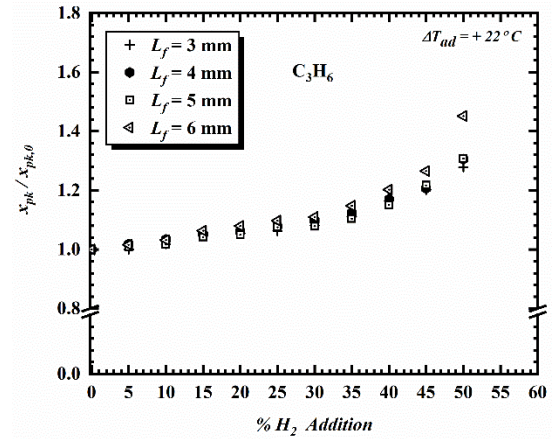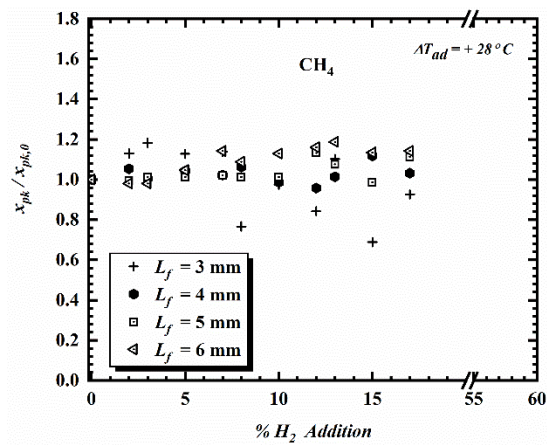
Figure 5.4: Variation in the normalised peak-to-peak distance (x_{pk}) between PAH and OH profiles as function of percentage H_2 additions at four different HABs for (a) C_2H_6 (b) C_2H_4 (c) C_3H_8 (d) C_3H_6 and (e) CH_4 . Change in adiabatic temperature, $\Delta T_{ad} = T_{ad,reference\ case} - T_{ad,fmax}$ (difference in the adiabatic temperatures of the reference case and the maximum H_2 addition)
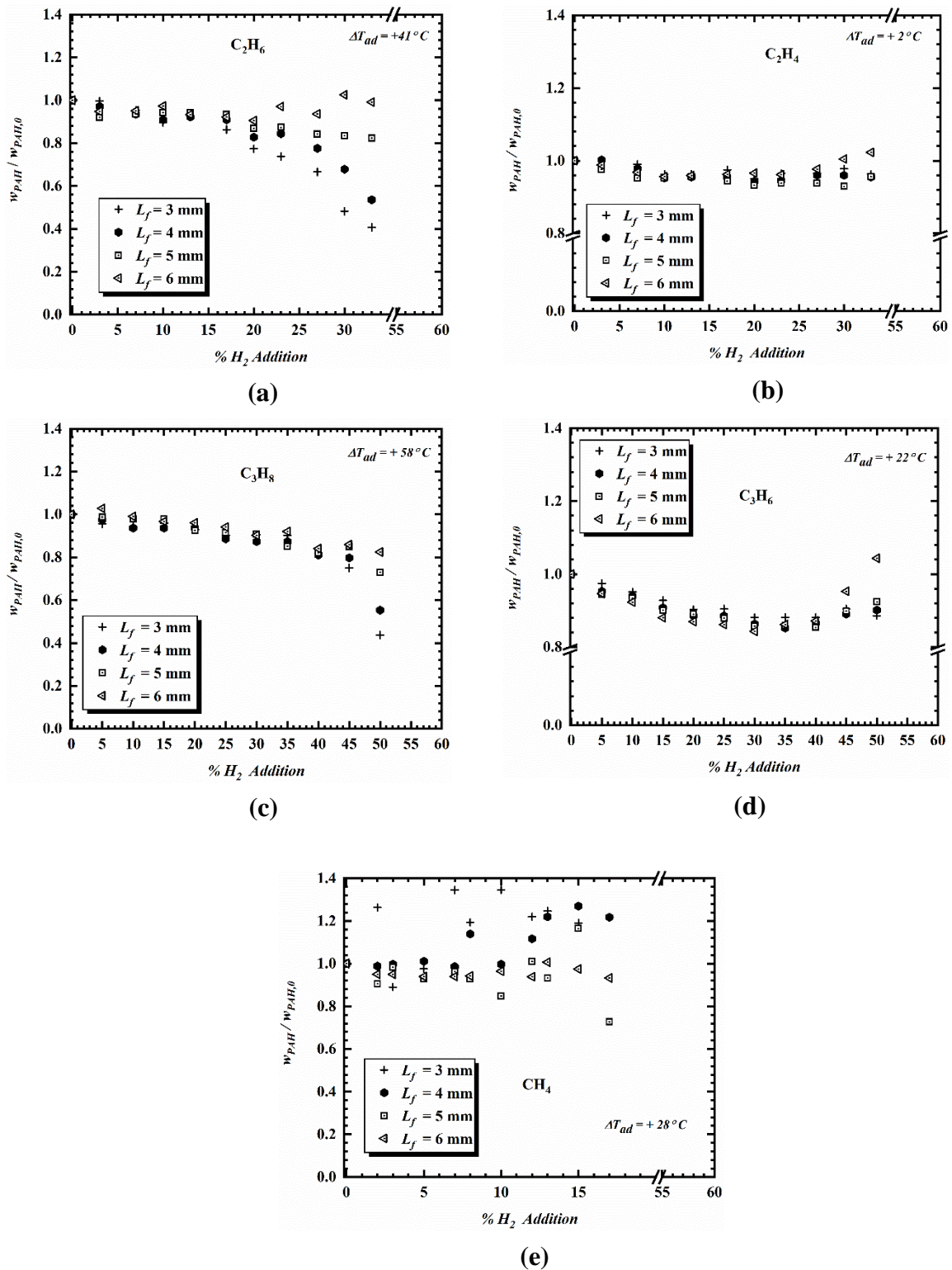
Figure 5.5: Variation in the PAH profile width as a function of percentage H_2 addition at four different HABs for (a) C_2H_6 (b) C_2H_4 (c) C_3H_8 (d) C_3H_6 and (e) CH_4 . Change in adiabatic temperature, $\Delta T_{ad} = Tad, reference\ case - Tad, fmax$ (difference in the adiabatic temperatures of the reference case and the maximum H_2 addition)

133
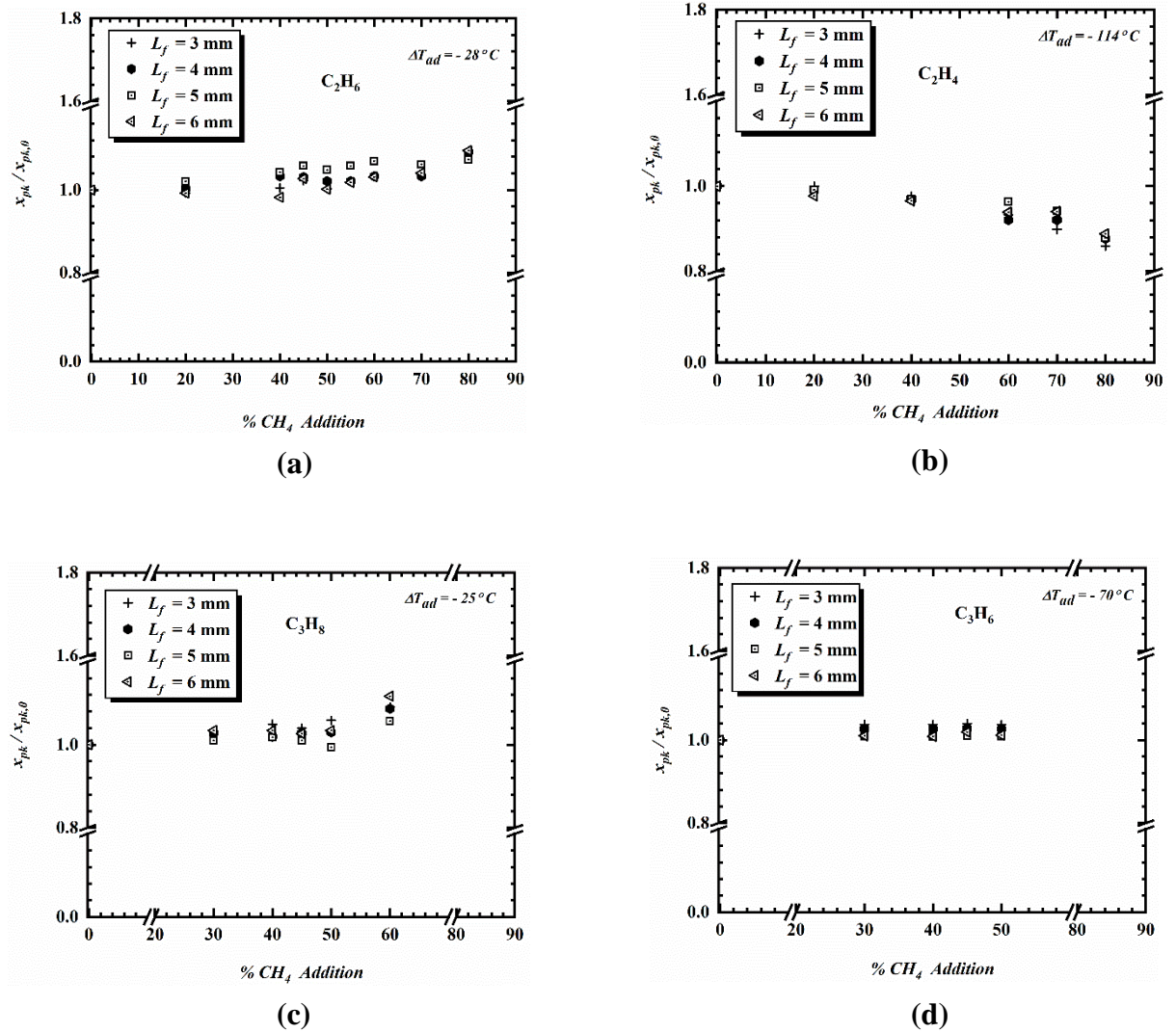
Figure 5.6: Variation in the peak-to-peak distance between PAH and OH profiles as function of percentage CH_4 additions at four different HABs for (a) C_2H_6 (b) C_2H_4 (c) C_3H_8 and (d) C_3H_6.

Figure 5.7 shows the PAH profile width at four different heights along the flame front, L_f, normalised with the w_{PAH} of the reference case and presented as a function of percent CH_4 addition for C_2H_6, C_2H_4, C_3H_8 and C_3H_6. Similar to observations with the addition of H_2 (Figure 5.5) there is no significant variation in w_{PAH} based on height in the primary hydrocarbon fuels investigated.
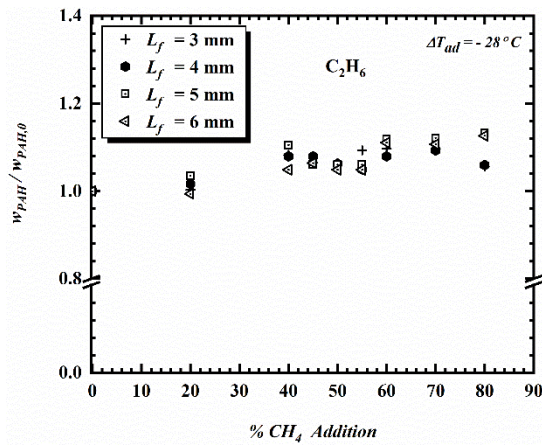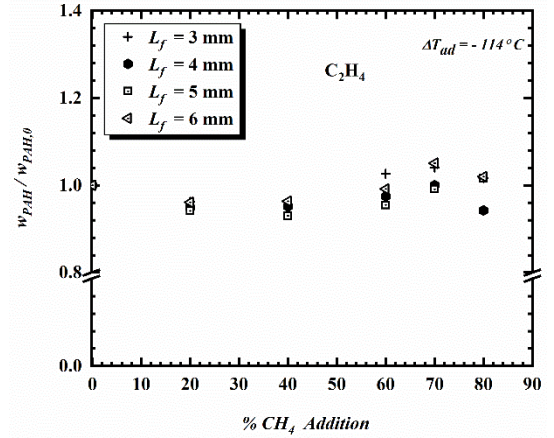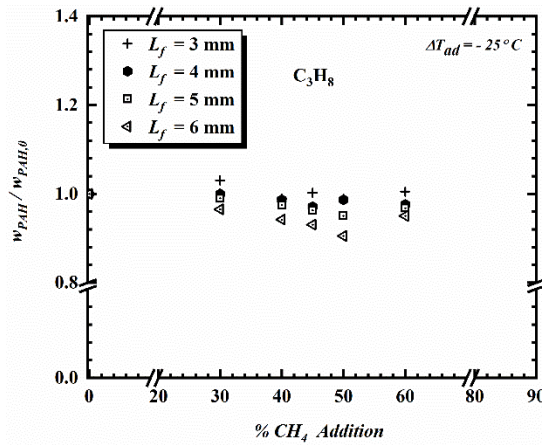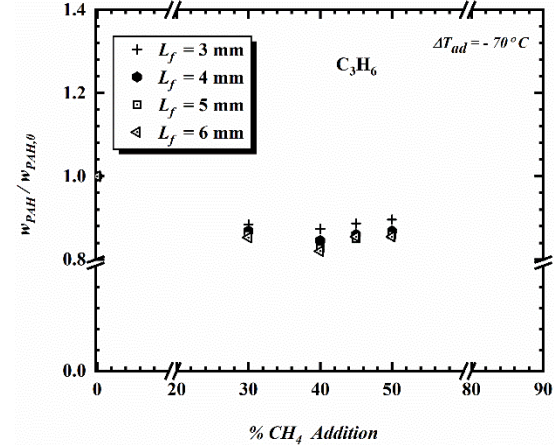
Figure 5.7: Variation in the PAH profile width as a function of percentage CH_4 addition at four different HABs for (a) C_2H_6 (b) C_2H_4 (c) C_3H_8 and (d) C_3H_6.

5.6 GROWTH RATE OF PAH LIF

5.6.1 Effect of H_2 addition

Figure 5.8 shows the growth rate of PAH, $d[PAH]/dL_f$ expressed as a function of PAH LIF signal for different levels of H_2 addition in C_2H_6, C_2H_4, C_3H_8, C_3H_6 and CH_4. Following on from the detailed description in section 3.5, it is

135

necessary to reiterate here that the growth rate refers to the rate of change of PAH LIF signal with L_f. PAH growth rate values as used here were determined relative to distance above the burner lip to indicate PAH formation tendencies. Figure 5.8 shows that for all the fuels tested, the magnitude of the peak growth rate was highest for the reference case (no H_2 addition) and subsequently reduced as the addition of H_2 increased in the primary fuel. It can also be observed from Figures 5.8 (b) and (c) that when the level of addition of H_2 in C_2H_4 and C_3H_8 is above 20%, and similarly in Figure 5.8 (e) when the H_2 addition in CH_4 is above 10%, the magnitude of the growth rate of PAH becomes similar. This could potentially suggest that there is a point (specific to each fuel) above which the global growth rate of PAH LIF in the fuels tested is not distinguishable even though the local reduction in PAH LIF is still present at this point. It was observed previously in Figures 5.1 (b), (c), and (e) that, at the same additions of H_2, the local PAH LIF showed significant reduction; with 20% H_2 addition in C_2H_4 and C_3H_8, ~ 60% reduction and 40 % reduction in PAH levels were observed respectively while 10% H_2 addition in CH_4 showed ~50% reduction in PAH LIF. This trend can be more clearly illustrated with the C_3H_6 case (see Figure 5.8 (d)); the graph for the reference case (0% H_2) is less steep when compared to the conditions with H_2 addition. It can be seen that as more H_2 is added in C_3H_6, the slope of the respective graphs becomes steeper indicating an increase in the potential for growth due to the reduced PAH level. In the formation and growth of PAH, it is expected that prior to observable PAH growth, an activation barrier point at the early growth stage involving typically 1-3 rings must be exceeded. There is a possibility that because the initial PAH concentration in the C_3H_6 flame with no H_2 addition is

orders of magnitude higher than the activation barrier requirements such that further growth in PAH levels as L_f increases is not distinguishable. If this is the case, it is reasonable to assume that there is a possibility that PAH growth in C_3H_6 is self-limiting (slower growth rates). The possibility of self-limiting growth of PAH suggests that the corresponding slower growth rates could possibly be due to self-assembly of PAH as an alternative growth mode. Furthermore, from the discussions above, it is evident that the addition of H_2 is not directly proportional to the growth rate of PAH as for all cases studied even tripling the level of H_2 addition does not result in a corresponding reduction in the rate of growth of PAH.
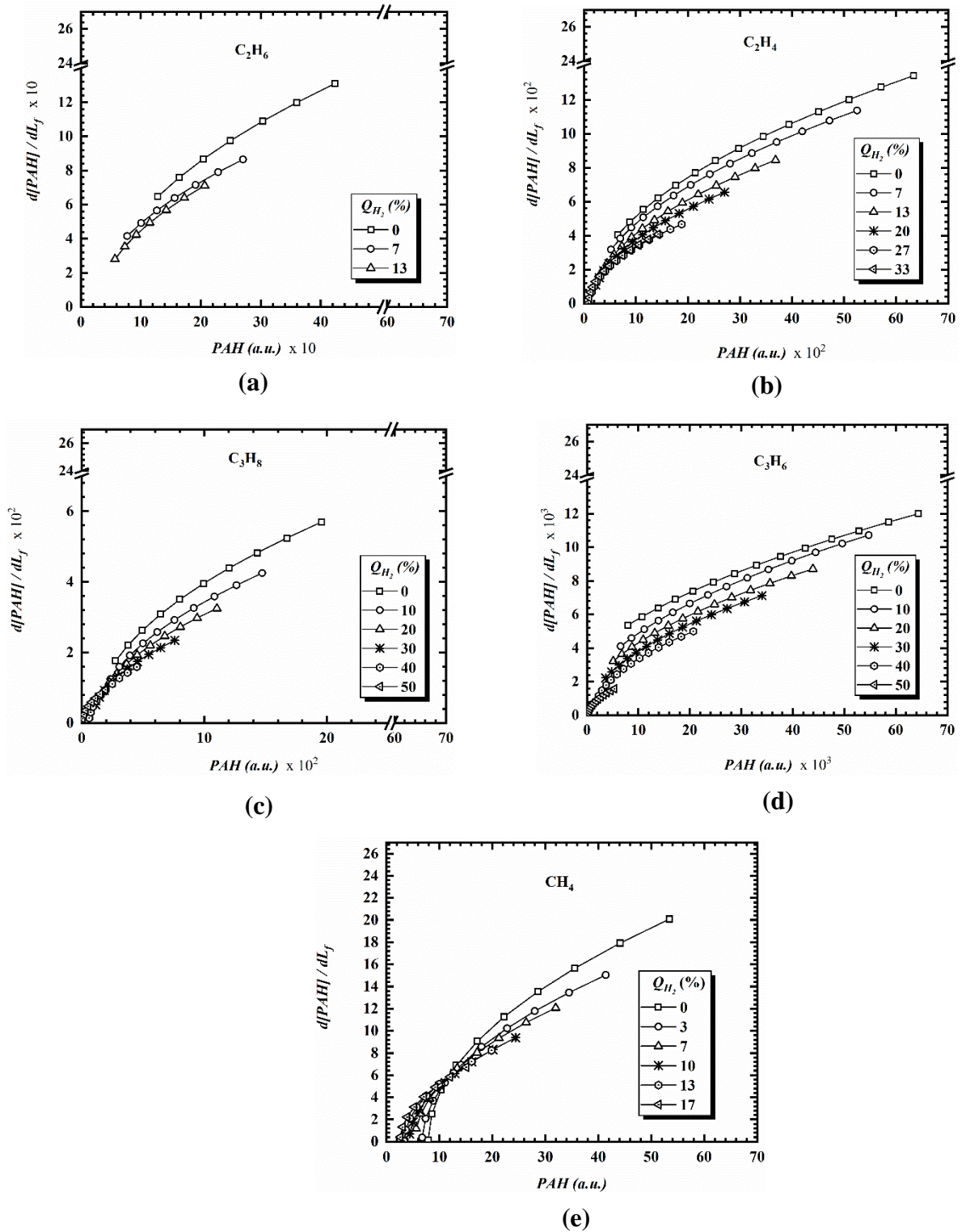
Figure 5.8: The growth rate of PAH expressed as a function of PAH LIF signal for different levels of H_2 addition in (a) C_2H_6 (b) C_2H_4 (c) C_3H_8 (d) C_3H_6 and (e) CH_4.

5.6.2 Effect of CH_4 addition

The rate of growth of PAH for C_2H_6, C_2H_4, C_3H_8, and C_3H_6 with different levels of CH_4 addition is presented in Figure 5.9. Similar to the observations in Figure 5.8 for the H_2 addition case, addition of CH_4 reduces the rate of growth of PAH LIF and above certain CH_4 additions, the growth rate become similar. For example, in C_3H_8 and C_2H_4 between the reference case and up to 40% CH_4 addition, the growth rate is not significantly different. With C_2H_4, the growth rate only shows difference above 60% CH_4 addition levels even though the local concentration of PAH showed marked reduction (~ 80% reduction in PAH levels in Figure 5.2 (b) with 60% CH_4 addition). Comparing Figures 5.8 and 5.9, it is evident that the addition of CH_4 is not as effective as H_2 in reducing the growth rate of PAH concentration. This could be attributed to difficulty in breaking the C-H bond in CH_4 to release H atom as compared to the addition of H_2 which provides H_2 molecule readily available for ring formation and growth of PAHs (Yoon, Lee and Chung, 2005). Additionally, preferential diffusive effects could play a role in the different effects on PAH growth observed with H_2 and CH_4 addition since H_2 is a considerably more diffusive and reactive molecule than CH_4 (H_2 is about 80% more diffusive than CH_4).

Now considering the rate of growth of PAH concentration for additions of both H_2 and CH_4, two regions of growth can be observed from Figures 5.8 and 5.9; an initial region where the growth rate of PAH concentration, $d[PAH]/dL_f$ is linear and faster and then a subsequent region where $d[PAH]/dL_f$ becomes non-linear and starts to slow down. The first region corresponds to early

formation stages with lower concentration of PAH. This is demonstrated in Figures 5.8 and 5.9 by very steep gradients. This could be attributed to the region in the flame mainly dominated by active formation of smaller PAHs, and the onset of growth from smaller PAHs to larger PAHs closer to the burner lip. Here, there is an abundance of active sites and higher propensity for further growth (early growth phase). In the experimental study of fuel rich laminar premixed CH_4 flame by Senkan and Castaldi (1996), the authors observed that the benzene mole fractions obtained by GC-MS analysis increased rapidly along the reaction zone due to the increase in methyl radicals which enhanced benzene formation through the C_3H_3 recombination routes. A similar rapid increase in the concentration of naphthalene was observed in the main reaction zone of the rich C_2H_4 premixed flame studied by Castaldi *et al.* (1996). The authors concluded that the increase in the production of benzene coupled with the O_2 molecule available in the main reaction zone favoured the rapid formation of cyclopentadienyl responsible for naphthalene formation. The second region corresponds to areas of increased PAH concentration where possibly only growth to larger ring PAHs prevail. Here, the concentration of larger PAHs increase until saturation point at which point the growth slows and nucleation to soot particles commences.
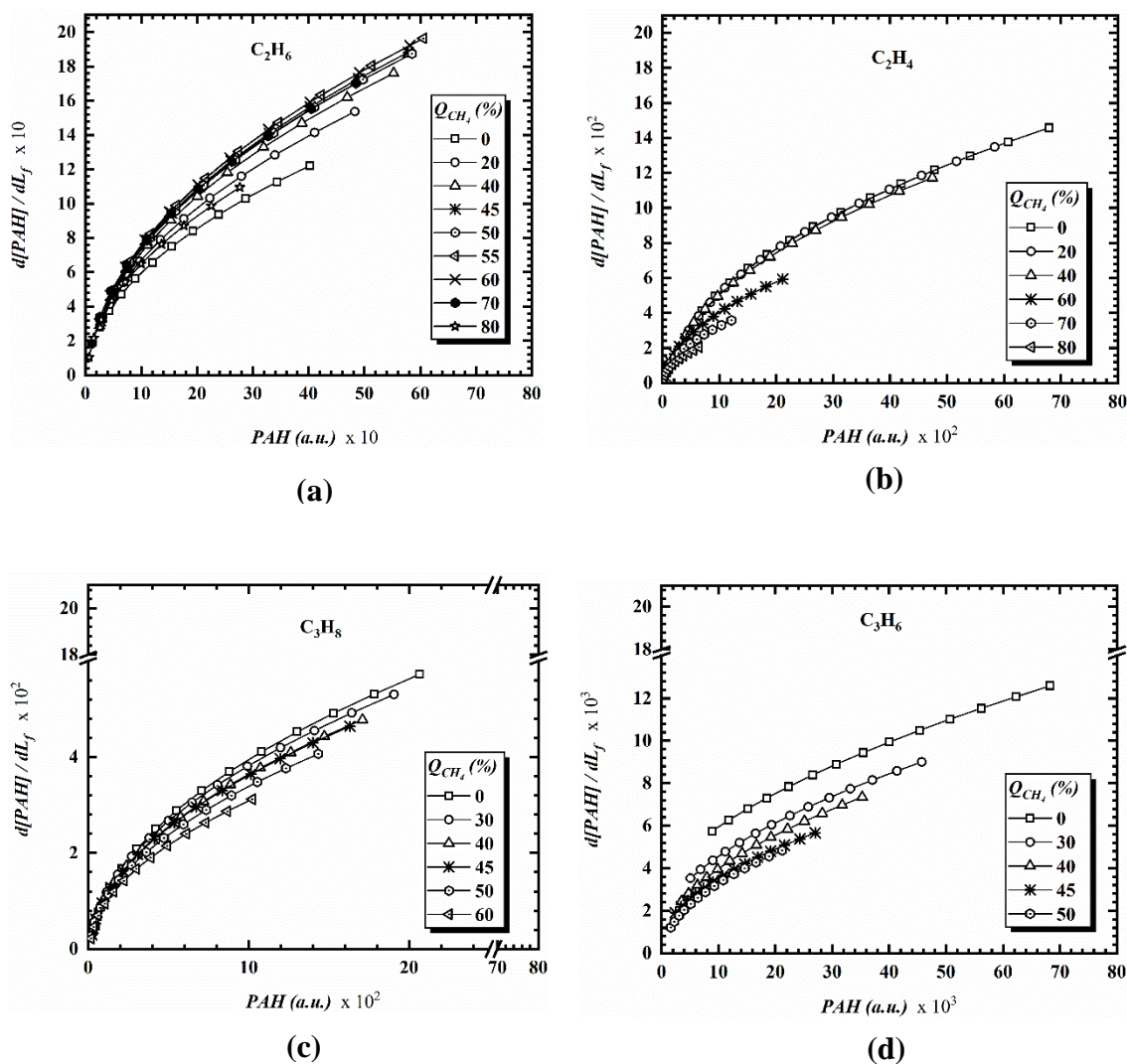
Figure 5.9: The growth rate of PAH expressed as a function of PAH LIF signal for different levels of CH_4 addition in (a) C_2H_6 (b) C_2H_4 (c) C_3H_8 and (d) C_3H_6.

A similar observation regarding saturation 'point' was presented by Mitra *et al.* (2019) in their study of n-dodecane doped methane co-flow diffusion flame using GC/MS analysis and numerical modelling. The authors reported a plateau in the concentration of cyclopenta(def)phenanthrene (A3R5 - 4 ring PAH) prior to soot nucleation which was attributed to PAHs being incorporated

into the young soot. Additionally, from the mole fraction profiles of larger PAHs (3 rings and above) presented in the experimental studies by Inal and Senkan, (2002), the near plateau region can be observed as the HAB increased which was also reproduced by the modelling study in Ref. (Park *et al.*, 2017). This observed saturation in the CH_4 addition cases shown in Figure 5.9, clarifies a similar observation for the binary mixture of H_2 and C_3H_6. As the concentration of PAH increases, the non-linear growth region dominates showing the saturation clearly. The saturation in PAH growth could be attributed to the self-limiting growth characteristics of PAH. With increased availability of PAHs for growth and the corresponding reduction in growth rate, it could be argued as in the H_2 and C_3H_6 case, that the slower growth observed is due to dynamic self-assembly of PAHs (maybe through dimerisation). This provides experimental insight to the popularly used method of PAH dimerisation in PAH/soot modelling to achieve comparable concentration between experimental and modelling results.

Considering the current study, it can be observed that the addition of both H_2 and CH_4 tends to move the trend to the initial region (that is, the region of linear growth rate with steeper gradients) with H_2 showing a more significant change. Also, the growth rate of PAH concentration has been shown to reduce with increasing volume of the secondary fuel (H_2 or CH_4) in the binary mixture.

To further explain the relationship between PAH LIF signal and PAH growth rate for all the conditions studied, the PAH LIF signal and their corresponding growth rate for all the cases in Figures 5.8 and 5.9 are presented as a log-log plot in Figure 5.10. Figure 5.10 also shows all binary fuel mixtures investigated

grouped into various range of H:C ratios. The growth rate function, $d[PAH]/dL_f$ is denoted by GR_{PAH}. The data shown in this figure includes the H:C ratios of all the mixtures that have been achieved by the addition of either H_2 (non-fuel bound H represented by subscript m) and CH_4 (fuel bound H represented by subscript f). A linear regression line has been fitted through the data in the figure to quantify (albeit, within margins of error) the effect of the addition of these secondary fuels on the growth rate of primary fuel PAHs. Consequently, the relationship between the growth rate and the PAH LIF signal for the mixtures investigated follows the empirical correlation:

$$ln\,[GR_{PAH}] \; = \; 0.8609 * ln\,[PAH] \; + \; ln\,[1.1383]$$

which could be further simplified to give $GR_{PAH} \; = \; 1.1383 * PAH^{0.8609}$

This empirical equation can be used to determine PAH growth rate for other hydrocarbon fuels/fuel mixtures with H:C ratios similar to those investigated in this study.
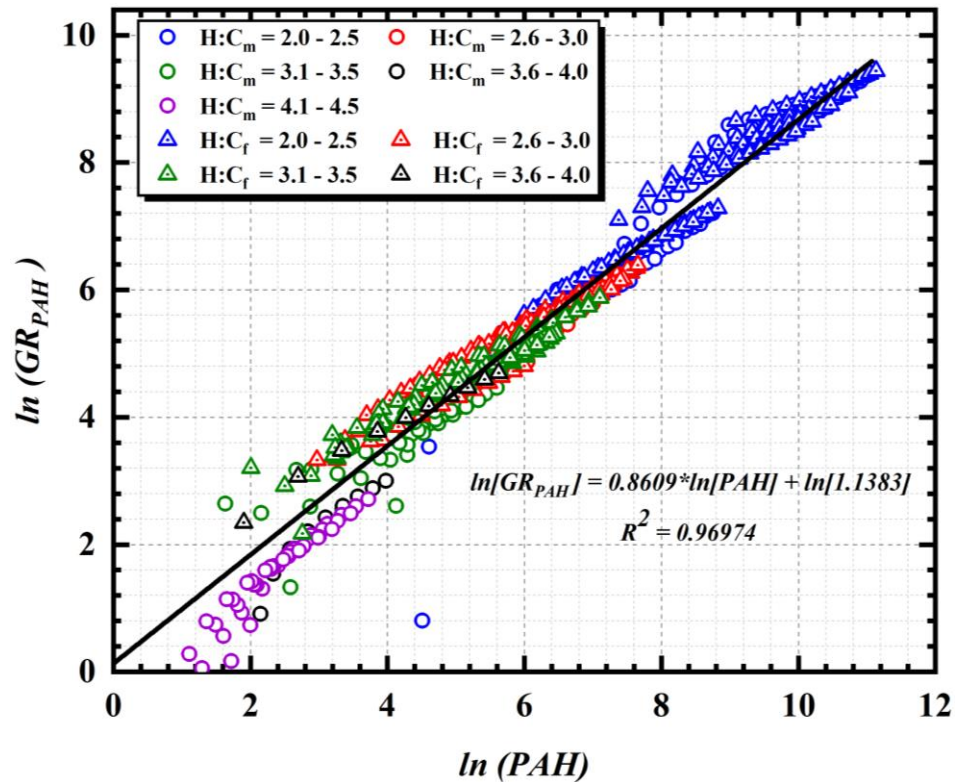
Figure 5.10: Rate of growth of PAH for all fuels according to different H:C ratio for the fuel-bound H represented by subscript f, and non-fuel-bound H represented by subscript m and linear regression fit through the data showing the band region of the growth rate.

The following paragraphs provide some further insights from Figure 5.10 and the empirical correlation. The early stages of PAH formation and growth is expected to be dominated by the reactions involving smaller PAHs (typically 1-3 rings, see Figure 2.1). It is expected that at this stage (typically lower in the flame closer to the burner exit nozzle) the rate of reaction is fast (and possibly efficient) which implies the effect of the added H_2 could be very effective leading to lower concentration of PAH. This is in agreement with the observation by Guo *et al.* (2006) in their numerical study of soot formation in H_2 and C_2H_4/air diffusion flame. The authors reported lower concentrations of

144

4-ring PAHs at lower heights in the flame as compared to the corresponding higher concentrations at higher heights with the addition of H_2. This explains the greater spread of data at the lower concentration region of Figure 5.10. However, beyond this region, a linear correlation (as mentioned earlier) can be seen in Figure 5.10. Notably, the gradient of the log of the growth rate lies within a band irrespective of the fuel bonding, molecular structure and the H:C ratio of the fuel mixtures. This implies that though there exist significant differences on the effect that the addition of either H_2 (non-fuel bound H) or CH_4 (fuel bound H) has on the growth of PAHs locally as discussed in previous sections (see Figures 5.1 & 5.2), there is a limit to how much the PAH grows globally as PAH LIF signal increases irrespective of the starting point or primary fuel.

To reiterate, in Figure 5.10, the fuel mixtures with higher H:C ratios correspond to lower PAH concentration and growth rate. As expected, fuels/fuel mixtures which have higher H:C ratio (lower carbon content) produce less PAHs and hence occupy the lower end of the log-log plot. Additionally, it can be seen from Figure 5.10 that the starting point for each H:C range (representative of the fuel/mixture molecular structure) is different; this is expected as PAH formation and increase in concentration will always be dependent on the molecular structure of the hydrocarbon fuel at the onset of PAH formation. For example, initially PAH formation (and concentration) from a hydrocarbon fuel with lower H:C ratio (high carbon content) such as C_3H_6 (unsaturated hydrocarbon) would be greater when compared with a hydrocarbon fuel of higher H:C ratio such as CH_4 (saturated hydrocarbon) (See Figures 5.8 & 5.9).

145

However, this effect seems to become insignificant on the growth rate function as the concentration of PAH and time (in terms of L_f) increases. A similar observation was made by Keller *et al.* (2000) which confirmed that PAHs undergo additional reactions simultaneously with growth reactions in the oxidation zone of flames to rapidly form the same products independent of the starting fuel. Figure 5.10 shows that even though the different H:C ratio mixtures start from different points on the curve, the gradient is the same except at the higher values of 4.1 - 4.5. However, the gradient of the mixtures with H:C ratios between 4.1 – 4.5 by extrapolation achieves same slope when $ln\ [PAH]$ value grows to around 6.5. This could potentially suggest that the growth rate of PAH is primarily dependent on the starting fuel at the early stages of PAH formation, beyond which the level of dependence becomes unclear (possibly independent of the fuel composition but the results from this study are not sufficient to confirm this).

5.7 CONCLUSIONS

The conclusions for this chapter are summarised below:

- It was found that the addition of H_2 to C_2H_4, C_3H_8 and C_3H_6 showed no significant variation in the magnitude of PAH reduction as the height along the flame front, L_f increases. However, with the addition of H_2 to CH_4, higher reductions in PAH levels were observed at higher L_f due to the effectiveness of H_2 in impeding the growth of smaller ring PAHs closer to the burner lip, hence resulting in reduced growth to larger ring PAHs. However, the addition of CH_4 showed higher reductions at lower L_f for all

the fuels tested. Generally, H_2 addition was observed to be more effective than CH_4 in reducing PAH LIF signal.

- The binary mixture of CH_4 and C_2H_6 showed a synergistic effect on PAH concentration for up to 70% of CH_4 addition, even though the H:C ratio increased (which implies a corresponding reduction in carbon content). This might be attributable to the formation of CH_3 radicals which may promote PAH formation via the propargyl recombination route.

- The addition of both H_2 and CH_4 reduced the rate of growth of PAH concentration with H_2 showing higher effectiveness. The addition of both fuels showed two distinct regions; a steep growth region (linear) followed by a slower growth region (non-linear).

- Though there exists significant difference locally between the addition of H_2 (non-fuel bound H) and CH_4 (fuel bound H) on the growth of PAHs, there is a limit to how much the PAH concentration grows globally irrespective of the starting fuel.

- The growth rate of PAH was observed to be primarily dependent on the starting fuel (that is, dependent on the H:C ratio) at the early stages of PAH formation, beyond which the level of dependence follows a log-log linear relationship with the empirical expression: $GR_{PAH} = 1.1383 * PAH^{0.8609}$.

CHAPTER SIX

6.0 EFFECT OF ADDITION OF NON-REACTIVE GAS TO HYDROCARBON FUELS ON PAH FORMATION

Several soot studies dilute hydrocarbon fuels with N_2 or Ar to either reduce soot yield in order to be able to use certain techniques such as laser light scattering which can be affected by broadband radiation from soot particles as in Ref. (Gleason, Carbone and Gomez, 2021) or to adjust flame temperatures to obtain a baseline for easy comparison of measured quantities (Nooren *et al.*, 2000; Qamar *et al.*, 2009; Boyette *et al.*, 2021; Dasappa and Camacho, 2021). In most cases, either the impact of the diluent added is not accounted for or it is assumed to be insignificant. However, the addition of an inert gas to either the fuel or oxidiser has been shown to modify the flame temperature and reactive species concentration which might have significant effect on the flame properties and consequently PAH/soot formation (Axelbalim, Flower and Law, 1988; Wu *et al.*, 2019). For example, Schug *et al.* (1980) showed that varying the composition of O_2 and N_2 in the oxidiser stream with N_2 dilution can affect the rate of oxygen penetration to the flame front which can then alter the soot formation rate. Hence, it is imperative to investigate the effects of these diluents when added to simple hydrocarbon fuels to ascertain the accuracy of these assumptions. Furthermore, oxy-fuel combustion and exhaust or flue gas recirculation (E/FGR) are well known strategies for reduction of pollutant emissions (NO_x, CO_2 and PAH/soot) (Shaddix and Williams, 2017). CO_2 is a major component of the recirculated combustion products used in these strategies, hence it is of practical importance to understand the effects of CO_2

addition on flame properties and PAH formation in simple hydrocarbon flames (Wang *et al.*, 2017). Finally, to develop a complete understanding of the effects of H_2 addition in hydrocarbon flames, it is important to qualify the degree of its overall reduction effects which can be attributed to dilution. Additionally, the results from this kind of a study could provide further insights into the correlations between various flame properties and PAH formation in diluted flames, which can potentially be relevant to fire safety research.

Therefore, this chapter presents results of experiments conducted to investigate the effect of the addition of non-reactive gases (diluents) to hydrocarbon fuels (CH_4, C_2H_6 and C_2H_4) on PAH formation. The diluents added include carbon dioxide (CO_2), nitrogen (N_2) and argon (Ar); CO_2 is an important component of biogas, while N_2 and Ar are nearly equi-diffusive gases which could provide insight on the effect of transport properties of diluents on PAH formation.

The flow rates of C_2H_6 and C_2H_4 were maintained at a constant value of 6 slpm while that of CH_4 was kept at a constant value of 12 slpm to maintain the number of carbon atoms at a constant value of 12. This is to allow comparison between the different hydrocarbon fuels. Up to 50% (v/v) of the diluents were added to C_2H_6 and C_2H_4 while that of CH_4 was limited to 33% (v/v) due to lower PAH LIF signals for additions above 33% (v/v). Each time simultaneous OH and PAH LIF images were obtained and saved for subsequent analysis. The selected properties of the gases utilised in this chapter are presented in Table 6.1 to aid discussion/analysis of the results.

Table 6.1: Selected properties for reactive and non-reactive gases employed in this study

Gases	Density (kg/m³)	Self-diffusion coefficient D_A (cm²/s)	Thermal Conductivity (W/mK) x 10⁻³	Volumetric Heat capacity (kJ/m³K)	Thermal Diffusivity (m²/s)	Dynamic viscosity (Pas) x 10⁻⁵
Ar	1.7572	0.157	17.9	0.914	1.96E-05	2.23
CO_2	1.9359	0.106	16.8	1.638	1.03E-05	1.47
N_2	1.2323	0.155	26	1.280	2.03E-05	1.76
CH_4	0.7057	0.188	34.1	1.567	2.18E-05	1.1
C_2H_6	1.3227	0.1453	21.3	2.315	9.20E-06	0.94
C_2H_4	1.234	0.1543	20.5	1.888	1.09E-05	1.03
H_2	0.0887	1.604	186.9	1.269	1.47E-04	0.88

6.1 EFFECT OF DILUENT ADDITION ON ADIABATIC FLAME TEMPERATURE

Figure 6.1 shows the normalised adiabatic flame temperatures of the hydrocarbon mixtures expressed as a function of percentage diluent addition (v/v). The adiabatic flame temperatures (calculated using GASEQ (Morley, 2005)) were normalised with the values of the pure hydrocarbon fuel condition (0% diluent addition). For all three hydrocarbon fuels (CH_4, C_2H_6 and C_2H_4) in Figure 6.1, there is a linear decrease in the adiabatic temperature value as the percent diluent in the mixture is increased. This could be attributed to the ability of the diluents to reduce the concentration of the reactive species (fuel or oxygen), modify the thermal properties of the fuel mixture (heat capacity, thermal diffusivity, enthalpy, etc.) and thus reduce the overall temperature of the flame, as observed in Ref. (Wang *et al.*, 2019). The addition of CO_2 showed the highest reduction in adiabatic temperature while Ar addition showed the lowest reduction. This could be due to their respective higher and lower volumetric heat capacities. A similar trend was observed by the study in Ref. (Abhinavam Kailasanathan *et al.*, 2013). It is important to also note that

Figures 3 (a) to (c) indicate that the temperature history for the different fuel mixtures are very similar even though the raw temperature values vary (there is an overall reduction of 639 K, 646 K and 655 K with up to 33% CO_2 addition in CH_4, and 50% CO_2 addition in C_2H_6, and C_2H_4 respectively.

6.2 EFFECT OF DILUENT ADDITION ON FLAME HEIGHT

The effect of diluent addition on the flame height is presented in Figure 6.2 for CH_4, C_2H_6 and C_2H_4. The flame height was determined as shown in Figure 3.6 (b) using an open source image processing program, ImageJ (Abràmoff, Magalhães and Ram, 2004). The pixel distance from the image was transformed to real world distance (in mm) by calibrating with a ruler target image taken on the same ICCD camera. The flame height described here, refers to the position of the maximum temperature along the axis on the flame centreline. It was extracted from the loci of the peak OH concentration relative to the burner lip (see Figure 3.6 (b)) and corresponds to the mixture-strength height as described by McEnally and Pfefferle (2000).
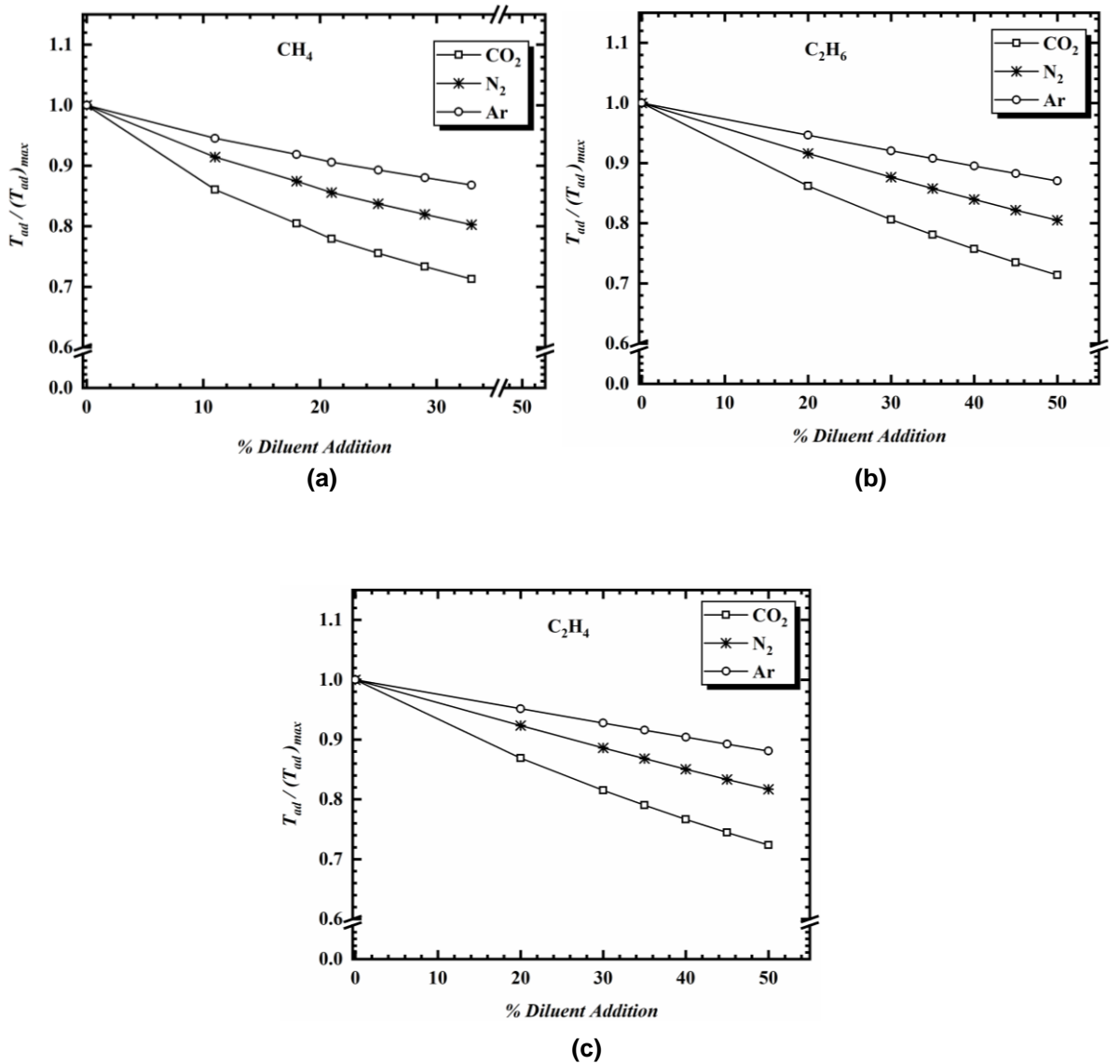
Figure 6.1: Normalised adiabatic temperature as a function of percent diluent addition for (a) CH_4 (b) C_2H_6 and (c) C_2H_4. Maximum adiabatic temperature for CH_4, C_2H_6, and C_2H_4 are 2226 K, 2260.4 K and 2370.1 K respectively

Flame height is a key parameter for the characterisation of the laminar co-flow diffusion flame. It is used in describing flame structure and can be an indicator of the residence time that PAHs undergo from inception to full oxidation (Wang *et al.*, 2019; Lou *et al.*, 2021). It can be seen in Figure 6.2 that the flame height increases monotonically for all the fuels investigated and at all percent dilution

of CO_2, N_2, and Ar. In Figure 6.2(a), the trend of increase in flame height with 33% diluent addition in CH_4 follows the sequence Ar (~6%) < CO_2 (~10%) < N_2 (~12%). However, in Figures 6.2 (b) and (c), the order is reversed between CO_2 and N_2 addition cases where CO_2 additions shows the highest increase in flame height. In C_2H_6 and C_2H_4, with addition of 50% CO_2, the flame height increased by ~23% compared to ~20% with 50% addition of N_2 for both fuels. Conversely, the addition of Ar showed the lowest increase in flame height for all the fuels studied.
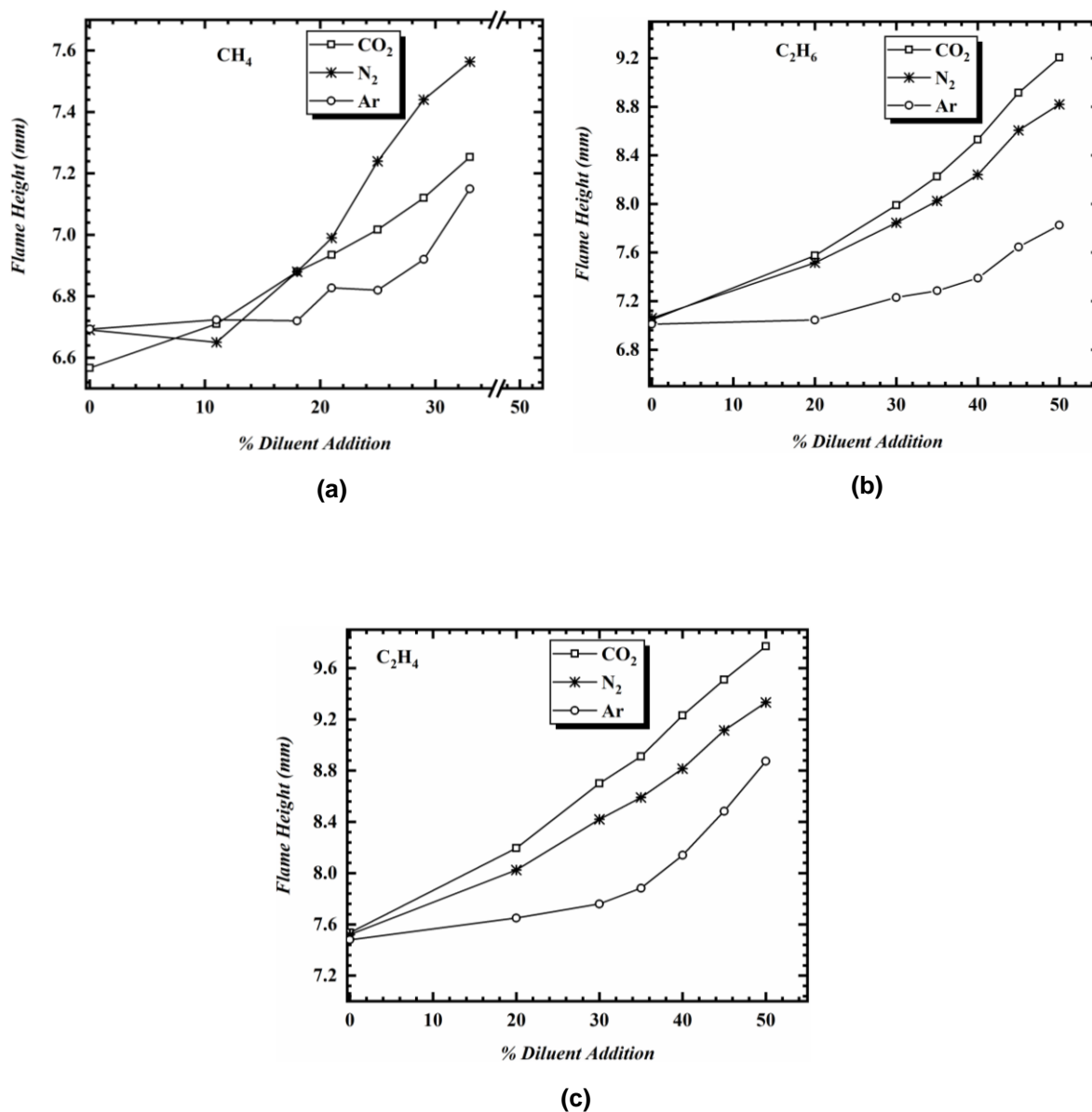
Figure 6.2: Flame height in mm expressed as function of percent dilution in (a) CH_4 (b) C_2H_6 and (c) C_2H_4. Each of (a), (b) and (c) was diluted with CO_2, N_2, and Ar

Considering that dilution decreases the adiabatic temperature of the flame, as shown in Figure 6.1, and consequently reduces the molecular diffusivity, it is reasonable to assume that increase in the level of diluent addition increases the time needed for the oxidiser to diffuse to the flame front (reduced convective transport) thereby elongating the flame (McEnally and Pfefferle,

2000). Comparing Figures 6.2 (b) and 6.2 (c), it can be seen that the trend of increase in flame height for the three diluents are similar. Though the magnitude of the flame height in C_2H_4 is higher than that of C_2H_6 (~9.8 mm for C_2H_4 as against 9.2 mm for C_2H_6), there is 25% increase in the overall flame height respectively when the addition of the three diluents is considered for both hydrocarbon fuels. This suggests that there could be a relationship between the effects produced by the addition of these diluents and the number of carbon atoms of the hydrocarbon fuel (C2 in this case). However, further investigations would be required to confirm this.

6.3 EFFECT OF DILUENT ADDITION ON PAH FORMATION

(a)

(b)

(c)
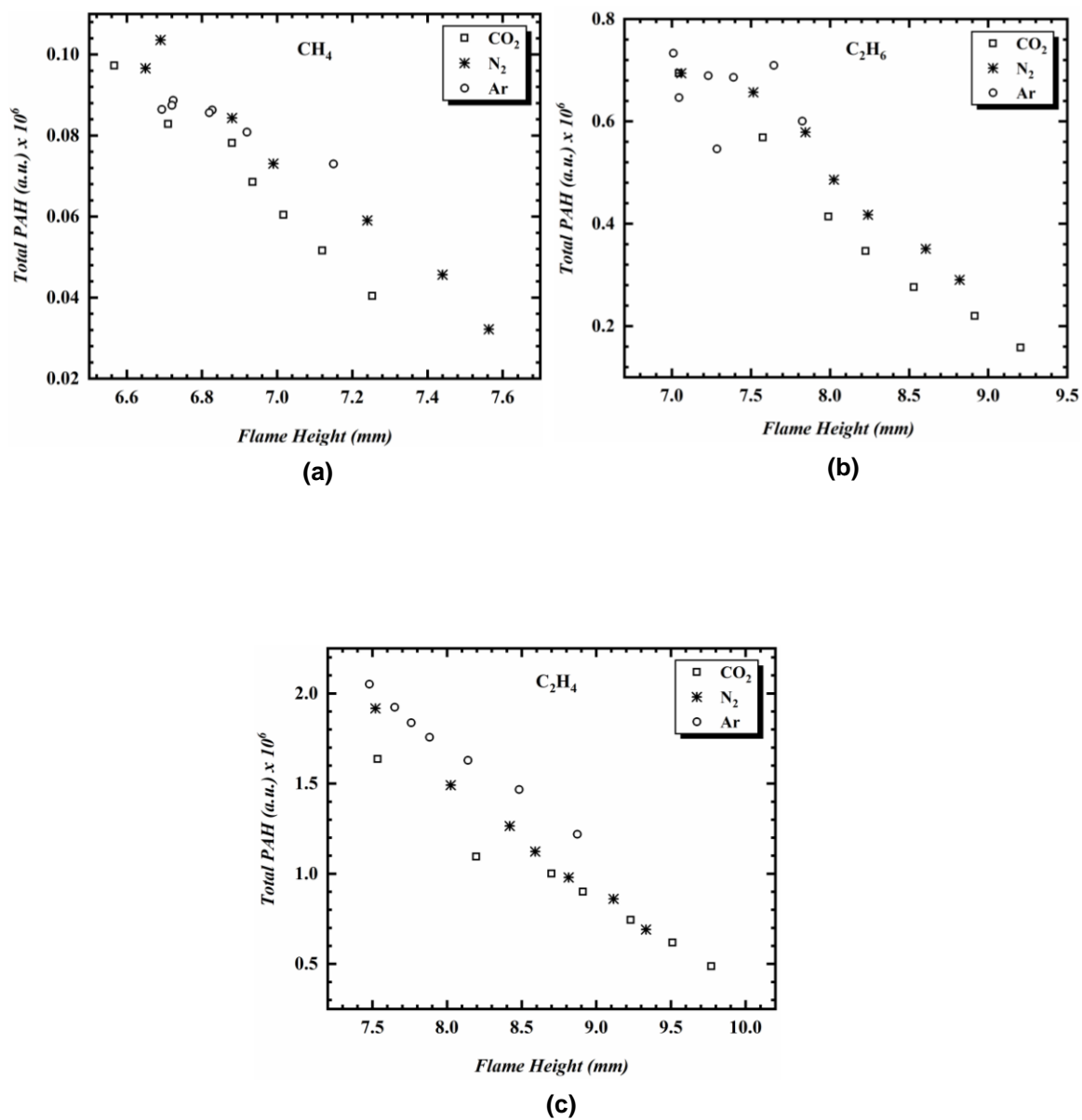
Figure 6.3: Radially integrated PAH LIF signal (Total PAH) as a function of flame height

The total PAH for every percent dilution shown in Figure 6.2 (a) to (c) is obtained and plotted for every corresponding flame height and presented in

Figure 6.3. It is evident from Figure 6.3 (a) to (c), that as the flame height increased, the total PAH reduced consistently for all percent dilution of CO_2, N_2 and Ar in CH_4, C_2H_6 and C_2H_4. Also, it can be seen from Figure 6.3 that for each hydrocarbon fuel tested, the inverse relationship between the flame height and total PAH becomes linear for higher percent dilution and higher flame height – above 6.8 mm for CH_4, 7.5 mm for both C_2H_6 and C_2H_4. It is possible that the observed increase in flame height, which implies an increase in residence time due to the addition of diluents allows more time for the oxidation of the PAH formation species and hence, further delays the growth of PAHs.

Several studies have argued that CO_2 addition to any hydrocarbon fuel has a chemical effect in addition to the dilution effect through the reaction $CO + OH \rightleftharpoons CO_2 + H$. Increasing the volume of CO_2 promotes the reverse reaction thereby increasing the concentration of the hydroxyl radical and depleting H radical. To investigate the relationship between CO_2, OH and PAH, line profiles of OH and PAH was obtained at a height of 6 mm for CO_2 diluted mixtures and presented in Figure 6.4. Firstly, each species set was normalised with the peak value of the respective reference case; that is, PAH and OH line profiles corresponding to 50% CO_2 addition were normalised with their respective 0% CO_2 case. Thereafter, the x-axis was normalised with respect to the FWHM value of the OH line profile.

It can be seen from Figure 6.4 that the OH line profile was similar for all conditions tested; no significant change observed in the shape, height and

width of the OH profiles (they can be seen to lie on top of each other). The peak-to-peak distance between the OH and PAH profiles increased as the percent dilution of CO_2 increased. The lowest and highest peak-to-peak distance were observed to occur in the C_2H_6 case and C_2H_4 cases respectively

<center>(a)</center>

<center>(b)</center>

<center>(c)</center>
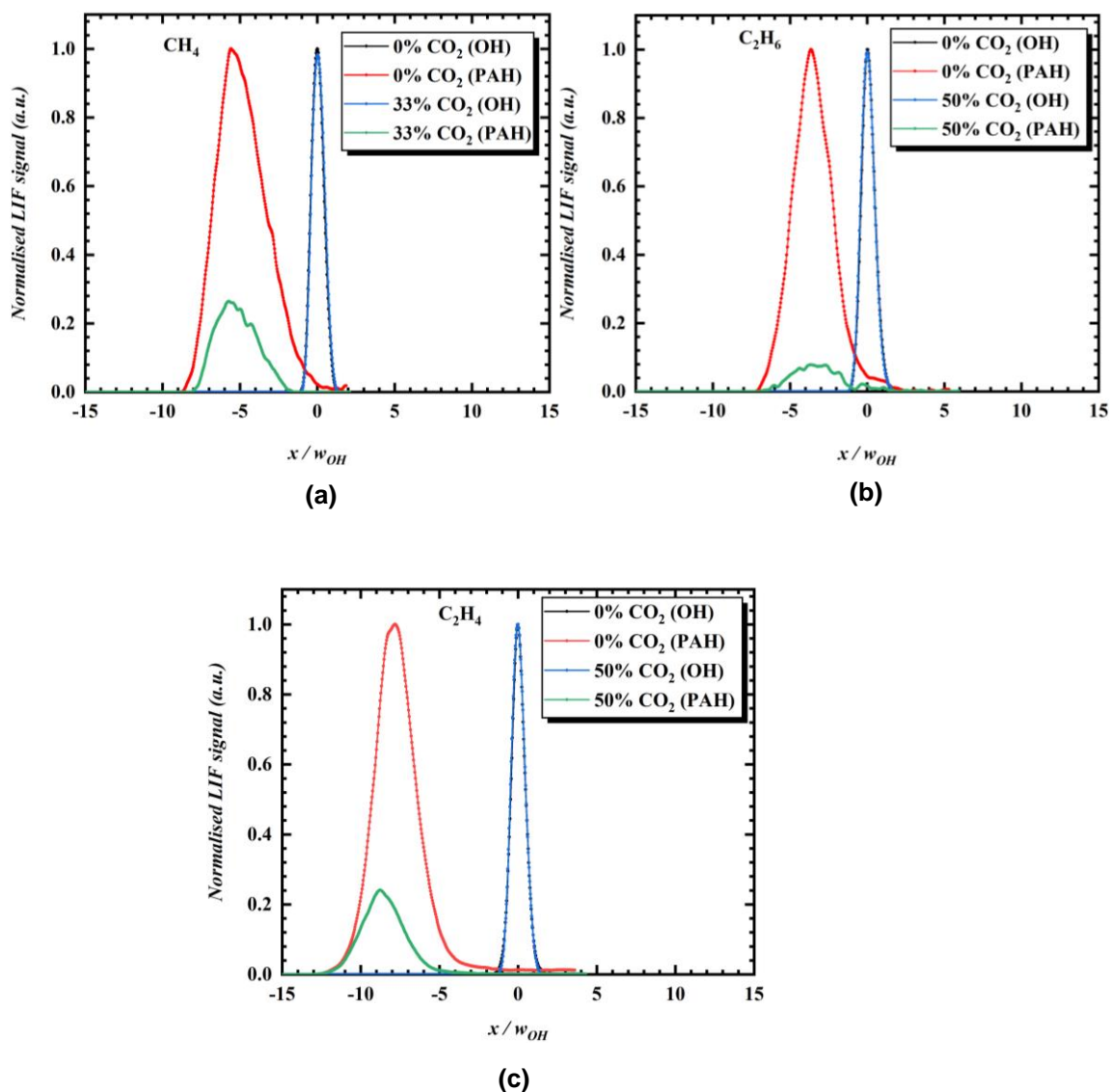
Figure 6.4: Normalised line profiles of OH and PAH LIF signals for 0% and 50% CO_2 addition in (a) CH_4 (b) C_2H_6 and (c) C_2H_4. The x-axis was normalised with respect to the FWHM value of the OH line profile while the OH and PAH LIF signals were normalised with the peak value of the respective reference case (0% CO_2) for OH and PAH.

<center>158</center>

(see Figure 6.4 (b) and (c)). Additionally, the PAH profile width reduced with increase in percent CO_2 addition in CH_4, C_2H_6 and C_2H_4. This could be a direct result of the dilution effects with CO_2 addition.
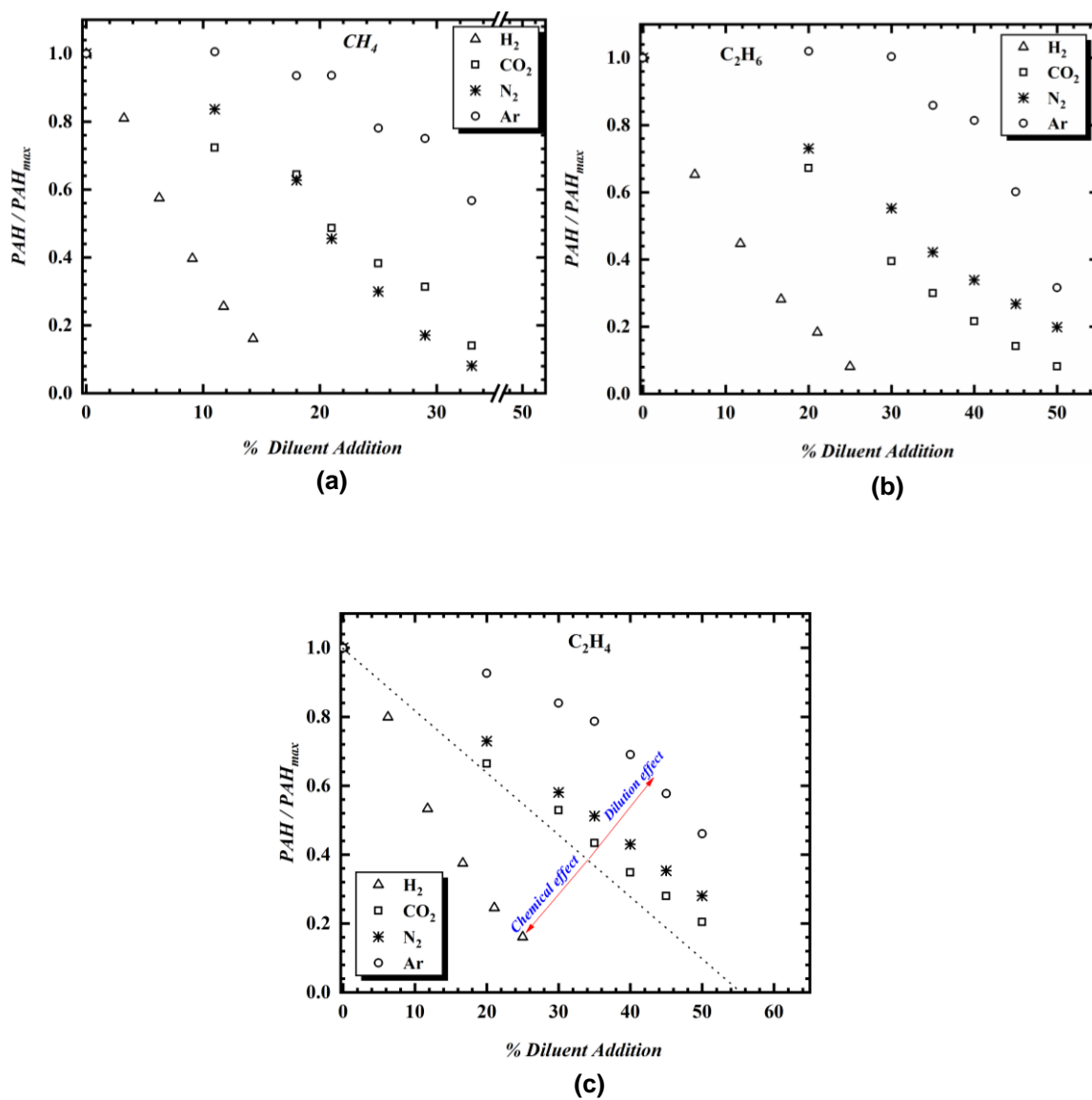
Figure 6.5: Normalised PAH for additions of H_2, CO_2, N_2 and Ar in (a) CH_4 (b) C_2H_6 and (c) C_2H_4

Even though the OH profile showed no significant changes with CO_2 addition as suggested by Fischer and Jiang (2016), the trends observed in this study of PAH reduction levels showing the dominance of CO_2 is consistent with conclusions from the studies in Refs. (Liu *et al.*, 2015; Fischer and Jiang, 2016).

Figure 6.5 shows the normalised PAH LIF signal presented as a function of percent dilution (CO_2, N_2 and Ar) for CH_4, C_2H_6 and C_2H_4. The PAH values were normalised with the corresponding PAH LIF signal of the no diluent addition case. The normalised PAH LIF signal with the addition of H_2 (obtained from data already presented in Chapter 5) is also shown in Figure 6.5. The inclusion of H_2 was done to highlight the difference in the effects of diluting the hydrocarbon fuel with a non-reactive and with a reactive gas on PAH growth.

In Figure 6.5 (a) to (c), it can be seen that for all additions of CO_2, N_2 and Ar in CH_4, C_2H_6 and C_2H_4, PAH levels reduced monotonically; this could be attributed to the dilution effect (a decrease in the fuel concentration) and to the thermal effect (a reduction in the flame temperature) of these additives. These complementary effects reduce the reaction rate of key species that contribute to PAH formation and also delay further growth of smaller PAHs to larger PAHs due to the increased residence times (Angrill *et al.*, 2000), as explained earlier when analysing Figure 6.2. It can be seen from Figure 6.5 that additions of Ar produced the reduction in PAH levels for all three cases (see Figure 6.5 (a) to (c)). This could be due to its low volumetric heat capacity and slightly lower diffusivity. In Figures 6.5 (b) and (c), the addition of CO_2 showed the highest

reduction of PAH levels for C_2H_6 and C_2H_4 when compared to the reduction levels with the addition of N_2 and Ar. This could be attributed to the additional role of CO_2 in the pathway for the formation of PAH and soot through the reaction $CO + OH \rightleftharpoons CO_2 + H$ as explained earlier (see discussions for Figure 6.4). Addition of CO_2 could reverse the direction of the above reaction, thus increasing the oxidation reactions with increased availability of OH radicals and reduced H radical concentration. This reduces the rate of acetylene (C_2H_2) addition in the HACA mechanism (Liu *et al.,* 2015). The trend of PAH reduction is slightly different in CH_4 (see Figure 6.5(a)) for additions of CO_2 and N_2. With additions of up to 30% diluent, CO_2 showed the lowest reduction when compared to N_2 addition which is similar to the observations in Figure 6.5 (b) and (c) for C_2H_6 and C_2H_4. However, beyond 30% diluent, the trend was reversed with N_2 showing more reduction in PAH levels than CO_2. A plausible explanation for this could be the hypothesis by Fischer and Jiang (2016) in their study of the effects of CO_2 addition to CH_4 (simulated biogas) on PAH chemistry. They observed that under certain conditions in biogas, CO_2 limits the efficiency of PAH oxidation which consequently slows down its ability to reduce PAH levels.

Comparing the effects of H_2 addition to that of the diluents - CO_2, N_2 and Ar, it is clear from Figure 6.5 that H_2 addition is more efficient in the reduction of PAH levels. which is due to a combination of chemical and dilution effect as illustrated in Figure 6.5 (c). The region above the dotted line in Figure 6.5 (c) can be described as the dilution effect while the region below the line can be attributed to the chemical effects due to H_2 addition (already explained in

Section 5.2). The H_2-hydrocarbon inverse diffusion flames studied in Chapter 5 showed no significant change in flame height or visible flame appearance (not shown) when H_2 was added to the pure fuel for all cases investigated; this implies that any change due to H_2 addition cannot be attributed to change in residence times. Therefore, any change observed in PAH level with H_2 addition could be attributed to two reasons. Firstly, dilution of the carbon concentration in the fuel mixture per unit volume and secondly, the direct chemical involvement of H_2 in key reactions leading to the formation of PAH (Gülder, Snelling and Sawchuk, 1996) as already detailed in the discussions in Chapter 5.

6.4 CONCLUSIONS

- There is a linear decrease in the adiabatic temperatures of CH_4, C_2H_6, and C_2H_4 flames as the percent dilution of CO_2, N_2 and Ar increased in the mixture. Additions of CO_2 showed the most reduction when compared with N_2 and Ar. This was attributed to $CO_2's$ higher volumetric heat capacity.

- The addition of CO_2, N_2 and Ar separately to CH_4, C_2H_6, and C_2H_4 flames increased the flame height monotonically. The smallest increase in flame height for all the conditions tested was observed with the addition of Ar. Also, for higher flame heights and dilution levels, an inverse linear relationship was observed between the total PAH LIF signal and the flame height.

- Overall reduction of PAH levels was observed to be greatest with the addition of CO_2. This was attributed to the additional role the addition of CO_2 potentially played in the formation of PAH through the reverse reaction of $CO + OH \rightleftharpoons CO_2 + H$. This produces more OH radicals and less H radicals which increases oxidation of intermediate species and reduces the rate of C_2H_2 addition via the HACA mechanism of PAH growth.

- H_2 addition was shown to be more effective at reducing PAH levels for all the fuels tested when compared with the diluents - CO_2, H_2 and Ar. This was attributed to a combination of dilution and chemical effects with H_2 addition.

CHAPTER SEVEN

7.0 CONCLUSIONS AND RECOMMENDATIONS FOR FUTURE WORK

The work conducted in this thesis focused mainly on understanding the effect of H_2 addition as a secondary gas to various hydrocarbon fuels on PAH formation and growth. Several binary mixtures were studied to provide further insight on the formation and growth rate of PAH using optical diagnostic techniques. In this chapter, the main conclusions of this work with reference to the corresponding objectives are presented followed by recommendations for future work.

7.1 SUMMARY AND CONCLUSIONS

To achieve the overarching aim of this work, an adequate experimental methodology was developed. A summary of the methodology is first presented in response to the objective: ***to set-up and optimise PAH PLIF system to detect 3-5 ring PAHs and use this system simultaneously with OH PLIF to get flame location***.

An inverse diffusion flame burner was designed and utilised to stabilise all the flame conditions tested in this thesis. Furthermore, an optical diagnostic system which comprised of a Litron Nd:YAG laser (532 nm fundamental wavelength) used to pump the Pulsare tunable dye laser equipped with Rhodamine 6G dye (tuned to near 283 nm wavelength) was set up and optimised to excite both OH and PAH species. This allowed simultaneous detection of OH and PAH PLIF signals. The fluorescence of the OH signal was

collected near 283 nm while that of PAH was between 420 nm - 480 nm to detect PAH of 3 – 5 rings. Simultaneous detection of OH and PAH PLIF signals enabled the development of a data reduction and image analysis routine in MATLAB for PAH formation and growth analysis. This was based on the flame normal statistics referenced to the flame location (represented by the loci of the peak OH signal). This methodology was employed for the subsequent analysis presented in chapters 4 to 6 of this thesis. The main conclusions from these results chapters are presented next.

7.1.1 EFFECT OF HYDROGEN ADDITION ON PAH FORMATION IN METHANE DIFFUSION FLAMES

In this chapter, the developed methodology was utilised to study PAH formation characteristics in hydrogen-enriched CH_4 gas which is representative of the popular hydrogen-enriched natural gas (HENG) being projected as a sustainable alternative for fossil fuel in heating homes and application in many domestic and industrial burners. The results were also compared with 1-D flame calculations. In response to the objective: ***understand the effect of H_2 - enriched natural gas (simulated with CH_4) on PAH formation***, the following main conclusions were reached:

- When considering H_2 addition to CH_4 , both experimental and computational results showed similar PAH profile widths, with no significant change observed with H_2 addition. However, the peak PAH location from the experimental campaign was observed to shift slightly

away from the OH peak (representing maximum temperature locations) with increasing H_2 addition.

- The rate of change in PAH with respect to the length of flame front (or height above burner) was highest for the methane only condition, with this rate reducing as H_2 was incrementally added.

- The reduction in PAH was observed to be monotonic with H_2 addition at all the heights above the burner tip, with higher reductions observed at higher heights above the burner. This could be attributed to H_2 preventing the formation of smaller PAHs at lower heights which would in turn impede the formation of larger PAHs at higher heights.

- The percentage reduction in PAH with H_2 addition at 5 mm above the burner tip was of similar magnitude to that observed from 1-D flame simulations. This is because the 1-D flame simulations cannot capture residence time, and hence are most comparable to heights closer to the burner tip but away from high strain and heat loss region.

- Based on simulation results, the reduction in PAH with H_2 addition was attributed to the increased oxidation of crucial species, such as acetylene and propargyl, hence reducing their availability for key PAH formation pathways. In addition, H_2 reduced the rate of H abstraction, hence impeding growth reactions on PAHs due to reduction of active sites for PAH growth.

7.1.2 PAH FORMATION CHARACTERISTICS IN VARIOUS BINARY MIXTURES OF H₂ OR CH₄ WITH C1 – C3 HYDROCARBON FUELS

Here, the addition of H_2 as a secondary gas to various hydrocarbon fuels was investigated and compared with the addition of CH_4 separately to the same fuels. Subsequently the growth rate of PAH was estimated based on the PAH LIF information obtained with respect to the flame front (flame normal statistics) for all conditions tested. Finally, an empirical growth rate function for all flame conditions tested was proposed by comparing the growth rate and the PAH LIF signal for all mixtures based on the H:C ratio. In response to the following objectives: (i) *understand the effect of binary fuel mixtures composed of varying levels of H_2 in C1-C3 hydrocarbon fuels on PAH formation and growth,* (ii) *Perform data reduction and image analysis to determine PAH growth rate in C1-C3 hydrocarbon fuels mixtures in relation to the flame front location and* (iii) *estimate PAH growth rate function from the binary hydrocarbon fuel mixtures,* the following main conclusions were reached:

- It was found that the addition of H_2 to C_2H_4, C_3H_8 and C_3H_6 showed no significant variation in the magnitude of reduction in PAH levels as the height along the flame front, L_f increased. However, with the addition of H_2 to CH_4, higher reduction in PAH levels was observed at higher L_f due to the effectiveness of H_2 in impeding the growth of smaller ring PAHs closer to the burner lip hence reduced growth to larger ring PAHs. However, the addition of CH_4 showed higher reductions at lower L_f for

all the fuels tested. Generally, H_2 addition was more effective than CH_4 in reducing PAH LIF signal.

- The addition of both H_2 and CH_4 reduced the rate of growth of PAH concentration with H_2 showing more effectiveness. The addition of both fuels shows two distinct regions; a steep growth region followed by a slower growth region.

- Though there exists significant difference on the local effects the addition of either H_2 (non-fuel bound H) or CH_4 (fuel bound H) on the growth of PAHs, there is a limit to how much the PAH grows globally as the PAH LIF signal increased irrespective of the starting fuel.

- The growth rate of PAH was observed to be primarily dependent on the starting fuel (as it is dependent on the H:C ratio) at the early stages of PAH formation, beyond which the level of dependence follows a log-log linear relationship with the empirical expression: $GR_{PAH} = 1.1383 * PAH^{0.8609}$.

7.1.3 EFFECT OF ADDITION OF NON-REACTIVE GAS TO HYDROCARBON FUELS ON PAH FORMATION

In this chapter, the effect of addition of non-reactive gases to hydrocarbon fuels on PAH formation was studied using CO_2, N_2 and Ar. This was subsequently compared with the data on H_2 effects on PAH formation shown in chapter 5 to highlight the possible contribution of the dilution effects to the overall reduction

of PAH formation observed in the mixtures in chapter 5 with H_2 addition. The following main conclusions were reached in response to the objective: ***to understand diluent effect of H_2 addition to hydrocarbon fuels on PAHs using control diluents***

- Overall reduction of PAH levels was observed to be greatest with the addition of CO_2. This was attributed to the additional role CO_2 addition could play in the formation of PAH through the reverse reaction of $CO + OH \rightleftharpoons CO_2 + H$. This produces more OH radicals and less H radicals which increases oxidation of intermediate species and reduces the rate of C_2H_2 addition via the HACA mechanism of PAH growth.

- H_2 addition was shown to be more effective at reducing PAH levels for all the fuels tested when compared with the diluents - CO_2, N_2 and Ar. This was attributed to a combination of dilution and chemical effects of H_2 addition.

7.2 RECOMMENDATION FOR FUTURE WORK

- In this thesis, PAH growth rate analysis was based on the detected 3 – 5 ring PAHs. It would be important to understand the evolution of PAHs from inception to soot formation using the growth rate analysis. Similar analysis could be repeated for 1 – 2 ring PAHs and soot volume fraction measurements to track the growth rate at the inception stages of PAH formation and growth to soot particles respectively. This will provide

further insight into other possible rate limiting steps and dependencies involved in PAH formation and growth to soot.

- In addition to the discussions on the effects of H_2 addition on PAH formation highlighted in this study, it would be interesting to understand how H atom directly affects the process of PAH formation by simultaneously measuring both species (H atom and PAH) under the same conditions. H atom species could be obtained using the interference free detection method proposed in the studies by Kulatilaka *et al.* (2012) and Jain *et al.* (2019, 2020). This will provide further insight that will enrich the development of kinetic mechanisms for PAH formation.

- In this thesis, CO_2, N_2 and Ar were used to highlight the dilution effects on PAH formation as a result of H_2 addition in the hydrocarbon fuels tested. However, it would be interesting to observe the impact of preferential diffusion due to the diffusive property of H_2 on the dilution effects by using a diluent with similar thermal diffusivity as H_2. This could be verified by comparing the effect on PAH reduction when similar volumes of H_2 and Helium (He) are added to hydrocarbon fuels. The dilution effect produced with He addition should be comparable to that of H_2 while other remaining effects could be attributed to the chemical effects of H_2 addition.

APPENDIX A1

A1: Detailed classification of 16 EPA priority PAH pollutants by IARC

The IARC of the World Health organisation (WHO) is the main organisation responsible globally for classifying compounds as carcinogens to humans (ACS, 2019). The classifications are based on extensive experimental evidence in animals and mechanistic data from humans exposed to these PAHs based on where they live or work (Steven N. Goodman, 2013; Jameson, 2019; IARC, 2020). These monographs for documenting the classifications are updated regularly as new evidences become available.

There are presently four groups of classification and they are detailed below

Group 1 – The substance under this group are labelled *carcinogens* because the evidence is very conclusive.

Group 2A – The substances here are labelled *probable carcinogens* because the evidence available is compelling but not considered very conclusive.

Group 2B - The substances here are labelled *possible carcinogens* because the evidence available is limited hence considered far from being conclusive.

Group 3 – Under this group, substances with inadequate or limited evidence are listed as *not classifiable*.

Table A1.1 below details the classification for the 16 PAHs considered as priority pollutants by EPA.

Table A1.1: Classification of 16 US EPA PAHs – priority pollutants by IARC for carcinogenicity to humans (EEA, 1999; Andersson and Achten, 2015; IARC, 2020).TEF values from EPA, number of rings and molecular weight of the PAHs are also included.

PAH	Group	Number of Rings	Molecular weight (g/mol)	TEF
Naphthalene	2B	2	128	0.001
Acenaphthylene	3	3	152	0.001
Acenaphthene	3	3	154	0.001
Fluorene	3	3	166	0.001
Anthracene	3	3	178	0.01
Phenanthrene	3	3	178	0.001
Fluoranthene	3	4	202	0.001
Pyrene	3	4	202	0.001
Benz[*a*]anthracene	2B	4	228	0.1
Chrysene	2B	4	228	0.01
Benzo[*b*]fluoranthene	2B	5	252	0.1
Benzo[*k*]fluoranthene	2B	5	252	0.1
Benzo[*a*]pyrene	1	5	252	1.0
Dibenz[*a,h*]anthracene	2A	5	278	1.0
Indeno[*1,2,3-cd*]pyrene	2B	6	276	0.1
Benzo[*g,h,i*]perylene	3	6	276	0.01

Table A2.1: Experimental data for the laser beam calibration used in comparing with the LIFBASE calculations in section 3.2.1.1

Wavelength	LIF intensity (a.u.)
282.5	0.1406
282.5125	0.1729
282.525	0.1844
282.5375	1.6288
282.55	0.1527
282.5625	5.0125
282.575	0.1594
282.5875	1.5606
282.6	0.1453
282.6125	0.1525
282.625	0.1586
282.6375	0.3287
282.65	7.8143
282.6625	0.2693
282.675	0.1304
282.6875	0.1411
282.7	0.1198
282.7125	0.1017
282.725	0.1066
282.7375	0.098
282.75	0.2272
282.7625	0.2455
282.775	0.2369
282.7875	0.2337
282.8	0.2047
282.8125	0.2532
282.825	0.2208
282.8375	0.1893
282.85	0.2088
282.8625	0.8111
282.875	1.5589
282.8875	0.3073
282.9	0.6973
282.9125	4.79
282.925	0.6802
282.9375	0.3733
282.95	0.3197

282.9625	0.2911
282.975	0.2794
282.9875	0.6317
283	0.3994
283.0125	1.1892
283.025	0.3127
283.0375	0.1688
283.05	0.1698
283.0625	0.2102
283.075	0.2175
283.0875	0.1695
283.1	0.1513
283.1125	0.1551
283.125	0.1977
283.1375	0.1719
283.15	0.2126
283.1625	2.1512
283.175	0.2724
283.1875	0.2483
283.2	1.255
283.2125	0.3817
283.225	0.2152
283.2375	0.2516
283.25	0.3229
283.2625	0.3278
283.275	0.2492
283.2875	0.2329
283.3	0.2287
283.3125	0.2293
283.325	0.2037
283.3375	0.2589
283.35	0.229
283.3625	0.8816
283.375	0.3526
283.3875	0.3075
283.4	2.7908
283.4125	0.1991
283.425	0.1828
283.4375	0.3692
283.45	0.9222
283.4625	0.249
283.475	0.1911
283.4875	0.2239
283.5	0.3421

283.5125	0.2747
283.525	0.383
283.5375	4.1856
283.55	1.0438
283.5625	0.4776
283.575	0.3971
283.5875	0.3358
283.6	0.4827
283.6125	2.8023
283.625	0.5209
283.6375	0.3835
283.65	0.4185
283.6625	0.5732
283.675	0.4184
283.6875	0.4037
283.7	0.8416
283.7125	0.288
283.725	0.2789
283.7375	0.3316
283.75	0.2668
283.7625	0.2786
283.775	0.1928
283.7875	0.1752
283.8	0.2118
283.8125	0.2858
283.825	0.2506
283.8375	0.2911
283.85	0.3224
283.8625	0.3002
283.875	0.3955
283.8875	0.3671
283.9	0.8767
283.9125	1.648
283.925	1.7604
283.9375	0.49
283.95	0.4075
283.9625	0.3353
283.975	0.2712
283.9875	0.2383
284	0.2666
284.0125	0.3065
284.025	0.3113
284.0375	0.2432
284.05	2.9351

284.0625	0.3393
284.075	0.3731
284.0875	0.3433
284.1	0.2806
284.1125	0.2877
284.125	0.5115
284.1375	0.4069
284.15	0.2985
284.1625	0.298
284.175	0.2933
284.1875	0.5027
284.2	0.6033
284.2125	0.9652
284.225	0.3711
284.2375	0.4083
284.25	0.934
284.2625	0.3585
284.275	0.3002
284.2875	0.2665
284.3	0.2716

<u>Some basic setting for the LIFBASE calculations</u>

Under Simulation:

Kind – Exc. LIF; Unit – Å; Noise – 0; Pressure – 1 bar; Start & End – 2810 Å & 2845 Å respectively; Resolution – 0.125; Lineshape – Gaussian; Lorentzian – 0; Temp. -2225 K

Under LIF emission settings:

Gated detection – Total integration; Fluorescent detection - window; Start & End window – 3000 Å & 3500 Å respectively; LIF regime – linear
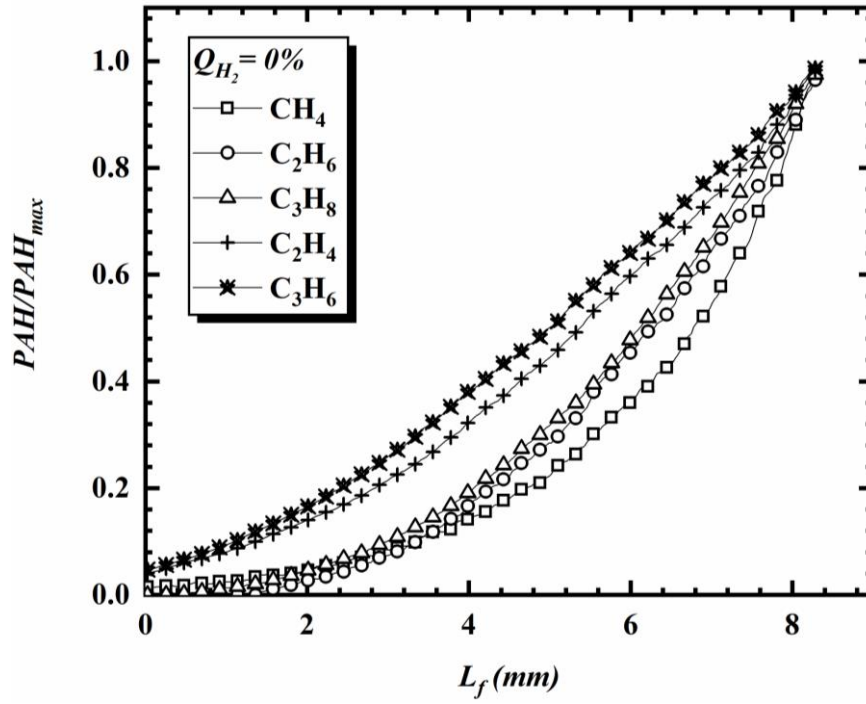
Figure A3.1: Normalised PAH LIF intensity as a function of L_f for reference fuels – CH_4, C_2H_6, C_3H_8, C_2H_4 and C_3H_6 for 0% H_2 addition levels. PAH_{max} values for CH_4, C_2H_6, C_3H_8, C_2H_4 and C_3H_6 are 69, 508, 2152, 6963, 68295 a.u. respectively.
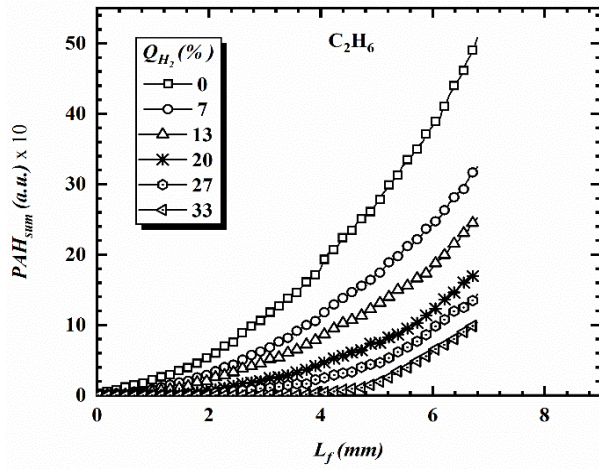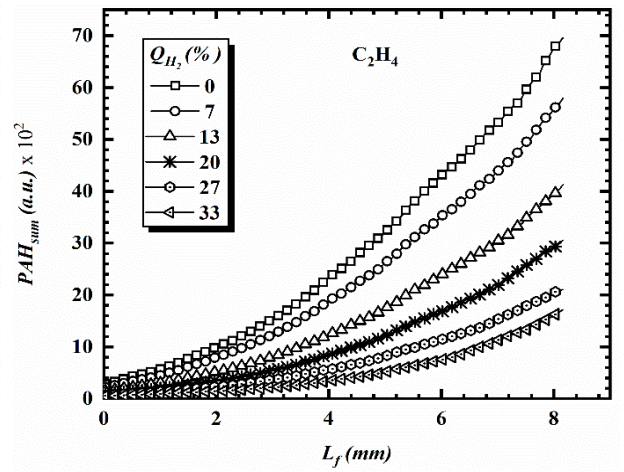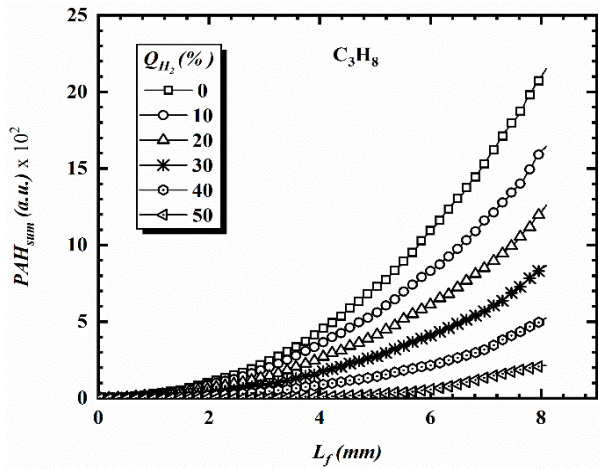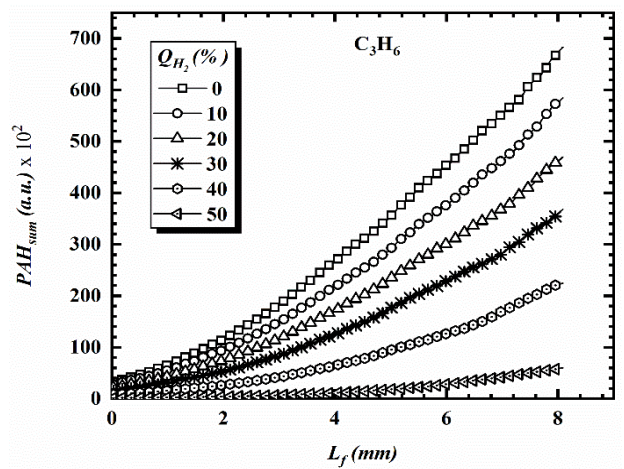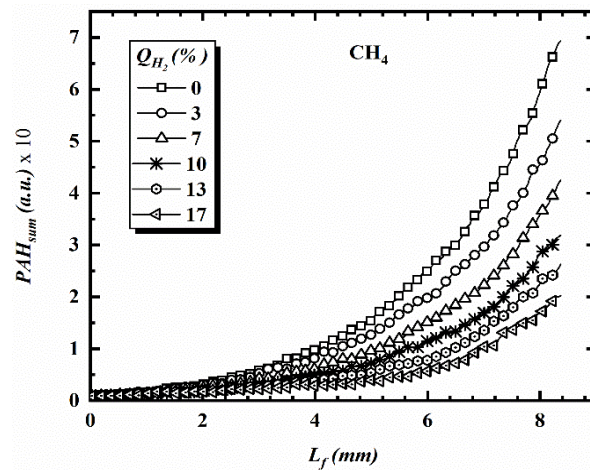
Figure A3.2: PAH_{sum} as a function of L_f for various H_2 addition levels in (a) C_2H_6 (b) C_2H_4 (c) C_3H_8 (d) C_3H_6 and (e) CH_4.

178
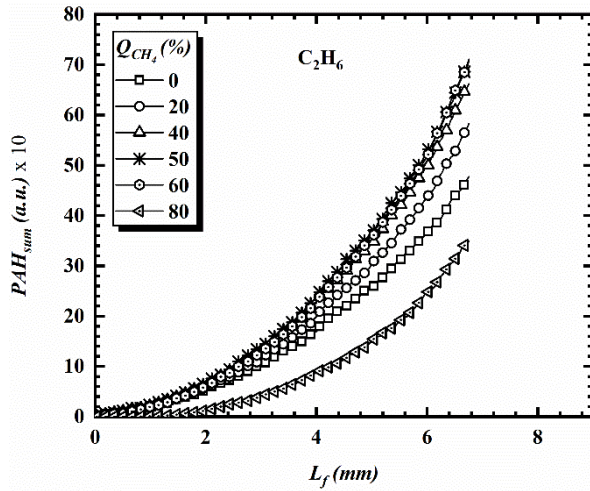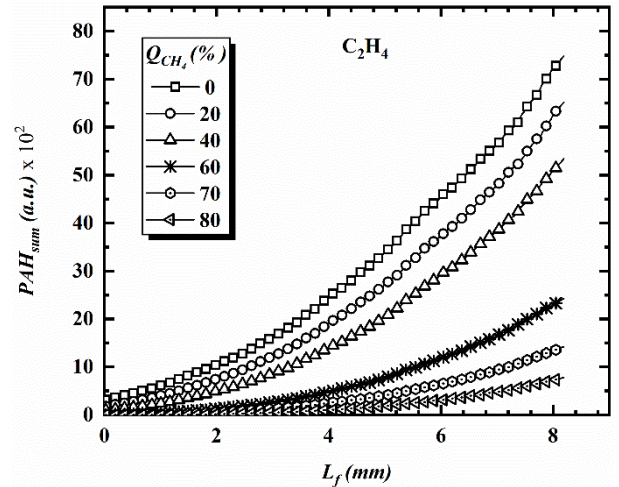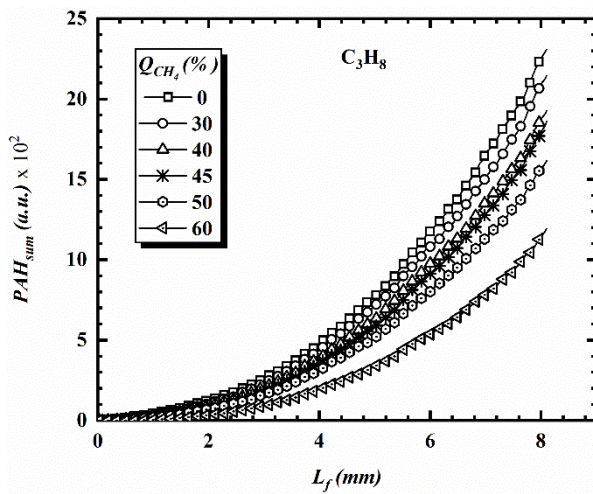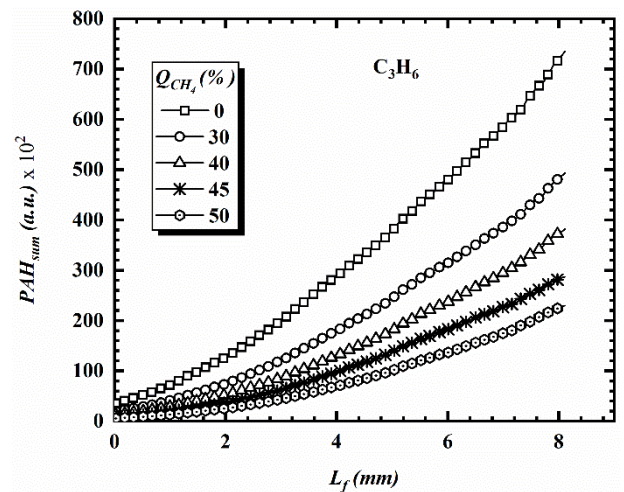
Figure A3.3: PAH_{sum} as a function of L_f for various CH_4 addition levels in (a) C_2H_6 (b) C_2H_4 (c) C_3H_8 and (d) C_3H_6.

179

APPENDIX A4

PROCEDURE FOR STARTING THE LASERS IN THE LASER ROOM

(B.05)

Setup A – Litron NanoPIV + doubler dye laser setup (LHS)

SWITCH ON

1. Switch ON Laser A (Nano PIV) power and dye circulator pumps from power strip mounted on LHS table. (Note: The dye laser power switch should be left switched ON)

2. Switch ON Laser A PSU (power supply unit) – the switch is located behind the PSU.

3. Turn the key to SYSTEM ON in front of PSU.

4. To control laser from computer switch in front of PSU should be set to LOCAL.

5. Switch SYSTEM ON, and press PUMP ON on the keypad control.

6. Wait until the temperature display at the back of the PSU shows 100°C.

7. Follow 'Start Dye Laser Doubler Software' as given below.

8. Once the temperature has reached, press LASER ON on the keypad control. The flashlamp should start flashing and a clicking sound heard from the laser.

9. **Wear safety glasses**. Press SHUTTER ON on the keypad control and laser beam should come out of LHS dye laser.

10. Measure energy using out of dye laser using power meter. Energy should be about 18.5 mJ

11. To control laser from computer (Insight 3G) switch in front of PSU should be set to REMOTE.

Start Dye Laser Doubler Software

1. Start Pulsar Doubler software on PC1 (MONITOR).

2. A window will pop up asking, Config loaded- do you want to initiate dye laser; click yes

3. Allow the resonator position to set (in steps)

4. Wait until the Drives detected, Serial port OK and Drives calibrated light turns green

5. Then under direct wavelength access, click on set wavelength (565 nm for the doubler and 615 nm for the Tripler)

6. Allow Position Reached light to turn solid green

7. Thereafter, you can optimise the energy with the manual positioning or use increment tabs (under direct wavelength access tab)

Note: FCU1 is for the doubler (Setup A and B) and FCU2 is for the Tripler (Setup B only)

Note: If the drives cannot be located, under the drives menu, go to Init system first and then Find Home-switch secondly to correct it.

SWITCH OFF

1. Press SHUTTER OFF, then LASER OFF, then SYSTEM OFF on keypad control.

2. Turn the key to OFF in front of PSU.

3. Switch of Laser A PSU from behind the PSU unit.

4. Switch OFF Laser A (Nano PIV) power and dye circulator pumps from power strip mounted on LHS table. (Note: The dye laser power switch should be left switched ON)

- This laser uses the **deioniser cartridge** only (for filter the water through the system)

Harmonics	Energy output (mJ)
532 nm (Nd:YAG)	175 -185
565 nm (dye laser - fundamental)	65
283 nm (dye laser – doubler)	18.5 - 20 (out of range)

Setup B – Litron LPY7000 + tripler dye laser setup (RHS)

SWITCH ON

1. Turn water ON at the back of the lab from the tap in the basin. Make sure ball valve A is set to open position and no leaks can be seen (it takes about 7 to 10minutes for the water to circulate and come out to the basin).

2. Switch ON Laser B (LPY7000) power and dye circulator pumps from power strip mounted on RHS table. (Note: The dye laser power switch should be left switched ON)

3. Laser B PSU should already be switched ON, otherwise release red emergency stop in front of PSU.

4. Turn the key to SYSTEM ON in front of PSU.

5. To control laser from computer switch in front of PSU should be set to LOCAL.

6. Switch SYSTEM ON, and press PUMP ON on the keypad control.

7. Wait until the temperature display at the back of the PSU shows 48°C on top and 55°C on bottom display (55ºC will not be displayed if the 355 nm harmonic is not installed).

8. Follow 'Start Dye Laser Tripler Software' as given below.

9. Once the temperature has reached, press LASER ON on the keypad control. The flashlamp should start flashing and a clicking sound heard from the laser.

10. **Wear safety glasses**. Reduce energy to 2 or 5 [i.e. 5(Amp) & 10 (Delay)] (using dial on keypad control). Press SHUTTER ON on the keypad control and laser beam should come out of LHS dye laser.

11. Measure energy using out of dye laser using power meter. Energy should be about 4 – 4.2 mJ.

12. To control laser from computer (Insight 3G) switch in front of PSU should be set to REMOTE.

Start Dye Laser Tripler Software

1. Start Pulsare Tripler software on PC2 (MONITOR).

2. A window will pop up asking, Config loaded- do you want to initiate dye laser; click yes

3. Allow the resonator position to set (in steps)

4. Wait until the Drives detected, Serial port OK and Drives calibrated light turns green

5. Then under direct wavelength access, click on set wavelength (565 nm for the doubler and 615 nm for the Tripler)

6. Allow Position Reached light to turn solid green

7. Thereafter, you can optimise the energy with the manual positioning or use increment tabs (under direct wavelength access tab)

Note: FCU1 is for the doubler (Setup A and B) and FCU2 is for the Tripler (Setup B only)

Note: If the drives cannot be located, under the drives menu, go to Init system first and then Find Home-switch secondly to correct it.

<u>SWITCH OFF</u>

1. Press SHUTTER OFF, then LASER OFF, then SYSTEM OFF on keypad control.
2. Allow the water to run for 5-8 minutes before turning it off.
3. Turn the key to OFF in front of PSU.
4. Leave Laser B PSU powered ON.
5. Switch OFF Laser B (LPY7000) power and dye circulator pumps from power strip mounted on RHS table. (Note: The dye laser power switch should be left switched ON)
   - This laser uses the **5 inch particle filter and deionisation resin cartridge** (for the filtering the water through the system)

   - *For both dye lasers, occasionally check the dye pumps to ensure the dye solution level is optimum (at least 500 ml) and listen to the sound to be sure it is normal.*

Harmonics	Energy output (mJ)
1064 nm (Nd:YAG)	1000 - 1200
532 nm (Nd:YAG)	500
615 nm (dye laser – fundamental)	
307.5 nm (dye laser - Doubler)	90
205 nm (dye laser - Tripler)	4 – 4.2

DYE CONCENTRATION:

<u>OH Dye Laser:</u>

Dye: Rhodamine 6G/590

Oscillator concentration – 0.09 g/l

Bethune cell concentration – 0.015 g/l

<u>H Dye Laser:</u>

Dye: Rhodamine 101/640

Oscillator concentration – 0.18 g/l

Bethune cell concentration – 0.03 g/l

REFERENCES

Abdel-Shafy, H. I. and Mansour, M. S. M. (2016) 'A review on polycyclic aromatic hydrocarbons: Source, environmental impact, effect on human health and remediation', *Egyptian Journal of Petroleum*. Egyptian Petroleum Research Institute, 25(1), pp. 107–123. doi: 10.1016/j.ejpe.2015.03.011.

Abhinavam Kailasanathan, R. K. *et al.* (2013) 'Effect of diluents on soot precursor formation and temperature in ethylene laminar diffusion flames', *Combustion and Flame*. The Combustion Institute., 160(3), pp. 656–670. doi: 10.1016/j.combustflame.2012.11.004.

Abràmoff, M. D., Magalhães, P. J. and Ram, S. J. (2004) 'Image processing with imageJ', *Biophotonics International*, 11(7), pp. 36–41. doi: 10.1201/9781420005615.ax4.

Achten, C. and Andersson, J. T. (2015) 'Overview of Polycyclic Aromatic Compounds (PAC)', *Polycyclic Aromatic Compounds*, 35(2–4), pp. 177–186. doi: 10.1080/10406638.2014.994071.

ACS (2019) *Determining if something is a carcinogen*, *The American Cancer Society*. Available at: https://www.cancer.org/cancer/cancer-causes/general-info/determining-if-something-is-a-carcinogen.html#written_by (Accessed: 4 March 2021).

Ahrens, J. *et al.* (1998) 'Large molecules, radicals, ions, and small soot particles in fuel-rich hydrocarbon flames: Part III: REMPI mass spectrometry

of large flame PAHs and fullerenes and their quantitative calibration through sublimation', *Berichte der Bunsengesellschaft für physikalische Chemie*, 102(12), pp. 1823–1839. Available at: https://doi.org/10.1002/bbpc.19981021213.

Akyüz, M. and Çabuk, H. (2010) 'Gas-particle partitioning and seasonal variation of polycyclic aromatic hydrocarbons in the atmosphere of Zonguldak, Turkey', *Science of the Total Environment*. Elsevier B.V., 408(22), pp. 5550–5558. doi: 10.1016/j.scitotenv.2010.07.063.

Andersson, J. T. and Achten, C. (2015) 'Time to Say Goodbye to the 16 EPA PAHs? Toward an Up-to-Date Use of PACs for Environmental Purposes', *Polycyclic Aromatic Compounds*, 35(2–4), pp. 330–354. doi: 10.1080/10406638.2014.991042.

Angrill, O. *et al.* (2000) 'Influence of exhaust gas recirculation on soot formation in diffusion flames', *Proceedings of the Combustion Institute*, 28(2), pp. 2643–2649. doi: 10.1016/S0082-0784(00)80683-9.

Appel, J., Bockhorn, H. and Frenklach, M. (2000) 'Kinetic modeling of soot formation with detailed chemistry and physics: laminar premixed flames of C2 hydrocarbons', *Combustion and Flame*, 121(1–2), pp. 122–136. doi: 10.1016/S0010-2180(99)00135-2.

Axelbalim, R. L., Flower, W. L. and Law, C. K. (1988) 'Dilution and Temperature Effects of Inert Addition on Soot Formation in Counterflow Diffusion Flames', *Combustion Science and Technology*, 61(1–3), pp. 51–73.

doi: 10.1080/00102208808915757.

Balachandran, R. (2005) *Experimental investigation of the response of turbulent premixed flames to acoustic oscillations*. University of Cambridge.

Ballester, J. M. *et al.* (1997) 'Investigation of low-NOx strategies for natural gas combustion', *Fuel*, 76(5), pp. 435–446. doi: 10.1016/S0016-2361(97)85521-4.

Barbella, R. *et al.* (1990) 'Behavior of a fuel oil during the combustion cycle of a direct injection diesel engine', *Combustion and Flame*, 82(2), pp. 191–198. doi: 10.1016/0010-2180(90)90097-B.

Bejaoui, S. *et al.* (2014) 'Laser induced fluorescence spectroscopy of aromatic species produced in atmospheric sooting flames using UV and visible excitation wavelengths', *Combustion and Flame*. The Combustion Institute., 161(10), pp. 2479–2491. doi: 10.1016/j.combustflame.2014.03.014.

Benish, T. G. *et al.* (1996) 'C2H2 and PAH as soot growth reactants in premixed C2H4-air flames', *Symposium (International) on Combustion*, 26(2), pp. 2319–2326. doi: 10.1016/S0082-0784(96)80060-9.

Beretta, F. *et al.* (1985) 'Ultraviolet and visible fluorescence in the fuel pyrolysis regions of gaseous diffusion flames', *Combustion and Flame*, 61(3), pp. 211–218. doi: 10.1016/0010-2180(85)90102-6.

Bittner, J. D. and Howard, J. B. (1981) 'Composition profiles and reaction mechanisms in a near-sooting premixed benzene/oxygen/argon flame',

Symposium (International) on Combustion. Elsevier, 18(1), pp. 1105–1116. doi: 10.1016/S0082-0784(81)80115-4.

Blevins, L. G. *et al.* (2002) 'The existence of young soot in the exhaust of inverse diffusion flames', *Proceedings of the Combustion Institute*, 29(2), pp. 2325–2333. doi: 10.1016/S1540-7489(02)80283-8.

Bockhorn, H. *et al.* (1983) 'Investigation of the Formation of High Molecular Hydrocarbons and Soot in Premixed Hydrocarbon-Oxygen Flames', *Ber. Bunsenges. Phys. Chem.*, 87, pp. 1067–1073.

Bockhorn, H. and Schäfer, T. (1994) 'Growth of Soot Particles in Premixed Flames by Surface Reactions', in, pp. 253–274. doi: 10.1007/978-3-642-85167-4_14.

Bohm, H. *et al.* (2000) 'Modelling of a fuel-rich premixed propene-oxygen-argon flame and comparison with experiments', *Physical Chemistry Chemical Physics*, 2(21), pp. 4956–4961. doi: 10.1039/b005252n.

Boyette, W. R. *et al.* (2021) 'Effects of pressure on soot production in piloted turbulent non-premixed jet flames', *Combustion and Flame*. Elsevier Inc., 227, pp. 271–282. doi: 10.1016/j.combustflame.2021.01.013.

Castaldi, M. J. *et al.* (1996) 'Experimental and modeling investigation of aromatic and polycyclic aromatic hydrocarbon formation in a premixed ethylene flame', *Symposium (International) on Combustion*, 26, pp. 693–702.

Chakraborty, A. and Chakravarthy, S. R. (2018) 'Formation of Soot in Ethylene – Air Partially Premixed Flames Over a Wide Range of Premixedness', *J. Eng. Gas Turbines Power*, 139(December 2017), pp. 1–6. doi: 10.1115/1.4037580.

Cherchneff, I. (2011) 'The formation of Polycyclic Aromatic Hydrocarbons in evolved circumstellar environments', *EAS Publications Series*. University College London (UCL), 46(2011), pp. 177–189. doi: 10.1051/eas/1146019.

Chernov, V. *et al.* (2014) 'Soot formation with C1 and C2 fuels using an improved chemical mechanism for PAH growth', *Combustion and Flame*. The Combustion Institute., 161(2), pp. 592–601. doi: 10.1016/j.combustflame.2013.09.017.

Cole, J. A. *et al.* (1984) 'Formation mechanisms of aromatic compounds in aliphatic flames', *Combustion and Flame*, 56(1), pp. 51–70. doi: 10.1016/0010-2180(84)90005-1.

Colket, M. B. (1986) 'The Pyrolysis of Acetylene and Vinylacetylene in a Single-Pulse Shock Tube', *Symposium (International) on Combustion*, 21, pp. 851–864.

Crosley, D. R. (1981) 'Collisional Effects On Laser-Induced Fluorescence Flame Measurements', *Optical Engineering*, 20(4), pp. 511–521.

D'Anna, A. (2008) 'Detailed kinetic modeling of particulate formation in rich premixed flames of ethylene', *Energy and Fuels*, 22(3), pp. 1610–1619. doi: 10.1021/ef700641u.

Dandajeh, H. A. *et al.* (2017a) 'Effects of unsaturation of C2 and C3 hydrocarbons on the formation of PAHs and on the toxicity of soot particles', *Fuel.* Elsevier Ltd, 194, pp. 306–320. doi: 10.1016/j.fuel.2017.01.015.

Dandajeh, H. A. *et al.* (2017b) 'Effects of unsaturation of C2 and C3 hydrocarbons on the formation of PAHs and on the toxicity of soot particles', *Fuel.* Elsevier Ltd, 194, pp. 306–320. doi: 10.1016/j.fuel.2017.01.015.

Dasappa, S. and Camacho, J. (2021) 'Evolution in size and structural order for incipient soot formed at flame temperatures greater than 2100 K', *Fuel.* Elsevier Ltd, 291(January), p. 120196. doi: 10.1016/j.fuel.2021.120196.

Defoeux, F. *et al.* (2005) 'Experimental investigation of the structure of a sooting premixed benzene/oxygen/argon flame burning at low pressure', *Proceedings of the Combustion Institute.* The Combustion Institute, 30(1), pp. 1407–1415. doi: 10.1016/j.proci.2004.08.014.

Desgroux, P., Mercier, X. and Thomson, K. A. (2013) 'Study of the formation of soot and its precursors in flames using optical diagnostics', *Proceedings of the Combustion Institute.* The Combustion Institute, 34(1), pp. 1713–1738. doi: 10.1016/j.proci.2012.09.004.

Do, H.-Q. *et al.* (2021) 'Experimental study of the influence of hydrogen as a fuel additive on the formation of soot precursors and particles in atmospheric laminar premixed flames of methane', *Fuel.* Elsevier Ltd, 287(September 2020), p. 119517. doi: 10.1016/j.fuel.2020.119517.

Dobbins, R. A. (2007) 'Hydrocarbon nanoparticles formed in flames and diesel engines', *Aerosol Science and Technology*, 41(5), pp. 485–496. doi: 10.1080/02786820701225820.

Du, D. X., Axelbaum, R. L. and Law, C. K. (1995) 'Soot formation in strained diffusion flames with gaseous additives', *Combustion and Flame*, 102(1–2), pp. 11–20. doi: 10.1016/0010-2180(95)00043-6.

Eckbreth, A. C. (1996) *Laser diagnostics for combustion temperature and species*. 2nd edn. Amsterdam: Gordon and Breach Publishers.

EEA (1999) 'An approach to estimation of PAH emissions', *European Environment Agency*. Available at: https://www.eea.europa.eu/publications/EMEPCORINAIR5/BPAH.pdf/view.

Elaine, L. (2020) *Japan aims for zero emissions, carbon neutral society by 2050 - PM*, *Reuters*. Available at: https://www.reuters.com/article/japan-politics-suga-idUSKBN27B0FB (Accessed: 2 March 2021).

Erika, H. *et al.* (2012) 'Human Health Risk Assessment of 16 Priority Polycyclic Aromatic Hydrocarbons in Soils of Chattanooga, Tennessee, USA', *Water Air Soil Pollut.*, 223(9), pp. 5535–5548. doi: 10.1007/s11270-012-1265-7.Human.

EU (2007) *REGULATION (EC) No 715/2007 OF THE EUROPEAN PARLIAMENT AND OF THE COUNCIL of 20 June 2007 on type approval of motor vehicles with respect to emissions from light passenger and commercial vehicles (Euro 5 and Euro 6) and on access to vehicle repair and mai*, *Official*

journal of the European Union.

EU (2019) 'Regulation (EU) 2019/1021 of the European Parliament and of the Council of 20 June 2019 on persistent organic pollutants (recast)', *Official Journal of the European Union*, L169(850), pp. 45–77.

Eveleigh, A. (2015) *The influence of fuel molecular structure on particulate emission investigated with isotope tracing*. University College London.

Ezenwajiaku *et al.* (2019) 'Study of polycyclic aromatic hydrocarbons (PAHs) in hydrogen-enriched methane diffusion flames', *International Journal of Hydrogen Energy*. Elsevier Ltd, 44(14), pp. 7642–7655. doi: 10.1016/j.ijhydene.2019.01.253.

Faccinetto, A. *et al.* (2020a) 'Evidence on the formation of dimers of polycyclic aromatic hydrocarbons in a laminar diffusion flame', *Communications Chemistry*. Springer US, 3(1), pp. 1–8. doi: 10.1038/s42004-020-00357-2.

Faccinetto, A. *et al.* (2020b) 'Evidence on the formation of dimers of polycyclic aromatic hydrocarbons in a laminar diffusion flame', *Communications Chemistry*. Springer US, 3(1), pp. 1–8. doi: 10.1038/s42004-020-00357-2.

Farmer, P. B. *et al.* (2003) 'Molecular epidemiology studies of carcinogenic environmental pollutants: Effects of polycyclic aromatic hydrocarbons (PAHs) in environmental pollution on exogenous and oxidative DNA damage', *Mutation Research - Reviews in Mutation Research*, 544(2–3), pp. 397–402. doi: 10.1016/j.mrrev.2003.09.002.

Fernández, I. (2020) 'Understanding the reactivity of polycyclic aromatic hydrocarbons and related compounds', *Chemical Science*, 11(15), pp. 3769–3779. doi: 10.1039/d0sc00222d.

Fialkov, A. B., Dennebaum, J. and Homann, K. H. (2001) 'Large molecules, ions, radicals, and small soot particles in fuel-rich hydrocarbon flames part V: Positive ions of polycyclic aromatic hydrocarbons (PAH) in low-pressure premixed flames of benzene and oxygen', *Combustion and Flame*, 125(1–2), pp. 763–777. doi: 10.1016/S0010-2180(00)00225-X.

Fischer, M. and Jiang, X. (2016) 'The chemical effects of CO 2 addition to methane on aromatic chemistry', *Fuel*. Elsevier Ltd, 183, pp. 386–395. doi: 10.1016/j.fuel.2016.06.106.

Fleurat-Lessard, P., Pointet, K. and Renou-Gonnord, M. F. (1999) 'Quantitative Determination of PAHs in Diesel Engine Exhausts by GC-MS', *Journal of Chemical Education*, 76(7), pp. 962–965. doi: 10.1021/ed076p962.

Frenklach, M. *et al.* (1988) 'Effect of fuel structure on pathways to soot', *Symposium (International) on Combustion*, 21(1), pp. 1067–1076. doi: 10.1016/S0082-0784(88)80337-0.

Frenklach, M. (1988) 'On the driving force of PAH production', *Twenty-Second S y m p o s i u m (International) on C o m b u s t i o n*, pp. 1075–1082.

Frenklach, M. (2002) 'Reaction mechanism of soot formation in flames', *Physical Chemistry Chemical Physics*, 4(11), pp. 2028–2037. doi:

10.1039/b110045a.

Frenklach, M. and Mebel, A. M. (2020) 'On the mechanism of soot nucleation', *Physical Chemistry Chemical Physics*. Royal Society of Chemistry, 22(9), pp. 5314–5331. doi: 10.1039/d0cp00116c.

Frenklach, M. and Wang, H. (1991) 'Detailed modeling of soot particle nucleation and growth', *Symposium (International) on Combustion*, 23(1), pp. 1559–1566. doi: 10.1016/S0082-0784(06)80426-1.

Frenklach, M. and Warnatz, J. (1987) 'Detailed Modeling of PAH Profiles in a Sooting Low- Pressure Acetylene Flame', *Combustion Science and Technology*, 51(4–6), pp. 265–283. doi: 10.1080/00102208708960325.

Fu, J. *et al.* (2013) 'Energy and exergy analysis on gasoline engine based on mapping characteristics experiment', *Applied Energy*. Elsevier Ltd, 102, pp. 622–630. doi: 10.1016/j.apenergy.2012.08.013.

García-Rodeja, Y. and Fernández, I. (2019) 'Impact of C=C/B−N Replacement on the Diels–Alder Reactivity of Curved Polycyclic Aromatic Hydrocarbons', *Chemistry - A European Journal*, 25(41), pp. 9771–9779. doi: 10.1002/chem.201901964.

Geitlinger, H. *et al.* (1998) 'Two-dimensional imaging of soot volume fractions, particle number densities, and particle radii in laminar and turbulent diffusion flames', *Symposium (International) on Combustion*, 27(1), pp. 1613–1621. doi: 10.1080/00102209908952102.

Georganta, E. *et al.* (2017) 'Growth of polycyclic aromatic hydrocarbons (PAHs) by methyl radicals : Pyrene formation from phenanthrene', *Combustion and Flame*. Elsevier Inc., 185, pp. 129–141. doi: 10.1016/j.combustflame.2017.07.011.

Gleason, K., Carbone, F. and Gomez, A. (2021) 'PAHs controlling soot nucleation in 0.101—0.811MPa ethylene counterflow diffusion flames', *Combustion and Flame*. Elsevier Inc., 227, pp. 384–395. doi: 10.1016/j.combustflame.2021.01.015.

Golea, D. *et al.* (2012) 'Reduction of PAH and soot precursors in benzene flames by addition of ethanol', *Journal of Physical Chemistry A*, 116(14), pp. 3625–3642. doi: 10.1021/jp211350f.

Gong, R., Hochmuth, M. and Weatherburn, D. (2003) 'Polycyclic Aromatic Hydrocarbons and Diesel Particulates', in *26th Australasian Transport Research Forum*. Wellington New Zealand, pp. 1–18. Available at: http://www.atrf.info/papers/2003/2003_gong_hochmuth_weatherburn.pdf.

Goodwin, D. G., Moffat, H. K. and Speth, R. L. (2017) 'Cantera: An Object-oriented Software Toolkit for Chemical Kinetics, Thermodynamics, and Transport Processes. Version 2.2.0'. doi: 10.5281/zenodo.48735.

Great Britain, Department for Business, E. & I. S. (2019) *UK becomes first major economy to pass net zero emissions law*, *GOV.UK*. Available at: https://www.gov.uk/government/news/uk-becomes-first-major-economy-to-pass-net-zero-emissions-law (Accessed: 2 March 2021).

Gu, M., Chu, H. and Liu, F. (2016) 'Effects of simultaneous hydrogen enrichment and carbon dioxide dilution of fuel on soot formation in an axisymmetric coflow laminar ethylene/air diffusion flame', *Combustion and Flame*. Elsevier Inc., 166, pp. 216–228. doi: 10.1016/j.combustflame.2016.01.023.

Gülder, Ö. L., Snelling, D. R. and Sawchuk, R. A. (1996) 'Influence of hydrogen addition to fuel on temperature field and soot formation in diffusion flames', *Symposium (International) on Combustion*, 26(2), pp. 2351–2358. doi: 10.1016/S0082-0784(96)80064-6.

Guo, H. *et al.* (2006) 'Numerical study on the influence of hydrogen addition on soot formation in a laminar ethylene-air diffusion flame', *Combustion and Flame*, 145(1–2), pp. 324–338. doi: 10.1016/j.combustflame.2005.10.016.

H. J. Curran *et al.* (2001) 'Detailed Chemical Kinetic Modeling of Diesel Combustion with Oxygenated Fuels', in *SAE Technical Paper 2001-01-0653*, p. 10. Available at: https://doi.org/10.4271/2001-01-0653.

Hansen, N. *et al.* (2009) 'Recent contributions of flame-sampling molecular-beam mass spectrometry to a fundamental understanding of combustion chemistry', *Progress in Energy and Combustion Science*, 35(2), pp. 168–191. doi: 10.1016/j.pecs.2008.10.001.

Hansen, N. *et al.* (2012) 'Exploring formation pathways of aromatic compounds in laboratory-based model flames of aliphatic fuels', *Combustion, Explosion and Shock Waves*, 48(5), pp. 508–515. doi: 10.1134/S0010508212050024.

Harris, S. J., Weiner, A. M. and Blint, R. J. (1988) 'Formation of Small Aromatic Molecules in a Sooting Ethylene Flame', *Combustion and Flame*, 72, pp. 91–109.

Harvey, R. . (1991) *Polycyclic Aromatic Hydrocarbons: Chemistry and Carcinogenicity*. 1st edn. Cambridge: Cambridge University Press.

Hayashida, K. *et al.* (2006) 'Experimental analysis of soot formation in sooting diffusion flame by using laser-induced emissions', *Journal of Engineering for Gas Turbines and Power*, 128(2), pp. 241–246. doi: 10.1115/1.2056536.

Haynes, B. S. and Wagner, H. G. (1981) 'Soot formation', *Progress in Energy and Combustion Science*, 7(4), pp. 229–273.

Hepp, H., Siegmann, K. and Sattler, K. (1995) 'New aspects of growth mechanisms for polycyclic aromatic hydrocarbons in diffusion flames', *Chemical Physics Letters*, 233(1–2), pp. 16–22. doi: 10.1016/0009-2614(94)01433-V.

Holme, J. A. *et al.* (2019) 'Potential role of polycyclic aromatic hydrocarbons as mediators of cardiovascular effects from combustion particles', *Environmental Health: A Global Access Science Source*. Environmental Health, 18(1), pp. 1–18.

Hwang, J. Y. *et al.* (1998) 'Synergistic effect of ethylene-propane mixture on soot formation in laminar diffusion flames', *Combustion and Flame*, 114(3–4), pp. 370–380. doi: 10.1016/S0010-2180(97)00295-2.

Hwang, J. Y., Chung, S. H. and Lee, W. (1998) 'Effects of oxygen and propane addition on soot formation in counterflow ethylene flames and the role of C3 chemistry', *Symposium (International) on Combustion*, 27(1), pp. 1531–1538. doi: 10.1016/S0082-0784(98)80561-4.

IARC (2020) *IARC monographs on the identification of carcinogenic hazards to humans, International agency for research on cancer (IARC) - world health organisation (WHO).* Available at: https://monographs.iarc.who.int/list-of-classifications (Accessed: 26 February 2021).

IEA (2019) *The future of hydrogen.* Paris. Available at: https://www.iea.org/reports/the-future-of-hydrogen.

IEA (2020) *Gas: key findings.* Available at: https://www.iea.org/fuels-and-technologies/gas (Accessed: 20 March 2021).

Ikeda, E. *et al.* (2000) 'The pyrolysis of methylcyclopentadiene: Isomerization and formation of aromatics', *Proceedings of the Combustion Institute*, 28(2), pp. 1725–1732. doi: 10.1016/S0082-0784(00)80573-1.

Inal, F. and Senkan, S. M. (2002) 'Effects of equivalence ratio on species and soot concentrations in premixed n-heptane flames', *Combustion and Flame*, 131(1–2), pp. 16–28. doi: 10.1016/S0010-2180(02)00388-7.

Jain, A., Wang, Y. and Kulatilaka, W. D. (2019) 'Effect of H-atom concentration on soot formation in premixed ethylene/air flames', *Proceedings of the Combustion Institute.* Elsevier Inc., 37(2), pp. 1289–1296. doi:

10.1016/j.proci.2018.07.093.

Jain, A., Wang, Y. and Kulatilaka, W. D. (2020) 'Simultaneous imaging of H and OH in flames using a single broadband femtosecond laser source', *Proceedings of the Combustion Institute*. Elsevier Inc., 000, pp. 1–9. doi: 10.1016/j.proci.2020.07.137.

Jameson, C. W. (2019) 'Polycyclic aromatic hydrocarbons and associated occupational exposures', in *Handbook of Combustion*, pp. 59–64. doi: 10.1002/9783527628148.hoc036.

Jia, C. *et al.* (2020) *Characterizing Community Exposure to Atmospheric Polycyclic Aromatic Hydrocarbons (PAHs) in The Memphis Tri-State Area Final Report Prepared by :* Memphis.

Jones, D. R., Al-Masry, W. A. and Dunnill, C. W. (2018) 'Hydrogen-enriched natural gas as a domestic fuel: An analysis based on flash-back and blow-off limits for domestic natural gas appliances within the UK', *Sustainable Energy and Fuels*. Royal Society of Chemistry, 2(4), pp. 710–723. doi: 10.1039/c7se00598a.

Ju, E. L., Oh, K. C. and Shin, H. D. (2005) 'Soot formation in inverse diffusion flames of diluted ethene', *Fuel*, 84(5), pp. 543–550. doi: 10.1016/j.fuel.2004.11.003.

Kamphus, M., Braun-Unkhoff, M. and Kohse-Höinghaus, K. (2008) 'Formation of small PAHs in laminar premixed low-pressure propene and cyclopentene

flames: Experiment and modeling', *Combustion and Flame*, 152(1–2), pp. 28–59. doi: 10.1016/j.combustflame.2007.09.005.

Katta, V. R., Blevins, L. G. and Roquemore, W. M. (2005) 'Dynamics of an inverse diffusion flame and its role in polycyclic-aromatic- hydrocarbon and soot formation', *Combustion and Flame*, 142(1–2), pp. 33–51. doi: 10.1016/j.combustflame.2005.02.006.

Keller, A., Kovacs, R. and Homann, K.-H. (2000) 'Large molecules, ions, radicals, and small soot particles in fuel-rich hydrocarbon flames; Part IV: Positive ions of polycyclic aromatic hydrocarbons (PAH) in low-pressure premixed flames of benzene and oxygen', *Physical Chemistry Chemical Physics*, 2(8), pp. 1667–1675. doi: 10.1016/S0010-2180(00)00225-X.

Kern, R. D. and Xie, K. (1991) 'Shock tube studies of gas phase reactions preceding the soot formation process', *Progress in Energy and Combustion Science*, 17(3), pp. 191–210.

Kim, K. H. *et al.* (2013) 'A review of airborne polycyclic aromatic hydrocarbons (PAHs) and their human health effects', *Environment International*. Elsevier Ltd, 60, pp. 71–80. doi: 10.1016/j.envint.2013.07.019.

Kiriluk, K. J. *et al.* (2012) 'Bladder cancer risk from occupational and environmental exposures', *Urologic Oncology: Seminars and Original Investigations*. Elsevier Inc., 30(2), pp. 199–211. doi: 10.1016/j.urolonc.2011.10.010.

Kislov, V. V. *et al.* (2005) 'Hydrogen abstraction acetylene addition and Diels-Alder mechanisms of PAH formation: A detailed study using first principles calculations', *Journal of Chemical Theory and Computation*, 1(5), pp. 908–924. doi: 10.1021/ct0500491.

Kislov, V. V., Sadovnikov, A. I. and Mebel, A. M. (2013) 'Formation Mechanism of Polycyclic Aromatic Hydrocarbons beyond the Second Aromatic Ring', *The Journal of Physical Chemistry A*, 117(23), pp. 4794–4816. doi: 10.1021/jp402481y.

Kohse-Höinghaus, K. *et al.* (2002) 'Contributions to the investigation of reaction pathways in fuel-rich flames', *Physical Chemistry Chemical Physics*, 4(11), pp. 2056–2062. doi: 10.1039/b110713e.

Kostka, S. *et al.* (2009) 'Comparison of line-peak and line-scanning excitation in two-color laser-induced-fluorescence thermometry of OH', *Applied Optics*, 48(32), pp. 6332–6343. doi: 10.1364/AO.48.006332.

Krestinin, A. V. (1998) 'Polyyne model of soot formation process', *Symposium (International) on Combustion*, 27(1), pp. 1557–1563. doi: 10.1016/S0082-0784(98)80564-X.

Krestinin, A. V. (2000) 'Detailed modeling of soot formation in hydrocarbon pyrolysis', *Combustion and Flame*, 121(3), pp. 513–524. doi: 10.1016/S0010-2180(99)00167-4.

Kulatilaka, W. D. *et al.* (2012) 'Photolytic-interference-free, femtosecond two-

photon fluorescence imaging of atomic hydrogen', *Optics Letters*, 37(15), p. 3051. doi: 10.1364/ol.37.003051.

Lee, S. M., Yoon, S. S. and Chung, S. H. (2004) 'Synergistic effect on soot formation in counterflow diffusion flames of ethylene-propane mixtures with benzene addition', *Combustion and Flame*, 136(4), pp. 493–500. doi: 10.1016/j.combustflame.2003.12.005.

Lemaire, R., Bejaoui, S. and Therssen, E. (2013) 'Study of soot formation during the combustion of Diesel, rapeseed methyl ester and their surrogates in turbulent spray flames', *Fuel*, 107, pp. 147–161. doi: 10.1016/j.fuel.2012.12.072.

Li, Hongyan *et al.* (2019) 'High cancer risk from inhalation exposure to PAHs in Fenhe Plain in winter: A particulate size distribution-based study', *Atmospheric Environment*. Elsevier, 216(August), p. 116924. doi: 10.1016/j.atmosenv.2019.116924.

Li, Y. *et al.* (2009) 'Experimental study of a fuel-rich premixed toluene flame at low pressure', *Energy and Fuels*, 23(3), pp. 1473–1485. doi: 10.1021/ef800902t.

Liu, F. *et al.* (2011) 'An experimental and numerical study of the effects of dimethyl ether addition to fuel on polycyclic aromatic hydrocarbon and soot formation in laminar coflow ethylene/air diffusion flames', *Combustion and Flame*, 158(3), pp. 547–563. doi: 10.1016/j.combustflame.2010.10.005.

Liu, F. *et al.* (2015) 'Numerical and experimental study of the influence of CO2 and N2 dilution on soot formation in laminar coflow C2H4/air diffusion flames at pressures between 5 and 20 atm', *Combustion and Flame*, 162(5), pp. 2231–2247. doi: 10.1016/j.combustflame.2015.01.020.

Liu, F. *et al.* (2018) 'Experimental investigation of polycyclic aromatic hydrocarbons growth characteristics of gasoline mixed with methanol, ethanol, or n-butanol in laminar diffusion flames', *Energy and Fuels*. American Chemical Society, 32, pp. 6823–6833. doi: 10.1021/acs.energyfuels.8b00693.

Liu, F., Ai, Y. and Kong, W. (2014) 'Effect of hydrogen and helium addition to fuel on soot formation in an axisymmetric coflow laminar methane/air diffusion flame', *International Journal of Hydrogen Energy*, 39(8), pp. 3936–3946. doi: 10.1016/j.ijhydene.2013.12.151.

Liu, Q. *et al.* (2021) 'Cylinder steam injection (CSI) for internal combustion (IC) engine waste heat recovery (WHR) and its application on natural gas (NG) engine', *Energy*. Elsevier Ltd, 214, p. 118892. doi: 10.1016/j.energy.2020.118892.

Lou, C. *et al.* (2021) 'Soot formation characteristics in laminar coflow flames with application to oxy-combustion', *Combustion and Flame*. Elsevier Inc., 227, pp. 371–383. doi: 10.1016/j.combustflame.2021.01.018.

Lunde, G. and Bjorseth, A. (1977) 'Polycyclic aromatic hydrocarbons in long-range transported aerosols', *Nature*, 268(5620), pp. 518–519. doi: 10.1038/268518a0.

Luque, J. and Crosley, D. R. (1999) 'LIFBASE: Database and Spectral Simulation Program (Version 1.5)," SRI International Report M "', p. P 99-009.

Maliszewska-Kordybach, B. (1999) 'Sources, Concentrations, Fate and Effects of Polycyclic Aromatic Hydrocarbons (PAHs) in the Environment. Part A: PAHs in Air', *Polish Journal of Environmental Studies*, 8(3), pp. 131–136.

Manzetti, S. (2013) 'Polycyclic Aromatic Hydrocarbons in the Environment: Environmental Fate and Transformation', *Polycyclic Aromatic Compounds*, 33(4), pp. 311–330. doi: 10.1080/10406638.2013.781042.

Masclet, P., Bresson, M. A. and Mouvier, G. (1987) 'Polycyclic aromatic hydrocarbons emitted by power stations, and influence of combustion conditions', *Fuel*, 66(4), pp. 556–562. doi: 10.1016/0016-2361(87)90163-3.

Masih, J. *et al.* (2010) 'Characteristics of polycyclic aromatic hydrocarbons in indoor and outdoor atmosphere in the North central part of India', *Journal of Hazardous Materials*. Elsevier B.V., 177(1–3), pp. 190–198. doi: 10.1016/j.jhazmat.2009.12.017.

Mastral, A. M. and Callén, M. S. (2000) 'A review on polycyclic aromatic hydrocarbon (PAH): Emissions from energy generation', *Environmental Science and Technology*, 34(15), pp. 3051–3057. doi: 10.1021/es001028d.

Mastrangelo, G., Fadda, E. and Marzia, V. (1996) 'Polycyclic aromatic hydrocarbons and cancer in man', *Environmental Health Perspectives*, 104(11), pp. 1166–1170. Available at: doi: 10.1289/ehp.961041166.

McEnally, C. S. *et al.* (2006) 'Studies of aromatic hydrocarbon formation mechanisms in flames: Progress towards closing the fuel gap', *Progress in Energy and Combustion Science*, 32(3), pp. 247–294. doi: 10.1016/j.pecs.2005.11.003.

McEnally, C. S. and Pfefferle, L. D. (2000) 'The effect of nitrogen dilution on nonfuel hydrocarbons in laminar nonpremixed flames', *Combustion Science and Technology*, 151(1–6), pp. 133–155. doi: 10.1080/00102200008924217.

McEnally, C. S. and Pfefferle, L. D. (2002) 'The effects of premixing on soot production in non- premixed flames fueled with unsaturated hydrocarbons', *Proceedings of the Combustion Institute*, 29, pp. 2407–2413.

Melius, C. F. *et al.* (1996) 'Reaction mechanisms in aromatic hydrocarbon formation involving the C5H5 cyclopentadienyl moiety', *Symposium (International) on Combustion*, 26(1), pp. 685–692.

Mercier, X. *et al.* (2008) 'Implementation of a new spectroscopic method to quantify aromatic species involved in the formation of soot particles in flames', *Applied Physics B: Lasers and Optics*, 91(2), pp. 387–395. doi: 10.1007/s00340-008-2997-3.

Mercier, X. *et al.* (2019) 'Dimers of polycyclic aromatic hydrocarbons: The missing pieces in the soot formation process', *Physical Chemistry Chemical Physics*. Royal Society of Chemistry, 21(16), pp. 8285–8294. doi: 10.1039/c9cp00394k.

Michelsen, H. A. (2017) 'Probing soot formation, chemical and physical evolution, and oxidation: A review of in situ diagnostic techniques and needs', *Proceedings of the Combustion Institute*. Elsevier Inc., 36(1), pp. 717–735. doi: 10.1016/j.proci.2016.08.027.

Mikofski, M. A. *et al.* (2006) 'Flame height measurement of laminar inverse diffusion flames', *Combustion and Flame*, 146(1–2), pp. 63–72. doi: 10.1016/j.combustflame.2006.04.006.

Mikofski, M. A. *et al.* (2007) 'Structure of laminar sooting inverse diffusion flames', *Combustion and Flame*. Elsevier, 149(4), pp. 463–478. doi: 10.1016/J.COMBUSTFLAME.2007.01.006.

Miller, J. A. and Melius, C. F. (1992) 'Kinetic and thermodynamic issues in the formation of aromatic compounds in flames of aliphatic fuels', *Combustion and Flame*, 91(1), pp. 21–39. doi: 10.1016/0010-2180(92)90124-8.

Miller, J. A., Pilling, M. J. and Troe, J. (2005) 'Unravelling combustion mechanisms through a quantitative understanding of elementary reactions', *Proceedings of the Combustion Institute*, 30(1), pp. 43–88. doi: 10.1016/j.proci.2004.08.281.

Miller, J. H., Mallard, W. G. and Smyth, K. C. (1982) 'The observation of laser-induced visible fluorescence in sooting diffusion flames', *Combustion and Flame*, 47(C), pp. 205–214. doi: 10.1016/0010-2180(82)90101-8.

Mitra, T. *et al.* (2019) 'Understanding the formation and growth of polycyclic

aromatic hydrocarbons (PAHs) and young soot from n-dodecane in a sooting laminar coflow diffusion flame', *Combustion and Flame*. Elsevier Inc., 202, pp. 33–42. doi: 10.1016/j.combustflame.2018.12.010.

Moreau, C. S. *et al.* (2004) 'Two-color laser-induced incandescence and cavity ring-down spectroscopy for sensitive and quantitative imaging of soot and PAHs in flames', *Applied Physics B: Lasers and Optics*, 78(3–4), pp. 485–492. doi: 10.1007/s00340-003-1370-9.

Morley, C. (2005) 'GASEQ, A Chemical Windows, Equilibrium Program for 0.79.'

Moskaleva, L. V, Mebel, A. M. and Lin, M. C. (1996) 'The CH3 + C5H5 reaction : A potential source of benzene at high temperatures', *Symposium (International) on Combustion*, 26, pp. 521–526.

Mulla, I. A. *et al.* (2016) 'Heat release rate estimation in laminar premixed flames using laser-induced fluorescence of CH 2 O and H-atom'. Elsevier Inc., 165, pp. 373–383. doi: 10.1016/j.combustflame.2015.12.023.

Ni, H. G. *et al.* (2011) 'Fate estimation of polycyclic aromatic hydrocarbons in soils in a rapid urbanization region, Shenzhen of China', *Journal of Environmental Monitoring*, 13(2), pp. 313–318. doi: 10.1039/c0em00470g.

Niranjan, R. and Thakur, A. K. (2017) 'The toxicological mechanisms of environmental soot (black carbon) and carbon black: Focus on Oxidative stress and inflammatory pathways', *Frontiers in Immunology*, 8(JUN), pp. 1–

20. doi: 10.3389/fimmu.2017.00763.

Nisbet, I. C. T. and LaGoy, P. K. (1992) 'Toxic equivalency factors (TEFs) for polycyclic aromatic hydrocarbons (PAHs)', *Regulatory Toxicology and Pharmacology*, 16(3), pp. 290–300. doi: 10.1016/0273-2300(92)90009-X.

Nooren, P. A. *et al.* (2000) 'Raman-Rayleigh-LIF measurements of temperature and species concentrations in the Delft piloted turbulent jet diffusion flame', *Applied Physics B: Lasers and Optics*, 71(1), pp. 95–111. doi: 10.1007/s003400000278.

Oh, K. C. and Shin, H. D. (2006) 'The effect of oxygen and carbon dioxide concentration on soot formation in non-premixed flames', *Fuel*, 85(5–6), pp. 615–624. doi: 10.1016/j.fuel.2005.08.018.

Pandey, P., Pundir, B. and Panigrahi, P. (2007) 'Hydrogen addition to acetylene–air laminar diffusion flames: Studies on soot formation under different flow arrangements', *Combustion and Flame*, 148(4), pp. 249–262. doi: 10.1016/j.combustflame.2006.09.004.

Park, S.-H., Choi, M. Y. and Yozgatligil, A. (2009) 'Nanostructure of Soot Collected from Ethanol Droplet Flames in Microgravity', *Combustion Science and Technology*, 181(9), pp. 1164–1186. doi: 10.1080/00102200903074154.

Park, S. *et al.* (2017) 'Compositional effects on PAH and soot formation in counterflow diffusion flames of gasoline surrogate fuels', *Combustion and Flame*. Elsevier Inc., 178, pp. 46–60. doi:

10.1016/j.combustflame.2017.01.001.

Pašková, V. *et al.* (2006) 'Toxic effects and oxidative stress in higher plants exposed to polycyclic aromatic hydrocarbons and their N-heterocyclic derivatives', *Environmental Toxicology and Chemistry*, 25(12), pp. 3238–3245. doi: 10.1897/06-162R.1.

Petarca, L. and Marconi, F. (1989) 'Fluorescence spectra and polycyclic aromatic species in a N-heptane diffusion flame', *Combustion and Flame*, 78(3–4), pp. 308–325.

Prado, G. *et al.* (1984) 'Polycyclic Aromatic Hydrocarbons formation and destruction in a laminar diffusion flame', *Symposium (International) on Combustion*, 20, pp. 989–996.

Prado, G. *et al.* (1985) 'Polycyclic aromatic hydrocarbons formation and destruction in a laminar diffusion flame', *Symposium (International) on Combustion*, 20(1), pp. 989–996. doi: 10.1016/S0082-0784(85)80588-9.

Qamar, N. H. *et al.* (2009) 'Soot volume fraction in a piloted turbulent jet non-premixed flame of natural gas', *Combustion and Flame*. The Combustion Institute. Published by Elsevier Inc. All rights reserved., 156(7), pp. 1339–1347. doi: 10.1016/j.combustflame.2009.02.011.

Qi, F. (2013) 'Combustion chemistry probed by synchrotron VUV photoionization mass spectrometry', *Proceedings of the Combustion Institute*. The Combustion Institute, 34(1), pp. 33–63. doi: 10.1016/j.proci.2012.09.002.

Qi, F. and McIlroy, A. (2005) 'Identifying combustion intermediates via tunable vacuum ultraviolet photoionization mass spectrometry', *Combustion Science and Technology*, 177(10), pp. 2021–2037. doi: 10.1080/00102200590956704.

Ramanakumar, A. V. *et al.* (2008) 'Risk of lung cancer following exposure to carbon black, titanium dioxide and talc: Results from two case-control studies in Montreal', *International Journal of Cancer*, 122(1), pp. 183–189. doi: 10.1002/ijc.23021.

Randall L.Vander Wal (1996) 'Soot precursor material: Visualization via simultaneous LIF-LII and characterization via tem', *Symposium (International) on Combustion*, 26(2), pp. 2269–2275. Available at: https://doi.org/10.1016/S0082-0784(96)80054-3.

Rehman, M. Y. A. *et al.* (2020) 'Elevated exposure to polycyclic aromatic hydrocarbons (PAHs) may trigger cancers in Pakistan: an environmental, occupational, and genetic perspective', *Environmental Science and Pollution Research*. doi: 10.1007/s11356-020-09088-2.

Reitz, R. D. (2013) 'Directions in internal combustion engine research', *Combustion and Flame*. The Combustion Institute., 160(1), pp. 1–8. doi: 10.1016/j.combustflame.2012.11.002.

Rengarajan, T. *et al.* (2015) 'Exposure to polycyclic aromatic hydrocarbons with special focus on cancer', *Asian Pacific Journal of Tropical Biomedicine*. Hainan Medical University, 5(3), pp. 182–189. doi: 10.1016/S2221-1691(15)30003-4.

Richter, H. and Howard, J. . (2000) 'Formation of polycyclic aromatic hydrocarbons and their growth to soot - a review of chemical reaction pathways', *Progress in Energy and Combustion Science*, 26(4–6), pp. 565–608. doi: 10.1016/S0360-1285(00)00009-5.

Roesler, J. F. *et al.* (2003) 'Investigating the role of methane on the growth of aromatic hydrocarbons and soot in fundamental combustion processes', *Combustion and Flame*, 134(3), pp. 249–260. doi: 10.1016/S0010-2180(03)00093-2.

Ruscic, B. (2015) 'Active Thermochemical Tables: Sequential Bond Dissociation Enthalpies of Methane, Ethane, and Methanol and the Related Thermochemistry', *The Journal of Physical Chemistry A*. American Chemical Society, 119(28), pp. 7810–7837. doi: 10.1021/acs.jpca.5b01346.

Santamaría, A. *et al.* (2006) 'FT-IR and1H NMR characterization of the products of an ethylene inverse diffusion flame', *Combustion and Flame*, 146(1–2), pp. 52–62. doi: 10.1016/j.combustflame.2006.04.008.

Sarathy, S. M. *et al.* (2015) 'Ignition of alkane-rich FACE gasoline fuels and their surrogate mixtures', *Proceedings of the Combustion Institute*. The Combustion Institute, 35(1), pp. 249–257. doi: 10.1016/j.proci.2014.05.122.

Sari, M. F., Esen, F. and Tasdemir, Y. (2020) 'Characterization, source apportionment, air/plant partitioning and cancer risk assessment of atmospheric PAHs measured with tree components and passive air sampler', *Environmental Research*. Elsevier Inc., (June), p. 110508. doi:

10.1016/j.envres.2020.110508.

Schenk, M. *et al.* (2015) 'PAH formation and soot morphology in flames of C4 fuels', *Proceedings of the Combustion Institute*, 35(2), pp. 1761–1769. doi: 10.1016/j.proci.2014.06.139.

Schiro, F., Stoppato, A. and Benato, A. (2020) 'Modelling and analyzing the impact of hydrogen enriched natural gas on domestic gas boilers in a decarbonization perspective', *Carbon Resources Conversion*. Elsevier B.V., 3(July), pp. 122–129. doi: 10.1016/j.crcon.2020.08.001.

Schug, K. P. *et al.* (1980) 'Sooting Behavior of Gaseous Hydrocarbon Diffusion Flames and the Influence of Additives', *Combustion Science and Technology*, 22(5–6), pp. 235–250. doi: 10.1080/00102208008952387.

Senkan, S. and Castaldi, M. (1996) 'Formation of polycyclic aromatic hydrocarbons (PAH) in methane combustion: Comparative new results from premixed flames', *Combustion and Flame*, 107(1–2), pp. 141–150. doi: 10.1016/0010-2180(96)00044-2.

Shaddix, C. R. *et al.* (2005) 'Flame structure of steady and pulsed sooting inverse jet diffusion flames', *Proceedings of the Combustion Institute*. The Combustion Institute, 30(1), pp. 1501–1508. doi: 10.1016/j.proci.2004.08.244.

Shaddix, C. R. and Williams, T. C. (2009) 'Measurements of the velocity field in laminar ethylene inverse jet diffusion flames', *Combustion and Flame*. Elsevier Inc., 156(4), pp. 942–945. doi: 10.1016/j.combustflame.2009.01.017.

Shaddix, C. R. and Williams, T. C. (2017) 'The effect of oxygen enrichment on soot formation and thermal radiation in turbulent, non-premixed methane flames', *Proceedings of the Combustion Institute*. Elsevier Inc., 36(3), pp. 4051–4059. doi: 10.1016/j.proci.2016.06.106.

Shen, H. *et al.* (2014) 'Global lung cancer risk from PAH exposure highly depends on emission sources and individual susceptibility', *Scientific Reports*, 4, pp. 1–8. doi: 10.1038/srep06561.

Shukla, B. *et al.* (2008) 'Role of Phenyl Radicals in the Growth of Polycyclic Aromatic Hydrocarbons', *The Journal of Physical Chemistry A*, 112(11), pp. 2362–2369. doi: 10.1021/jp7098398.

Shukla, B. and Koshi, M. (2010) 'A highly efficient growth mechanism of polycyclic aromatic hydrocarbons', *Physical Chemistry Chemical Physics*, 12(10), pp. 2427–2437. doi: 10.1039/b919644g.

Shukla, B. and Koshi, M. (2011) 'Comparative study on the growth mechanisms of PAHs', *Combustion and Flame*. The Combustion Institute., 158(2), pp. 369–375. doi: 10.1016/j.combustflame.2010.09.012.

Shukla, B., Miyoshi, A. and Koshi, M. (2010) 'Role of Methyl Radicals in the Growth of PAHs', *Journal of the American Society for Mass Spectrometry*. Elsevier Inc., 21(4), pp. 534–544. doi: 10.1016/j.jasms.2009.12.019.

Sidebotham, G. W. and Glassman, I. (1992) 'Flame temperature, fuel structure, and fuel concentration effects on soot formation in inverse diffusion

flames', *Combustion and Flame*, 90(3–4), pp. 269–283. doi: 10.1016/0010-2180(92)90088-7.

Siegmann, K., Hepp, H. and Sattler, K. (1995) 'Reactive dimerization: A new pah growth mechanism in flames', *Combustion Science and Technology*, 109(1–6), pp. 165–181. doi: 10.1080/00102209508951900.

Singh, P. and Sung, C. J. (2016) 'PAH formation in counterflow non-premixed flames of butane and butanol isomers', *Combustion and Flame*. Elsevier Inc., 170, pp. 91–110. doi: 10.1016/j.combustflame.2016.05.009.

Sirignano, M. and D'Anna, A. (2020) 'The role of CO2 dilution on soot formation and combustion characteristics in counter-flow diffusion flames of ethylene', *Experimental Thermal and Fluid Science*, 114(January). doi: 10.1016/j.expthermflusci.2020.110061.

Slavinskaya, N. A. *et al.* (2012) 'Detailed numerical modeling of PAH formation and growth in non-premixed ethylene and ethane flames', *Combustion and Flame*. The Combustion Institute., 159(3), pp. 979–995. doi: 10.1016/j.combustflame.2011.10.005.

Smyth, K. C., Shaddix, C. R. and Everest, D. A. (1997) 'Aspects of soot dynamics as revealed by measurements of broadband fluorescence and flame luminosity in flickering diffusion flames', *Combustion and Flame*. Elsevier, 111(3), pp. 185–207. doi: 10.1016/S0010-2180(97)00017-5.

Solomon, B. D. and Banerjee, A. (2006) 'A global survey of hydrogen energy

research, development and policy', *Energy Policy*, 34(7), pp. 781–792. doi: 10.1016/j.enpol.2004.08.007.

Solomons, T. W. G. and Fryhle, C. B. (2011) *Organic Chemistry*. Tenth edit. New York: Wiley.

Stein, S. E. *et al.* (1991) 'A new path to benzene in flames', *Symposium (International) on Combustion*, 23(1), pp. 85–90.

Stepowski, D., Puechberty, D. and Cottereau, M. J. (1981) 'Use of laser-induced fluorescence of OH to study the perturbation of a flame by a probe', *Symposium (International) on Combustion*, 18(1), pp. 1567–1573.

Steven N. Goodman, & J. G. (2013) *Mechanistic Evidence in Evidence-Based Medicine : A Conceptual Framework Research White Paper Mechanistic Evidence in Evidence-Based Medicine : A Conceptual Framework*, *Agency for Healthcare Research and Quality (US)*. Available at: https://www.ncbi.nlm.nih.gov/books/NBK154587/#background.s1.

Talibi, M. (2011) *Experimental study to determine laminar flame speeds of multi-fuel gaseous mixtures*. University College London.

Tamamura, S. *et al.* (2007) 'Long-range transport of polycyclic aromatic hydrocarbons (PAHs) from the eastern Asian continent to Kanazawa, Japan with Asian dust', *Atmospheric Environment*, 41(12), pp. 2580–2593. doi: 10.1016/j.atmosenv.2006.11.021.

Trottier, S. *et al.* (2007) 'Measurement and modeling of the sooting propensity of binary fuel mixtures', *Proceedings of the Combustion Institute*, 31 I(1), pp. 611–619. doi: 10.1016/j.proci.2006.07.229.

Tsukimori, O. (2020) *Japan faces high costs in achieving Suga's 2050 carbon neutrality target*, *thejapantimes*. Available at: https://www.japantimes.co.jp/news/2020/11/09/business/japan-2050-carbon-neutrality-costs/ (Accessed: 2 March 2021).

Ukaogo, I. J. C. P. O. (2015) 'Environmental Effects of Polycyclic Aromatic Hydrocarbons', *Journal of Natural Sciences Research*, 5(7), pp. 117–131. Available at: www.iiste.org.

USDOE (2020) *Hydrogen strategy - Enabling a low-carbon economy*. Available at: https://www.energy.gov/sites/prod/files/2020/07/f76/USDOE_FE_Hydrogen_Strategy_July2020.pdf.

USEIA (2016) *U.S. Energy Information Administration. International energy outlook*.

USEPA (2020) *Overview of Greenhouse Gases*. Available at: https://www.epa.gov/ghgemissions/overview-greenhouse-gases (Accessed: 20 March 2021).

Verhoeven, L. M. *et al.* (2013) 'A numerical and experimental study of Polycyclic Aromatic Hydrocarbons in a laminar diffusion flame', *Proceedings*

of the Combustion Institute. Elsevier, 34(1), pp. 1819–1826. doi: 10.1016/J.PROCI.2012.06.016.

Vander Wal, R. L. (1996) 'Soot precursor material: Visualization via simultaneous IIF-LII and characterization via tem', *Symposium (International) on Combustion*, 26(2), pp. 2269–2275. doi: 10.1016/S0082-0784(96)80054-3.

Vander Wal, R. L. (1997) 'LIF-LII measurements in a turbulent gas-jet flame', *Experiments in Fluids.* Springer-Verlag, 23(4), pp. 281–287. doi: 10.1007/s003480050112.

Vander Wal, R. L. (1998) 'Soot precursor carbonization: Visualization using LIF and LII and comparison using bright and dark field TEM', *Combustion and Flame*, 112(4), pp. 607–616. doi: 10.1016/S0010-2180(97)00171-5.

Vander Wal, R. L., Jensen, K. A. and Choi, M. Y. (1997) 'Simultaneous laser-induced emission of soot and polycyclic aromatic hydrocarbons within a gas-jet diffusion flame', *Combustion and Flame*. Elsevier, 109(3), pp. 399–414. doi: 10.1016/S0010-2180(96)00189-7.

Wang, H. and Frenklach, M. (1997) 'A detailed kinetic modeling study of aromatics formation in laminar premixed acetylene and ethylene flames', *Combustion and Flame*, 110(1–2), pp. 173–221. doi: 10.1016/S0010-2180(97)00068-0.

Wang, Q. *et al.* (2017) 'Experimental characterization of the different nitrogen dilution effects on soot formation in ethylene diffusion flames', *Proceedings of*

the Combustion Institute. Elsevier Inc., 36(2), pp. 3227–3235. doi: 10.1016/j.proci.2016.07.063.

Wang, Y. *et al.* (2018) 'A comparative study on the sooting tendencies of various 1-alkene fuels in counterflow diffusion flames', *Combustion and Flame*. Elsevier Inc., 192, pp. 71–85. doi: 10.1016/j.combustflame.2018.01.033.

Wang, Y. *et al.* (2019) 'Numerical Simulation of the Effects of Hydrogen Addition to Fuel on the Structure and Soot Formation of a Laminar Axisymmetric Coflow C2H4/(O2-CO2) Diffusion Flame', *Combustion Science and Technology*. Taylor & Francis, 191(10), pp. 1743–1768. doi: 10.1080/00102202.2018.1532413.

Wang, Y. *et al.* (2020) 'An experimental and numerical study of soot formation of laminar coflow H2/C2H4 diffusion flames in O2CO2 atmosphere', *Combustion and Flame*. Elsevier Inc., 221, pp. 50–63. doi: 10.1016/j.combustflame.2020.07.026.

Wang, Y. and Chung, S. H. (2019) 'Soot formation in laminar counterflow flames', *Progress in Energy and Combustion Science*. Elsevier Ltd, 74, pp. 152–238. doi: 10.1016/j.pecs.2019.05.003.

Wartel, M. *et al.* (2010) 'Quantitative measurement of naphthalene in low-pressure flames by Jet-Cooled Laser-Induced Fluorescence', *Applied Physics B: Lasers and Optics*, 100(4), pp. 933–943. doi: 10.1007/s00340-010-4135-2.

Wartel, M. *et al.* (2011) 'Pyrene measurements in sooting low pressure

methane flames by jet-cooled laser-induced fluorescence', *Journal of Physical Chemistry A*, 115(49), pp. 14153–14162. doi: 10.1021/jp206970t.

Weilmünster, P., Keller, A. and Homann, K. H. (1999) 'Large molecules, radicals, ions, and small soot particles in fuel-rich hydrocarbon flames Part I: Positive ions of polycyclic aromatic hydrocarbons(PAH) in low-pressure premixed flames of acetylene and oxygen', *Combustion and Flame*, 116(1–2), pp. 62–83. doi: 10.1016/S0010-2180(98)00049-2.

Wu, J. *et al.* (2006) 'Reduction of PAH and soot in premixed ethylene-air flames by addition of dimethyl ether', *Combustion Science and Technology*, 178(5), pp. 837–863. doi: 10.1080/00102200500269942.

Wu, Y. *et al.* (2019) 'Effects of Carbon Dioxide and Water Vapor Addition on Benzene and PAH Formation in a Laminar Premixed CH4/O2/Ar Flame', *Combustion Science and Technology*. Taylor & Francis, 191(10), pp. 1866–1897. doi: 10.1080/00102202.2018.1536881.

Xi, J. and Zhong, B.-J. (2006) 'Soot in Diesel Combustion Systems', *Chemical Engineering & Technology*, 29(6), pp. 665–673. doi: 10.1002/ceat.200600016.

Xiao, J., Austin, E. and Roberts, W. L. (2005) 'Relative polycyclic aromatic hydrocarbon concentrations in unsteady counterflow diffusion flames', *Combustion Science and Technology*, 177(4), pp. 691–713. doi: 10.1080/00102200590917239.

Xu, L. *et al.* (2020) 'Chemical effects of hydrogen addition on soot formation in

counterflow diffusion flames: Dependence on fuel type and oxidizer composition', *Combustion and Flame*. Elsevier Inc., 213, pp. 14–25. doi: 10.1016/j.combustflame.2019.11.011.

Yamamoto, K. and Takemoto, M. (2013) 'Measurement of PAH and soot of diffusion flames in a triple port burner', *Fuel Processing Technology*. Elsevier, 107, pp. 99–106. doi: 10.1016/J.FUPROC.2012.06.006.

Yamamoto, K. and Takemoto, M. (2014) 'Reductions of PAH and Soot by Center Air Injection', *Environments*, 1(1), pp. 42–53. doi: 10.3390/environments1010042.

Yan, F. *et al.* (2019) 'On the opposing effects of methanol and ethanol addition on PAH and soot formation in ethylene counterflow diffusion flames', *Combustion and Flame*. Elsevier Inc., 202, pp. 228–242. doi: 10.1016/j.combustflame.2019.01.020.

Yoon, S. S., Anh, D. H. and Chung, S. H. (2008) 'Synergistic effect of mixing dimethyl ether with methane, ethane, propane, and ethylene fuels on polycyclic aromatic hydrocarbon and soot formation', *Combustion and Flame*. Elsevier, 154(3), pp. 368–377. doi: 10.1016/J.COMBUSTFLAME.2008.04.019.

Yoon, S. S., Lee, S. M. and Chung, S. H. (2005) 'Effect of mixing methane, ethane, propane, and propene on the synergistic effect of PAH and soot formation in ethylene-base counterflow diffusion flames', *Proceedings of the Combustion Institute*. The Combustion Institute, 30(1), pp. 1417–1424. doi:

10.1016/j.proci.2004.08.038.

Zhang, Y. *et al.* (2018) 'Experimental and kinetic study of the effects of CO_2 and H_2O addition on PAH formation in laminar premixed $C_2H_4/O_2/Ar$ flames', *Combustion and Flame*. Elsevier Inc., 192, pp. 439–451. doi: 10.1016/j.combustflame.2018.01.050.

Zizak, G. *et al.* (1996) 'Detection of aromatic hydrocabons in the exhaust gases of a i.c. engine by laser-induced fluorescence technique', *Recent Res. Devel. in Applied Spectro.*, 1(January 1996).